Found 61 Records

SESSION TITLE: Late Breaking Session 01: Probe Concepts & Preclinical Imaging (basic bio, neuro, onc)
CONTROL ID: 2790384
TITLE: Luciferin Analogues Extend Firefly Bioluminescence into the Near-Infrared for Deep Bioluminescence Imaging
PRESENTER: Yuma Ikeda
AUTHORS (FIRST NAME, LAST NAME): Yuma Ikeda[1], Shigeru Nishiyama[2], Koji Suzuki[1], Daniel Citterio[1]
INSTITUTIONS (ALL):
1. Department of Applied Chemistry, Keio University, Yokohama, Kanagawa, Japan.
2. Department of Chemistry, Keio University, Yokohama, Kanagawa, Japan.
ABSTRACT BODY:
Abstract Body: Bioluminescence (BL)-based assays are widely used as in vitro and in vivo reporters of biologically relevant substances, gene expression, and tumor progression, among others. Among the available systems, firefly bioluminescence shows the highest emission efficiency (φ_{BL} = 0.41). Although bioluminescence-based assays show much lower background signals than fluorescence-based assays and are applicable for more sensitive in vivo imaging, their application is limited due to a lack of luciferins especially emitting in the near-infrared (NIR) wavelength (650–900 nm), where tissue is more light transparent.

In order to expand the firefly bioluminescence applications and its emission wavelength, we have developed novel firefly luciferin analogues modified with allyl groups at the C-7' position of its benzothiazole core. The terminal olefin of allyl groups is for example available for further modification as a linker, or the allyl groups can also be converted to aldehyde groups, which can then react with various functional groups. Therefore, it is considered that allyl modification of firefly luciferin leads to useful possibilities, such as the development of various analogues and labeling applications by using allyl luciferin as a platform. Additionally, we hypothesized that this steric modification would result in red-shifted bioluminescence emission due to the conformational change that creates an extremely hydrophobic microenvironment in the luciferase active site.

As expected, the developed luciferin showed 45 nm red-shifted emission, presumably due to the change in the interaction between the luciferin and amino acid residues at the active site of the luciferase enzyme. This result indicates that bioluminescence emission wavelength can be controlled by stereoscopic effect. Additionally, live cell assays of the allyl-luciferin with some beetle luciferases were performed. Recent studies revealed that steric modifications to the luciferin potentially have the ability to bolster bioluminescence properties. Surprisingly, the allyl-luciferin showed luciferase-selective response. This result suggests that this synthetic luciferin can be applied to luciferin-luciferase based multiple in vivo imaging. Based on these findings, five types of allyl modified luciferin analogues were newly developed. These analogues extended the bioluminescence emission into the NIR wavelength with wild type luciferase.

In summary, we successfully synthesized 6 types of firefly luciferin analogues with allyl group. One of them, allyl luciferin showed luciferase selective response with live cell. Further modification of allyl luciferin resulted in remarkable red-shifted emission into NIR. We believe that this new synthetic luciferin will contribute to the expansion of bioluminescence imaging applications both in vitro and in vivo. Studies are now in progress to develop artificial beetle luciferases that display stronger bioluminescence emission with allyl luciferins compared to that of natural substrate, D-luciferin, and also apply its selective response to bioluminescence based reporter assays.

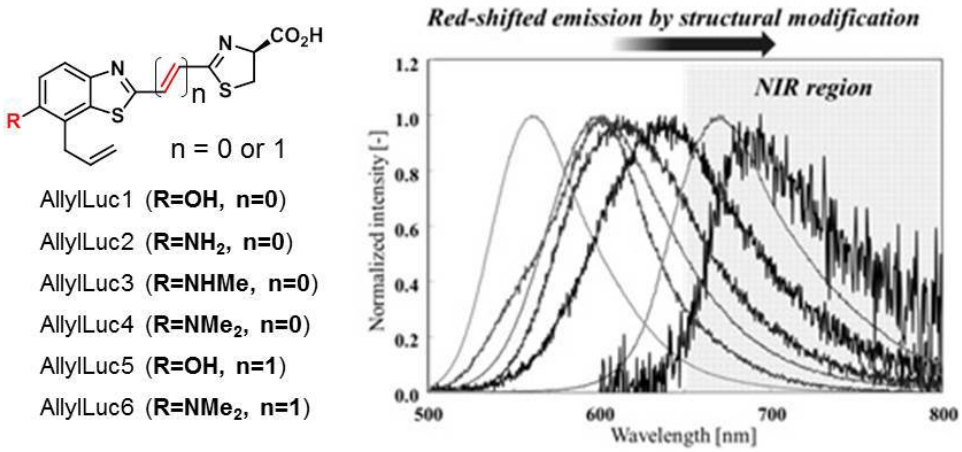

Structure of firefly luciferin analogues and their emission wavelength

IMAGE CAPTION: Structure of firefly luciferin analogues and their emission wavelength

SESSION TITLE: Late Breaking Session 01: Probe Concepts & Preclinical Imaging (basic bio, neuro, onc)
CONTROL ID: 2799618
TITLE: Highly Sensitive ^{19}F MR Imaging of in Vivo Enzyme Activity Using Perfluorocarbon-Encapsulated Silica Nanoparticle
PRESENTER: Kazuki Akazawa
AUTHORS (FIRST NAME, LAST NAME): Kazuki Akazawa[1], FUMINORI SUGIHARA[2], KAZUYA KIKUCHI[1, 2]
INSTITUTIONS (ALL):
1. Graduate school of enginnering, Osaka University, Osaka, Japan.
2. Immunology Frontier Research Center, Osaka University, Osaka, Japan.
ABSTRACT BODY:
Abstract Body: Highly sensitive imaging of in vivo enzyme activities is important for analyzing their biological roles and the response of drug treatment. Magnetic resonance imaging (MRI) is an in vivo imaging modality that offers highly spatial resolution images without concern for tissue depth. Especially, ^{19}F MRI has little endogenous background signal, so this imaging technique is suitable for specific detection of the signals from ^{19}F MRI probes. Thus, various types of ^{19}F MRI probes for imaging enzyme activities have been reported. For example, activatable ^{19}F MRI probes have been designed on the basis of paramagnetic relaxation enhancement (PRE) effect (Figure 1).[1] However, the sensitivity using small-molecule ^{19}F MRI probes was not sufficient for in vivo experiments. There are two main challenges when boosting up the sensitivity of ^{19}F MRI probes. First, an increase of the number of fluorine atoms in a molecule decreases the solubility of the probes. Second, a suppression of molecular mobility caused by the increase of molecular size shortens the transverse relaxation time (T_2), which is a crucial factor affecting the MRI contrast, resulting in the attenuation of the MRI signals. To overcome these challenges, a novel ^{19}F MRI contrast agent, FLuorine Accumulated silica nanoparticle for MRI contrast Enhancement (FLAME), was developed (Figure 2).[2] FLAMEs are composed of a liquid perfluorocarbon (PFC) core, where PFC molecules show high molecular mobility to achieve the long T_2, and a robust silica shell. FLAME has superior properties such as high sensitivity, stability in organic and aqueous solution, and enables versatile surface modification. Through appropriate surface modification of FLAMEs, transplanted tumors in living mice were successfully detected by ^{19}F MRI.
To monitor specific biological events such as reducing environment and enzyme activities, activatable ^{19}F MRI nanoprobes were developed by combining OFF/ON-switching strategy based on PRE effect and FLAME. Initially, multiple Gd^{3+} complexes were conjugated on the FLAME surface via disulfide linkers (FLAME-SS-Gd^{3+}), and it was revealed that PRE effect of Gd^{3+} complexes can efficiently attenuate ^{19}F MRI signals of FLAMEs (Figure 3).[3] After the treatment of reducing agents, FLAME-SS-Gd^{3+} showed a high ^{19}F MRI signal enhancement. By taking this knowledge, activatable ^{19}F MRI nanoprobes for monitoring in vivo enzyme activities were developed. ^{19}F MR imaging of in vivo enzyme activity using activatable ^{19}F MRI nanoprobe will be introduced in this presentation.

[1] S. Mizukami, R. Takikawa, F. Sugihara, Y. Hori, H. Tochio, M. Wälchli, M. Shirakawa, K. Kikuchi, J. Am. Chem. Soc., 2008, 130, 794–795.
[2] H. Matsushita, S. Mizukami, F. Sugihara, Y. Nakanishi, Y. Yoshioka, K. Kikuchi, Angew. Chem. Int. Ed., 2014, 53, 1008–1011.
[3] T. Nakamura, H. Matsushita, F. Sugihara, Y. Yoshioka, S. Mizukami, K. Kikuchi, Angew. Chem. Int. Ed., 2015, 54, 1007–1010.

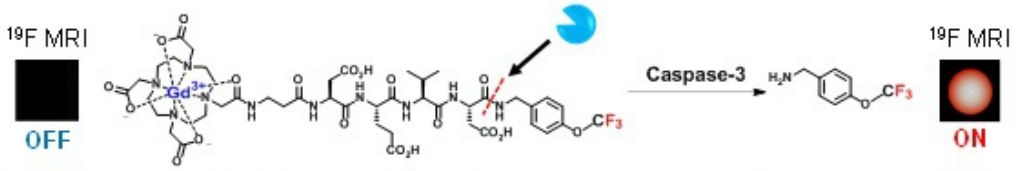

Figure 1. Activatable ^{19}F MRI probe based on paramagnetic relaxation enhancement (PRE) effect.

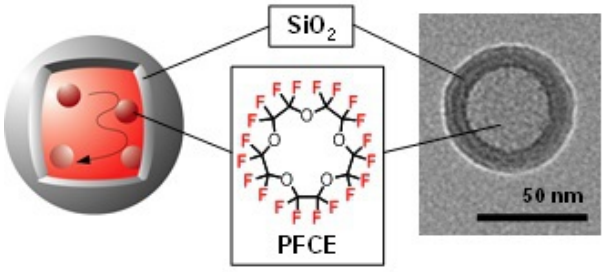

Figure 2. Highly sensitive ^{19}F MRI nanoprobe.

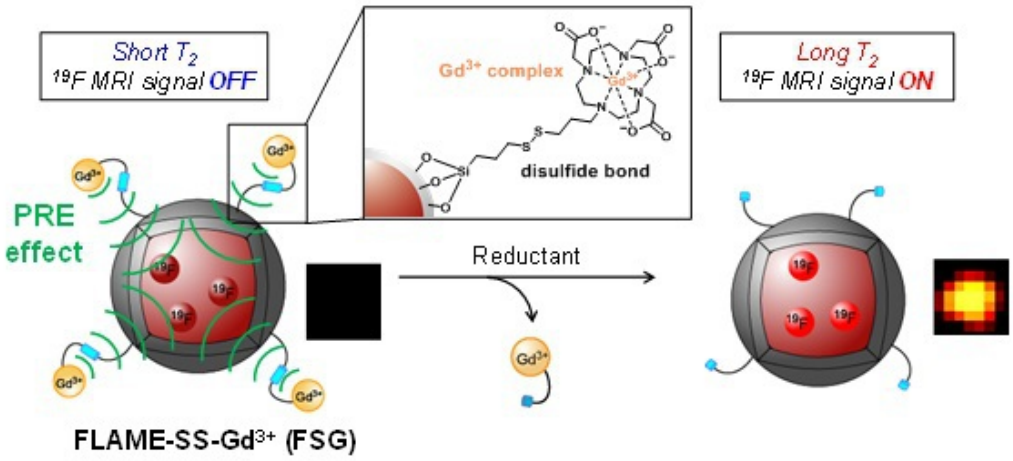

Figure 3. Activatable ^{19}F MRI nanoprobes for the detection of reducing environment.

IMAGE CAPTION:

SESSION TITLE: Late Breaking Session 01: Probe Concepts & Preclinical Imaging (basic bio, neuro, onc)
CONTROL ID: 2804836
TITLE: ^{18}F-Labelled Perfluorocarbon Nanoemulsion for PET Imaging
PRESENTER: Yun Xiang
AUTHORS (FIRST NAME, LAST NAME): Nagina Amir[1], David R. Green[2], Jeff Kent[1], Yun Xiang[3], Ivan Gorelikov[2], Minseok Seo[2], Megan Blacker[1], Nancy Janzen[1], Shannon Czorny[1], John Valliant[1, 4], Naomi Matsuura[3, 5, 6]
INSTITUTIONS (ALL):
1. Department of Chemistry and Chemical Biology, McMaster University, McMaster, ON, Canada.
2. Physical Sciences, Sunnybrook Research Institute, Toronto, ON, Canada.
3. Department of Medical Imaging, University of Toronto, Toronto, ON, Canada.
4. Centre for Probe Development and Commercialization, McMaster University, Hamilton, ON, Canada.
5. Department of Materials Science and Engineering, University of Toronto, Toronto, ON, Canada.
6. Institute of Biomaterials and Biomedical Engineering, University of Toronto, Toronto, ON, Canada.
ABSTRACT BODY:
Abstract Body: Introduction: Nanoscale perfluorocarbon (PFC) emulsions have been used to create imaging agents and drug delivery vehicles (1, 2). However, development and characterization of new formulations of PFC emulsions are hindered because of the lack of simple methods for quantitative and sensitive assessment of whole body tissue distribution and pharmacokinetics of the emulsions. To address this issue, a general-purpose method for radiolabeling the inner core of nanoscale perfluorocarbon emulsions with a hydrophobic and lipophobic fluorine-18 compound was developed, so that positron emission tomography (PET) and quantitative biodistribution studies can be employed to evaluate PFC nanoemulsions in vivo.
Methods: A robust method to produce $[^{18}F]CF_3(CF_2)_7(CH_2)_3F$ from a tosylate precursor using $[^{18}F]F^-$ was developed. The product's effectiveness as a general label for different PFCs and its ability to distinguish the in vivo behavior of different PFC emulsion formulations was evaluated using two types of PFC nanoemulsions: fluorosurfactant-stabilized perfluorohexane (PFH) nanoemulsions and lipid-stabilized perfluorooctylbromide (PFOB) nanoemulsions. In vivo assessment of the ^{18}F-labelled PFH and PFOB nanoemulsions were conducted in normal mice following intravenous injection using small animal PET imaging and gamma counting of tissues and fluids.
Results: $[^{18}F]CF_3(CF_2)_7(CH_2)_3F$ was produced in modest yield and was stable with respect to loss of fluoride in vitro. The labeled perfluorocarbon was successfully integrated into PFH nanoemulsions (~175 nm) and PFOB nanoemulsions (~260 nm) without altering their mean sizes, size distributions, or surface charges compared to their non-radioactive analogues. No leakage of the radiolabel from the nanoemulsions was detected after emulsion formation in vitro. PET imaging and biodistribution data for the two emulsion types tested showed significantly different tissue uptake and clearance patterns.
Conclusion: A convenient method for producing ^{18}F-labelled PFC emulsions was developed. The results highlight the potential utility of the strategy for pre-clinical evaluation of different PFC emulsion formulations through direct PFC core labeling using a fluorinated radiolabel. The strategy can be used for sensitive and quantitative assessment of the whole-body pharmacokinetics of novel nanoscale PFC emulsions. With the advent of PET-MRI, the emulsions reported also represent a multi-modal contrast agent that can be imaged by ^{19}F-MRI and PET simultaneously (3). This provides the means to combine high-resolution anatomical imaging with the ability to obtain quantitative pharmacokinetic data.

Reference

1. E. Strohm, M. Rui, I. Gorelikov, N. Matsuura, M. Kolios, Biomed. Opt. Express. 2, 1432–42 (2011).
2. N. Rapoport, Z. Gao, A. Kennedy, J. Natl. Cancer Inst. 99, 1095–106 (2007).
3. C. Giraudeau et al., NMR Biomed. 25, 654–60 (2012).

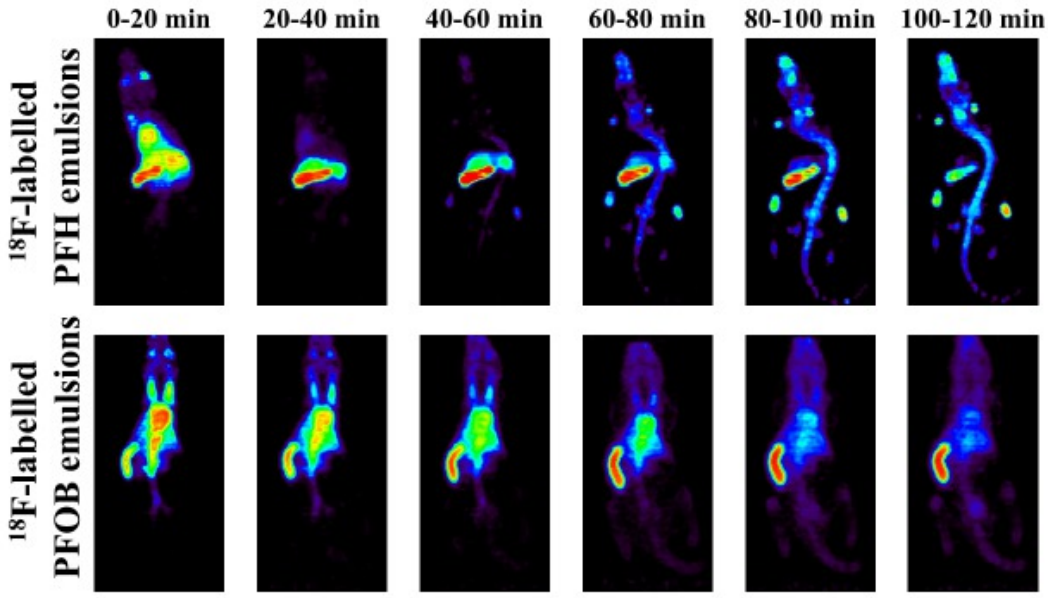

Figure 1. Coronal small animal PET images of a C3H/HeJ female mouse after injection of ^{18}F-labelled PFH nanoemulsions (2.86 MBq, top) and ^{18}F-labelled PFOB nanoemulsions (9.62 MBq, bottom) over a 2 h scan time at 20 min intervals. The mouse was placed on the scanner 8 min after tracer injection. All images shown were taken from the same coronal slice and displayed using equivalent imaging parameters.

IMAGE CAPTION: Figure 1. Coronal small animal PET images of a C3H/HeJ female mouse after injection of ^{18}F-labelled PFH nanoemulsions (2.86 MBq, top) and ^{18}F-labelled PFOB nanoemulsions (9.62 MBq, bottom) over a 2 h scan time at 20 min intervals. The mouse was placed on the scanner 8 min after tracer injection. All images shown were taken from the same coronal slice and displayed using equivalent imaging parameters.

SESSION TITLE: Late Breaking Session 01: Probe Concepts & Preclinical Imaging (basic bio, neuro, onc)

CONTROL ID: 2805123

TITLE: Novel click beetle luciferase mutant and near infrared luciferins for improved bioluminescence imaging

PRESENTER: Laura Mezzanotte

AUTHORS (FIRST NAME, LAST NAME): Mary Hall[1], Carolyn C. Woodroofe[2], Monika Wood[1], Ce Shi[2], Thomas A. Kirkland[2], Lance Encell[1], Keith Wood[1], Clemens Lowik[3], Laura Mezzanotte[3]

INSTITUTIONS (ALL):

1. Promega Corporation, Madison, WI, United States.
2. Promega Biosciences , San Luis Obispo, CA, United States.
3. Radiology, Erasmus Medical Center, Rotterdam, Netherlands.

ABSTRACT BODY:

Abstract Body: The sensitivity of bioluminescence imaging in animals is primarily dependent on the amount of photons emitted by the luciferase enzyme at wavelengths greater than 620 nm, where there is low light absorption by tissue. This area of work has been dominated Firefly luciferase and its substrate, D-luciferin, due to the system's broad emission spectrum and the favorable biodistribution of D-Luciferin in vivo. Here we describe a novel codon optimized mutant of Click beetle red luciferase (peak emission of 620 nm with D-luciferin) that produces substantially more light output compared to Firefly luciferase when equimolar levels of the two enzymes are compared in transplanted cells within different organs of nude and black fur mice. The same mutant Click beetle sequence was originally designed to function with two novel napthyl-luciferin substrates that produce spectral emissions of 730 and 750 nm, respectively, well within the desirable near infrared range. The system providing 730 nm emission produces a stable luminescence signal over time and provides unprecedented sensitivity for performing deep tissue tomography in mice.

(No Image Selected)

SESSION TITLE: Late Breaking Session 05: Basic Bio - New Probe & Systems/Engineered Biology

CONTROL ID: 2805240

TITLE: Engineering Acoustic Biomolecules as Dynamic Molecular Sensors for Ultrasound Imaging

PRESENTER: Anupama Lakshmanan

AUTHORS (FIRST NAME, LAST NAME): Anupama Lakshmanan[1], Suchita P. Nety[2], David Maresca[2], Mikhail G. Shapiro[2]

INSTITUTIONS (ALL):

1. Biology and Biological Engineering, California Institute of Technology, Pasadena, CA, United States.
2. Chemistry and Chemical Engineering, California Institute of Technology, Pasadena, CA, United States.

ABSTRACT BODY:

Abstract Body: Background: Ultrasound enables the imaging of deep tissues with high spatial and temporal resolution. However, this modality has limited ability to visualize dynamic molecular and cellular processes due to the lack of functional contrast agents. Gas Vesicles (GVs) - hollow protein nanostructures isolated from buoyant microbes, have emerged as a new class of biomolecular imaging agents for ultrasound (Shapiro, Nat. Nano., 2014). The genetic encodability of these acoustic biomolecules provides a unique platform for engineering mechanical and functional properties at the protein level. Recently, we demonstrated that modifying a key GV shell protein results in nanostructures with enhanced non-linear contrast, as well as tunable collapse pressures for multiplexed imaging (Lakshmanan, ACS Nano, 2016). Now, we extend this platform to engineer GVs whose ultrasound signals change dynamically in response to the activity of specific molecules in their environment. In particular, we set out to produce GVs that change their non-linear ultrasound contrast in response to specific proteases, an important class of enzymes underlying homeostatic and disease processes, and a target of drug discovery.

Innovation: Here, we present initial evidence that genetic engineering of the gas vesicle shell protein GvpC (Fig. 1A-C) can be used to generate GVs whose non-linear ultrasound signals depend on the activity of proteases. We hypothesized that incorporation of protease recognition motifs at specific sites within the GvpC sequence would enable its cleavage by the active enzyme, modifying the mechanical properties of the GV shell and thereby producing a change in GV acoustic properties (Fig. 1C-D). The target enzyme may be an always-on protease or one whose function depends on the concentration of another analyte of interest, such as calcium. Here, we demonstrate this concept with two different proteases.

Methods: GVs containing genetically engineered, recombinantly expressed protease-sensitive GvpC were incubated with their cognate proteases and evaluated with ultrasound and pressurized absorbance spectroscopy. Ultrasound images were acquired at 18 MHz, with non-linear signals acquired using a custom amplitude modulation sequence (Maresca, Appl. Phys. Lett., 2017).

Results: Incubation of engineered GVs with the always-on protease resulted in a change in the mechanical properties of GVs, as seen by a reduction in their critical hydrostatic collapse pressure and an increase in non-linear ultrasound signal (Fig. 1E). Similar results were obtained with GVs designed to sense a calcium-dependent protease, where a change in non-linear ultrasound signal was observed in response to calcium.

Impact: These results provide the first demonstration of a genetically engineered molecular sensor for ultrasound. The platform presented here can be used to engineer the next generation of acoustic contrast agents that can be used to dynamically monitor physiologically relevant molecules, adding a new functional capability to this imaging modality.

Figure 1: Engineering Acoustic Biomolecules as Dynamic Molecular Sensors for Ultrasound Imaging

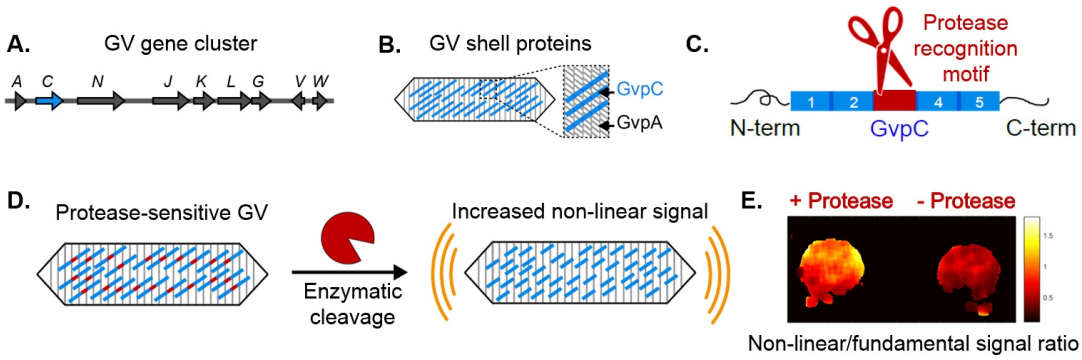

IMAGE CAPTION:

SESSION TITLE: Late Breaking Session 05: Basic Bio - New Probe & Systems/Engineered Biology

CONTROL ID: 2805382

TITLE: Sensing and imaging through tissue with radioluminescent phosphors

PRESENTER: Jeffrey Anker

AUTHORS (FIRST NAME, LAST NAME): Jeffrey N. Anker[1, 2], Gretchen Schober[1], Hongyu Chen[1], Fenglin Wang[1], Thomas L. Moore[2], Dino Sulejmanovic[1], Bin Qi[3], Shiou-Jyh Hwu[1], Olin T. Mefford[3], Fank Alexis[2]

INSTITUTIONS (ALL):

1. Chemistry, Clemson University, Clemson, SC, United States.
2. Bioengineering, Clemson University, Clemson, SC, United States.
3. Materials Science and Engineering, Clemson University, Clemson, SC, United States.

ABSTRACT BODY:

Abstract Body: Radioluminescent nanophosphors are promising contrast agents for deep tissue optical imaging applications because they can be excited by deeply penetrating X-rays and generate a low background signal.[1] High resolution X-ray luminescence tomography (XLT) images can be acquired by scanning a narrow X-ray beam and recording light escaping from the tissue at each X-ray position point. In addition, the nanophosphors can serve as a local radioluminescent sensor to measure accumulation or release of radiolabeled drugs. For all these bioimaging applications, the nanophosophors should ideally be small, monodispersed and brightly luminescent. However, most methods used to improve luminescence yield by annealing the particles to reduce crystal and surface defects (e.g. using flux or sintering agents) also cause particle fusion or require multiple component core-shell structures. We describe a method to prepare bright, uniformly sized X-ray nanophosphors (Gd_2O_2S:Eu or Tb) and upconversion nanophosphors (Y_2O_2S: Yb/Er, or Yb/Tm) with large crystal domain size without causing aggregation by encapsulating NaF as a sintering agent in the core and encasing with a protective shell containing no sintering agent.[2] Increasing the sintering agent concentration up to 7.6 mol% increases both crystal domain size and luminescence intensity (up to 40% of commercial microphosphors) without affecting the physical particle diameter. The prepared bright nanophosphors were subsequently functionalized with PEG-folic acid to target MCF-7 breast cancer cells which overexpress folic acid receptors. Both X-ray and upconversion nanophosphors provided low background and bright luminescence which was imaged through 1 cm chicken breast tissue at a low dose of nanophosphors 200 µL (0.1 mg/mL). X-ray scintillators were also detected in a mouse brain tumor.[3] These monodispersed and bright X-ray and upconversion nanophosphors have promise for sensing and imaging through tissue.

Acknowlegment: This work was supported in part by NSF CAREER award CHE1255535 and The South Carolina Bioengineering Center of Regeneration and Formation of Tissues (BioCRAFT) funded under NIGMS of the National Institutes of Health, award number 5P20GM103444-07.

References:

1. Chen H., Rogalski M., and Anker, J.N.: “Advances in functional X-ray imaging techniques and contrast agents.” Physical Chemistry

2. Chemical Physics, 14 13469-13486 (2012).1. Chen H., Moore T., Qi B., Mefford, O.T., Alexis F., and Anker J.N.: “Enhanced performance of targeted X-ray and up-conversion nanophosphors using an encapsulated sintering agent.” Chemistry of Materials B, (Accepted 2017)

3. Moore L.T., Wang F., Chen H., Grimes S.W., Anker J.N., and Alexis F.: “Polymer-Coated Radioluminescent Nanoparticles for Imaging Drug Delivery into Cells.” Advanced Functional Materials, 24, 5815-5823 (2014).

(No Image Selected)

SESSION TITLE: Late Breaking Session 05: Basic Bio - New Probe & Systems/Engineered Biology

CONTROL ID: 2805412

TITLE:

Tumor-Targeted and Clearable Human Protein MRI probes

PRESENTER: gang han

AUTHORS (FIRST NAME, LAST NAME): gang han[1]

INSTITUTIONS (ALL):

1. university of massachusetts-medical school, Worcester, MA, United States.

ABSTRACT BODY:

Abstract Body:

Herein, we report on a fisrt human protein based MRI probes . In particuar, this is a new tumor-targeting, gadolinium biomineralized human transferrin (Tf) protein-based nanoparticle (Gd@Tf NP) . As compared to the conventionally used gadolinium chelates, the resultant Gd@Tf NPs possess outstanding chemical stability and exhibited superior longitudinal relaxation. More importantly, our MR images show that Gd@Tf indeed retained the natural tumor targeting ability and the subsequent tumor retrieval biofunctions of Tf. Thus, such Tf protein-based MR NPs integrate T1 signal amplification, precise tumor targeting, and systematic clearance capabilities. They offer a new approach to design biocompatible multifunctional MRI contrast agents for a wide range of clinical imaging and treatment applications.

(No Image Selected)

SESSION TITLE: Late Breaking Session 09: Basic Biology - New Probe Concepts

CONTROL ID: 2781392

TITLE: Photoacoustic Ocular Imaging of Retina Oxygen Gradients In Vivo

PRESENTER: Ali Hariri

AUTHORS (FIRST NAME, LAST NAME): Ali Hariri[1], Junxin Wang[1], Jesse V. Jokerst[1, 2]

INSTITUTIONS (ALL):

1. Nanoengineering, University of California San Diego, San Diego, CA, United States.
2. Radiology, University of California San Diego, San Diego, CA, United States.

ABSTRACT BODY:

Abstract Body: Introduction:

Many eye diseases including glaucoma result from dysregulated intraocular pressure (IOP)—the choroidal blood flow decreases as the IOP increases. In turn, oxygen availability decreases along with a decrease in retinal oxygenation (sO_2). Thus, the quantification of sO_2 could play a significant role in detecting and monitoring glaucoma. Photoacoustic imaging is an emerging tool that can satisfy many ocular imaging requirements while also making functional measurements of sO_2 with high temporal resolution. Here, we show that photoacoustic ocular imaging (PAOI) can measure sO_2 gradients in a rabbit model with increased IOP.

Methods:

New Zealand white rabbits (n=5; 2-3 kg) were anesthetized with i.m. injection of ketamine (35 mg/kg) and xylazine (5 mg/kg). The pupils were dilated and anesthetized using 2.5% phenylephrine hydrochloride, 0.5% proparacaine hydrochloride, and 1% tropicamide. To calibrate the PAOI, the animal was given different oxygen tensions (0% - 100% O2 with the balance as nitrogen). The sO_2 was monitored with both a pulse oximeter and PAOI. The IOP was increased with an ischemia-reperfusion model using a 25-gauge needle placed in the anterior chamber of the eye. Saline was infused to increase the pressure. This pressure increase was measured before (baseline), during (ischemia), and after stopping the PBS injection using a Tonopen. Both PO and PAOI were monitored during the experiment via photoacoustic imaging used a Vevo 2100 commercial photoacoustic scanner (Visualsonics, 15 MHz-centered transducers (LZ201), 750 and 850 nm as wavelength).

Results:

We first showed that the photoacoustic data reflected oxygen tension. We used both PAOI and a PO with different oxygen tensions and showed good correlation between the two techniques (R^2> 0.95; Supplementary data). Next, we created a model of IOP and validated it with a Tonopen. Fig. 1A and B show a B-mode photoacoustic/ultrasound and a sO2 map, respectively. At baseline (no IOP increase; 9.667 ± 0.577 mmHg), the sO_2 is 67.871 ± 1.947. When the IOP was increased to 50 ± 1.732 mmHg the sO_2 decreased to 8.806 ± 1.612. This recovered to 65.443 ± 1.016 after the IOP returned to 15.5 ± 0.707 mmHg. Fig. 1C shows sO_2 map during the ischemia, and Fig. 1D shows reperfusion. Fig. 1E demonstrates real time monitoring of both PO and PAOI during ischemia-reperfusion experiment. The ischemia- reperfusion model did not affect the sO_2 using PO on the animal's paw, but the PAOI shows a nearly 8-fold decrease in sO_2 (n=5, $p<0.01$). Fig. 1F demonstrates that sO_2 and IOP are negatively correlated. The sO2 decreased with increased IOP (n=5, $p<0.01$).

Conclusions:

Photoacoustic imaging was utilized to measure hemoglobin oxygen saturation. The PAOI was evaluated using different oxygen percentages (See supplement) and with an in vivo model of increased IOP.

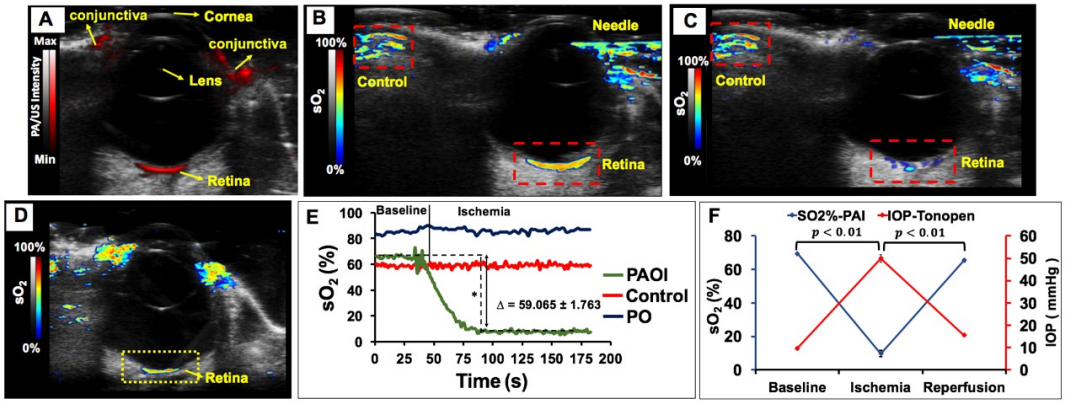

Figure 1. (A) B-mode photoacoustic/ultrasound image in baseline condition, (B) B-mode sO_2 map using 750 and 850 nm excitation while a 25-gauge needle is inside the anterior segment of eye. (C) B-mode sO_2 map during the ischemia. The blood flow and retina blood vessel diameter will decrease in ischemia. (D) B-mode sO_2 map during reperfusion. sO_2 (E) Real time monitoring of sO_2 using PO and PAOI. The PAOI shows 8-fold decrease in sO_2 during ischemia (n=5, p<0.01). The Δ shows sO_2 difference between baseline and ischemia. (F) Statistical analysis of IOP and sO_2 measurement using a Tonopen and PAOI respectively. There is negative correlation between IOP and sO_2 (n=5, $p < 0.01$). In this imaging system OPO-laser source is operating at 20 Hz between 680 and 970 nm with a 1 nm step size and a pulse of 4 to 6 ns. The laser was coupled into 15 MHz-centered transducers (LZ201). To measure sO_2, 750 and 850 nm were used in our experiments. The frame for sO_2 measurement is 1 Hz.

IMAGE CAPTION:

SESSION TITLE: Late Breaking Session 09: Basic Biology - New Probe Concepts

CONTROL ID: 2784215

TITLE: Measuring Dental Pocket Depths with Photoacoustic Imaging and a Food Grade Contrast Agent.

PRESENTER: Jesse Jokerst

AUTHORS (FIRST NAME, LAST NAME): Ching-Yu Lin[1], Fang Chen[1], Ali Hariri[1], Chien-Ju Chen[1], Jesse V. Jokerst[1]

INSTITUTIONS (ALL):

1. University of California, San Diego, La Jolla, CA, United States.

ABSTRACT BODY:

Abstract Body: Introduction: Periodontal probing is a useful diagnostic tool to estimate the periodontal pocket depth and assess the status of periodontal disease, but is limited by systematic and random errors. Here, we used photoacoustic imaging in tandem with a food grade cuttlefish contrast agent to specifically measure pocket depths in swine models and then compared this to Williams probe.

Methods: The contrast agent was made of 2% (w/v) cornstarch and 5% (w/v) cuttlefish ink. Photoacoustic imaging used a Vevo LAZR imaging system (Visualsonics) at 40 MHz. Both photoacoustic and ultrasound image were collected before and after application of the contrast agent to a swine model (n=27 teeth). Spectral data was collected at both 680 and 800 nm to discriminate between the photoacoustic signal from stains and contrast agent. The pocket depths were measured on the sagittal view of the 3D images as well as with a Williams probe before photoacoustic imaging. In the maxilla, the pocket depths were recorded at four sites per tooth i.e. mesial, distal and two buccal locations below the anterior and posterior cusps of maxillary molar and fourth premolar. In the mandible, pocket depths were recorded mesial, distal, and at two lingual locations below the anterior and posterior cusps of the mandibular molar.

Results: The mean size of melanin nanoparticles were first shown to be pH stable (Fig. S1). The contrast agent had similar photoacoustic signal at 800 nm and 680 nm, but the signal from endogenous stains decreased 50% at 800 nm (Fig. 1). The photoacoustic signal of contrast agent in the pocket started from the gingival margin and extended along the root. We validated the photoacoustic measurements with a gold-standard Williams probe and Bland-Altman analysis. The Bland-Altman plots show that 97% of our samples fell within 1.96 standard deviations of the differences between the depths measured by photoacoustic imaging and the probe (95% confidence interval) at mesial, lingual and buccal, and distal locations. Small bias values of -0.04, +0.17, and -0.2 mm were identified at mesial, lingual and buccal, and distal locations, respectively; the 95% confidence intervals are plotted as well and all are < 1.0 mm (Fig. 1). The photoacoustic imaging approach also offered 0.01 mm precision and could cover the entire pocket versus the probe-based approach that is limited to only a few sites. The gingival thickness can also be precisely measured via the ultrasound mode data (Fig. S2).

Conclusion: This study demonstrated for the first time that pocket depths could be measured with photoacoustic imaging. The values we achieved with this novel technique agreed nicely with the gold-standard periodontal probe approach, but were more precise and covered all areas of the tooth. Future work will use models of periodontal disease as well as automated algorithms to collect and process the data.

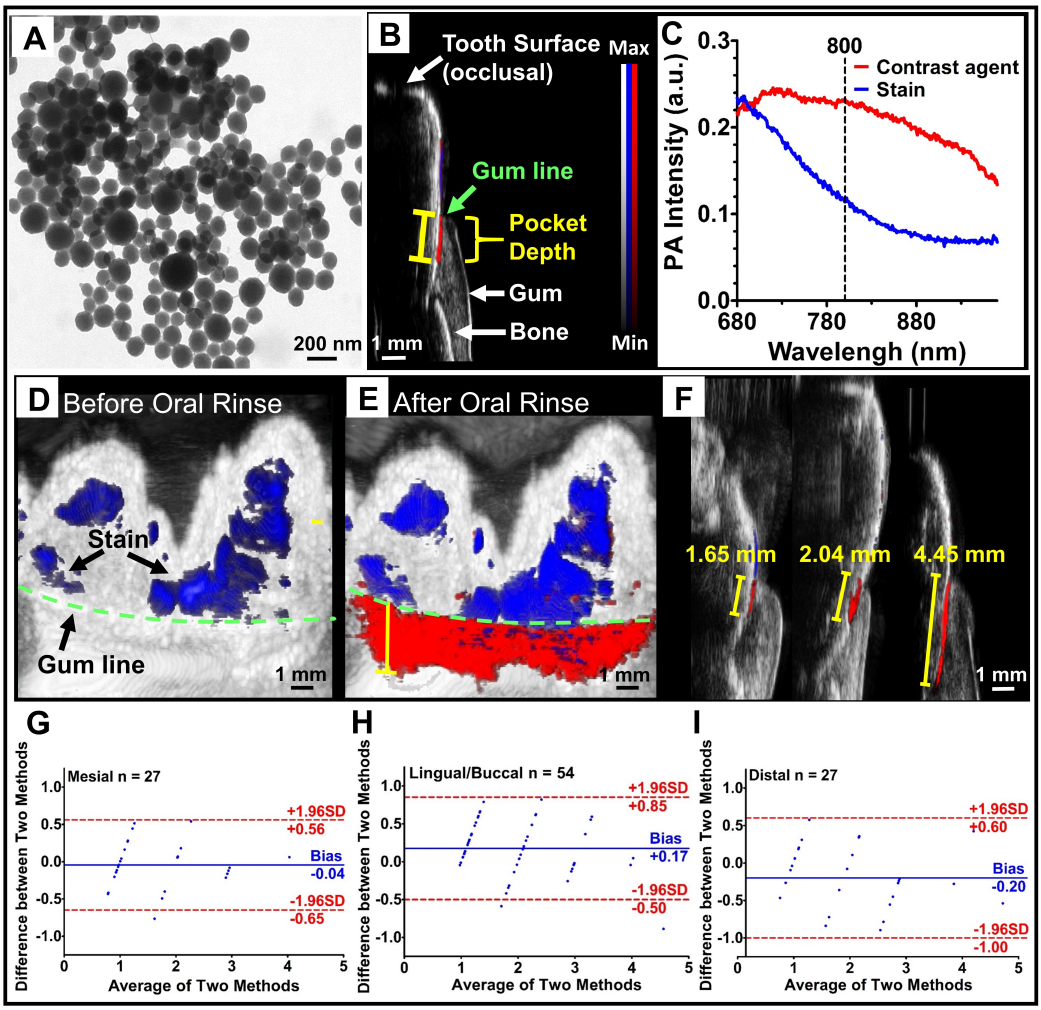

Figure 1. (A) TEM image illustrates spherical melanin nanoparticles in cuttlefish ink. (B) Sagittal view shows hard and soft dental tissues. Photoacoustic signal of the contrast agent in a pocket starts at the gingival margin and extends along the root. (C) The contrast agent and stain had similar signal at 680 nm, but the signal of the stain decreased ~50% at 800 nm. Photoacoustic/ultrasound images before (D) and after (E) contrast agent treatment. Blue color is the signal from stains, and red color is from contrast agents. Yellow bar represents pocket depth. Panel (F) contains representative images including small, medium and large pocket depths obtained via photoacoustic imaging. Bland-Altman plots compare the agreement between pocket depths measured by photoacoustic imaging and Williams probe at (G) mesial, (H) lingual/buccal and (I) distal locations of molars; 97% of samples fell within 95% confidence interval at mesial, lingual/buccal and distal locations. Bias values < 0.20 mm.

IMAGE CAPTION: **Figure 1.** (A) TEM image illustrates spherical melanin nanoparticles in cuttlefish ink. (B) Sagittal view shows hard and soft dental tissues. Photoacoustic signal of the contrast agent in a pocket starts at the gingival margin and extends along the root. (C) The contrast agent and stain had similar signal at 680 nm, but the signal of the stain decreased ~50% at 800 nm. Photoacoustic/ultrasound images before (D) and after (E) contrast agent treatment. Blue color is the signal from stains, and red color is from contrast agents. Yellow bar represents pocket depth. Panel (F) contains representative images including small, medium and large pocket depths obtained via photoacoustic imaging. Bland-Altman plots compare the agreement between pocket depths measured by photoacoustic imaging and Williams probe at (G) mesial, (H) lingual/buccal and (I) distal locations of molars; 97% of samples fell within 95% confidence interval at mesial, lingual/buccal and distal locations. Bias values < 0.20 mm.

SESSION TITLE: Late Breaking Session 09: Basic Biology - New Probe Concepts

CONTROL ID: 2798513

TITLE: Gas-generating nanoparticles for molecular ultrasound imaging

PRESENTER: In-Cheol Sun

AUTHORS (FIRST NAME, LAST NAME): In-Cheol Sun[1], Stanislav Y. Emelianov[1, 2]

INSTITUTIONS (ALL):

1. Wallace H. Coulter Department of Biomedical Engineering, Georgia Institute of Technology, Atlanta, GA, United States.
2. School of Electrical and Computer Engineering, Georgia Institute of Technology, Atlanta, GA, United States.

ABSTRACT BODY:

Abstract Body: Microbubbles (MBs) are often used as ultrasound imaging contrast agents. Given their micrometer size, MBs are confined in vascular compartments because they cannot escape through endothelial barriers and, as such, MBs are primarily useful in microcirculation or vascular-targeting molecule imaging. To penetrate outside of vasculature, the size of the contrast agent should be in the nanometer range. Reducing MBs to nanometer size does not help because nanobubbles have low echogenicity. Therefore, a desired contrast agent should consist of nanoparticles that are capable of escaping from vasculature, penetrating into tissue, and generating sufficient contrast once they reach the target site. We develop a novel contrast agent—plasmonic nanoparticles covered by azide compounds, capable of on-demand laser-induced gas generation via photolysis of azide functional groups (Figure 1a). The developed nanoparticles are small enough to escape vasculature and, upon laser activation, serve as ultrasound contrast agent due to photo-induced generation of nitrogen gas.

Gas-generating nanoparticles (ggNPs) were synthesized by reducing chloroauric acid with glycol chitosan at 70°C for 24 h and azide compounds were chemically conjugated to the nanoparticles with EDC/NHS. Spectrophotometer measurements confirmed the stability of ggNPs by showing the surface plasmon resonance peaks during the synthesis were at around 530 nm and, as expected, did not change significantly after surface modification. The changes in zeta-potential measurements were indicative of chemical conjugation and reflected the corresponding changes in gold nanoparticles after gas generation. TEM images of nanoparticles during the synthesis and after laser irradiation showed the expected morphology of nanoparticles and supported the zeta potential and spectrophotometry. Finally, DLS measurements indicated that the hydrodynamic size of the ggNPs was 35.72 ± 8.83 nm.

Following synthesis of ggNPs, the feasibility of ggNPs to serve as an ultrasound contrast agent was tested. Within a glass tube, upon a single laser pulse irradiation, the gas-generating nanoparticles produced large amount of gas bubbles visible with the naked eye (Figure 2b). Further, upon laser irradiation, ggNPs generated significant signal enhancement in US images obtained using the Vevo LAZR system (Figure 1c). The gas generation and, therefore, signal enhancement increases with the intensity of excitation laser energy.

The significance of this study is in the discovery of the photocatalytic function of gold nanoparticles in the photolysis of azide and subsequent gas generation. Among many applications of the gas-generating nanoparticles, we demonstrated their utility in contrast-enhanced ultrasound imaging. Indeed, measuring the ultrasound signal from nanoparticles smaller than 50 nm is unprecedented. The nanometer scale size and the on-demand contrast enhancement of ggNPs would enable molecular ultrasound imaging and diagnosis of various diseases that conventional microbubbles cannot detect. Furthermore, these particles can also be used for ultrasound-guided photoacoustic imaging, focused ultrasound, and photothermal therapy.

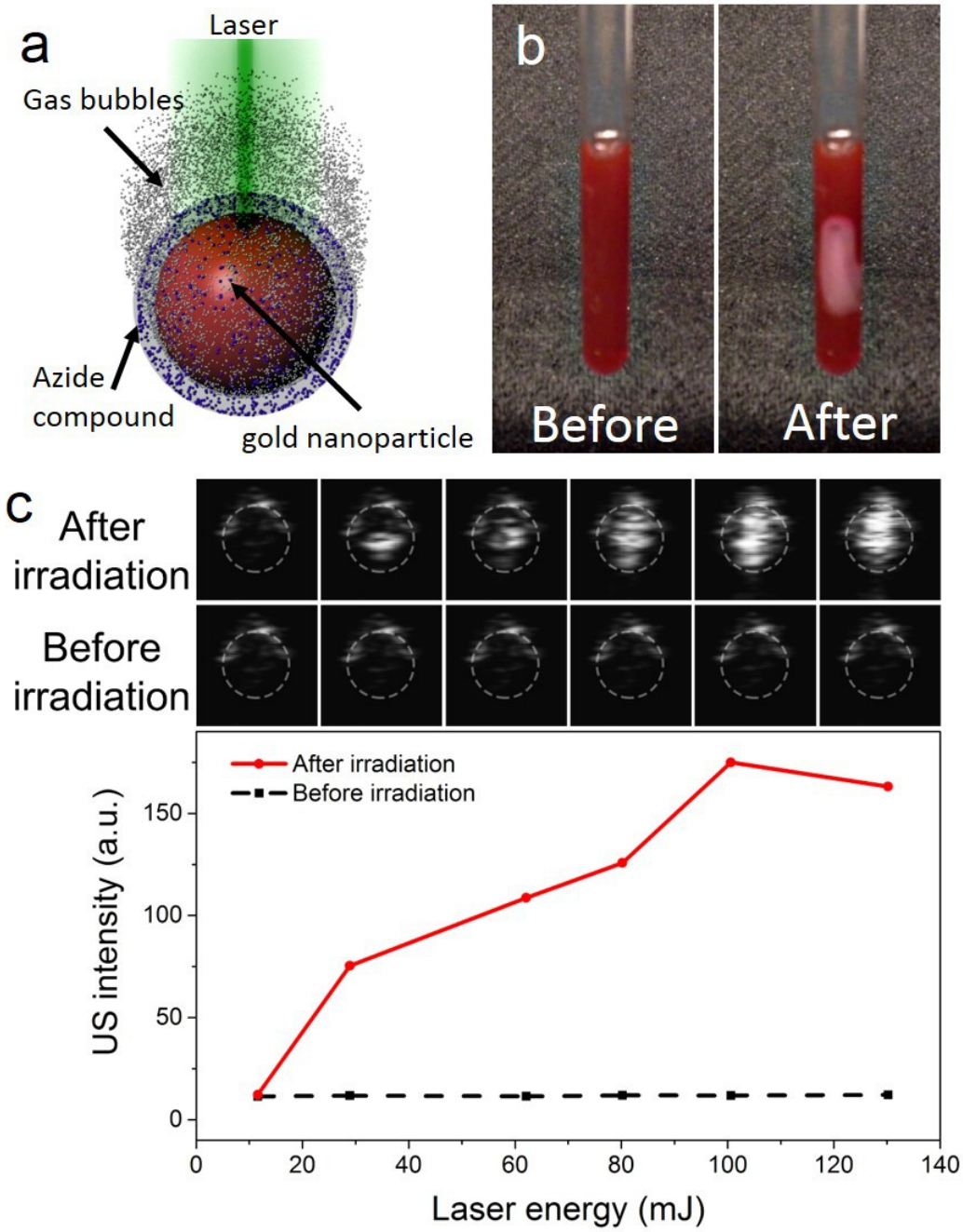

(a) A scheme of gas-generating nanoparticle. (b) Photograph of a glass tube with gas-generating nanoparticle colloid before (left) and after (right) irradiation irradiation by a single laser pulse. (c) Ultrasound images show correlation between excitation laser energy and ultrasound signal intensity.

IMAGE CAPTION: (a) A scheme of gas-generating nanoparticle. (b) Photograph of a glass tube with gas-generating nanoparticle colloid before (left) and after (right) irradiation irradiation by a single laser pulse. (c) Ultrasound images show correlation between excitation laser energy and ultrasound signal intensity.

SESSION TITLE: Late Breaking Session 09: Basic Biology - New Probe Concepts

CONTROL ID: 2805107

TITLE: Dark yet bright: Non-radiative and high performance optoacoustic nanoemulsions

PRESENTER: Sheryl Roberts

AUTHORS (FIRST NAME, LAST NAME): Sheryl Roberts[1], Chrysafis Andreou[1], Patrick L. Donabedian[1], Madhumitha Jayaraman[1], Crystal S. Choi[1], Carlos Perez-Medina[2], Willem Mulder[2], Jan Grimm[3], Moritz Kircher[1], Thomas Reiner[1]

INSTITUTIONS (ALL):

1. Radiology, Memorial Sloan Kettering Cancer Center, New York, NY, United States.
2. Translational and Molecular Imaging Institute, Department of Radiology, Mount Sinai School of Medicine, New York, NY, United States.
3. Molecular Pharmacology and Chemistry, Memorial Sloan Kettering Cancer Center, New York, NY, United States.

ABSTRACT BODY:

Abstract Body: Objectives: Optoacoustic imaging offers high spatial resolution and penetration depth well beyond the conventional optical techniques, advantages that could be favorable for a variety of applications. However, similar to PET imaging and optical fluorescence imaging, exogenous contrasts agents, known as sonophores, need to be developed for molecularly targeted optoacoustic imaging agents. Despite some contrast agents having been reported, more rational development of sonophores needs to be performed (1). Here, we systematically identified and evaluated twelve commercially available near infrared and highly absorbing dyes (690-900 nm) for multi-spectral optoacoustic tomography (MSOT).

Methods: We have formulated the near-infrared dyes in nanoemulsions (NE) adapting a previously described method (2). Size, zeta potential, stability, dye encapsulation, loading efficiency and photophysical properties were evaluated. Optical and optoacoustic intensities as a function of concentration using standardized approaches were measured. Using the optoacoustic signal intensities directly measured from the phantom experiments as our reference, a direct classical least-square (DCLS) approach was implemented (3). The mouse breast cancer cell line 4T1 was used for in-vivo mouse experiments. In-vivo MSOT imaging was performed before and after (24 h) intravenous injection of sonophores.

Results: The NEs had a mean effective diameter of 130-160 nm that form a more stable, biocompatible optoacoustic agent as compared to its native dye form. Comparisons made between absorbers reveal compelling evidence for higher optoacoustic signals with dark quenchers as opposed to weakly fluorescent dyes. Using the most promising near-infrared NE, we have confirmed in in vivo 4T1 tumor model experiments using MSOT that the dark quencher IRDyeQC-1 COOH is a highly potent tumor targeting candidate when encapsulated in a biocompatible (O/W) NE system. IRDye QC-1 carboxylic acid is non-fluorescent but exhibits a high extinction coefficient and broad near infrared UV/Vis and optoacoustic spectrum, all favorable characteristics of an optoacoustic agent.

Conclusions: MSOT in combination with our NE system enables non-invasive detection of tumors. Specifically, NE IRDye QC-1 offers a superior optoacoustic performance and detection compared to related near-infrared NEs. Using a library-screening approach, we have demonstrated that NEs when loaded with dark quenchers represent a flexible and new class of exogenous sonophores suitable for non-invasive pre-clinical optoacoustic imaging.

Acknowledgements: The authors thank the support of MSKCC's Animal Imaging Core, Radiochemistry & Molecular Imaging Probes Core and Molecular Cytology Facilities. This work was supported by NIH grants R01 HL125703 (T.R.), R01 CA204441 (T.R.), R01 CA214820 (T.R.), R21CA191679 (T.R.), P30 CA008748, NIH R01 EB017748 (M.F.K.) and K08 CA16396 (M.F.K.); M.F.K. is a Damon Runyon-Rachleff Innovator supported (in part) by the Damon Runyon Cancer Research Foundation (DRR-29-14).

References: (1)Weber, J. et al., Nature Methods, 2016 (2)Pérez-Medina, C. et al., Nat. Commun., 2016. (3)Tzoumas, S. et al., Nat. Commun., 2016

(No Image Selected)

SESSION TITLE: Late Breaking Session 09: Basic Biology - New Probe Concepts

CONTROL ID: 2805144

TITLE: Theranostic GNR@Ag Nanoparticles for Photoacoustic Imaging and Therapy of Bacterial Infections

PRESENTER: Taeho Kim

AUTHORS (FIRST NAME, LAST NAME): Taeho Kim[1], Qiangzhe Zhang[1], Liangfang Zhang[1], Jesse V. Jokerst[1, 2]

INSTITUTIONS (ALL):

1. NanoEngineering, University of California, San Diego (UCSD), La Jolla, CA, United States.
2. Radiology, University of California, San Diego (UCSD), La Jolla, CA, United States.

ABSTRACT BODY:

Abstract Body: Introduction: Silver nanoparticles (AgNPs) are broad-spectrum antibacterial agents via Ag^+ ions. However, there are no tools to effectively trigger the release of Ag^+ ions and monitor this release and subsequent antibacterial activities in vivo. Photoacoustic (PA) imaging is an emerging non-invasive imaging tool, and gold nanorods (GNRs) are an excellent contrast agent for PA imaging. Here, we developed a gold nanorod/silver (GNR@Ag) hybrid nanoparticle as a theranostic antibacterial/photoacoustic agent.

Methods: GNRs were synthesized via seed-mediated growth followed by a silver shell that could be cleaved via oxidative etching with 1 mM hexacyanoferrate (III). To examine bacterial inhibitions, E. coli and MRSA (OD=0.1, respectively) were suspended in LB (1 mL) after addition of GNR@Ag (2 µL, 1 mM Ag^+) and hexacyanoferrate (III) silver etchant (5 µL, 1 mM). The bacterial solutions were serially diluted and plated on LB agar plates; the number of colonies were counted after overnight incubation. To confirm the theranostic potential, GNR@Ag in 50% matrigel/PBS (200 µL) were injected subcutaneously into wild-type male mice (n=3) and imaged 4 h after i.p. injection of 1 mM of silver etchant (hexacyanoferrate (III) in PBS (500 µL)). PA imaging used a Visualsonics LAZR PA scanner with pulsed laser excitation at 800 nm.

Results: A schematic of the experiments and representative TEM images are shown in Fig. 1A. Ag-coated GNRs (GNR@Ag) were successfully synthesized (width: 10-15 nm, length: 50-60 nm, shell thickness of Ag: 10 nm) (Fig. 1A, left). Exposure to the mild oxidant ferricyanide ions ($[Fe(CN)_6]^{3-}$) selectively etches the AgNPs from GNR@Ag as confirmed by the TEM (Fig. 1A, right). The absorption intensity of the GNR@Ag has a peak at 450 nm with no absorption at 750 nm. However, the particles show strong absorption at 750 nm after etching (Fig. 1B). When co-treated with the etchant, the GNR@Ag exhibited a strong bactericidal efficacy similar to equivalent free Ag^+ ions ($AgNO_3$) (Fig. 1C). Ferricyanide oxidant alone had no significant bacterial killing, and GNR@Ag without the oxidant showed substantially less bactericidal efficacy. As a broad-spectrum antibacterial agent, the GNR@Ag killed >99.99% of both (Gram-positive) MRSA (32 µM Ag^+ equivalent) and (Gram-negative) E. coli (8 µM Ag^+ equivalent) (Fig. 1D). When the GNR@Ag particles were implanted subcutaneously into mice followed by etching, there was a 730% increase in the PA signal ($p<0.01$) comparing pre- (Fig. 1E bottom) and post- etching (Fig. 1E top). Similar to the PA spectrum of colloidal GNR@Ag (Fig. 1B), the in vivo PA spectrum recovered as the silver dissociates. This spectral data can distinguish the area being treated from the surrounding tissues (Fig. 1F).

Conclusions: This study presented a theranostic GNR@Ag nanoparticle system with biochemically-triggered antibacterial activity. These nanoparticles show a strong bactericidal activity and also facilitate non-invasive monitoring of localized release of Ag^+ ions with PA imaging. Follow-up studies are underway to determine the in vivo therapeutic efficacy of GNR@Ag nanoparticles against bacterial infections.

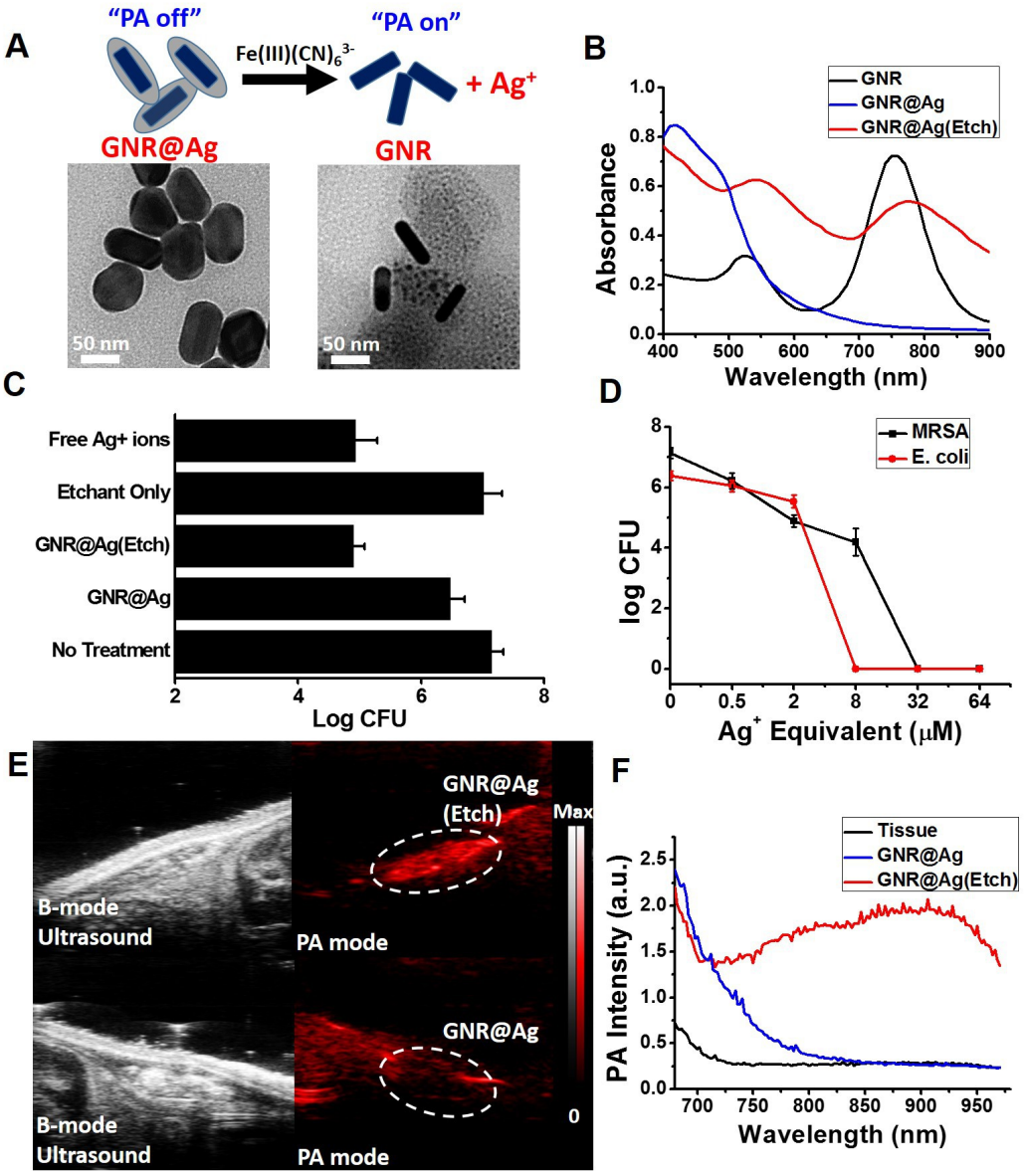

(A) A schematic of the experiments and representative TEM images of GNR@Ag and etched GNR@Ag. (B) UV/Visible absorbance of GNR, GNR@Ag, and etched GNR@Ag. (C) Bacterial counts showing the bactericidal action of etched GNR@Ag. *MRSA* (OD=0.1) was treated with GNR@Ag (2 μM Ag^+), GNR@Ag (2 μM Ag^+) with 1 mM $[Fe(CN)_6]^{3-}$, 1 mM $[Fe(CN)_6]^{3-}$ (etchant only), and a $AgNO_3$ solution (2 μM Ag^+; free Ag^+ ions), respectively. Error bars represent s.d. (D) The growth inhibition of Gram-positive *MRSA* and Gram-negative *E. coli*, evaluated by bacterial colony counts (log CFU *vs* concentration of Ag^+; error bars, s.d.). (E) B-mode ultrasound (gray scale) and photoacoustic (red) images of subcutaneously injected GNR@Ag (bottom) and GNR@Ag with successive addition of etchant (top). The spectral analysis (from Fig. E) of GNR@Ag (with and without AgNPs etching) and the background host tissues.

IMAGE CAPTION: (A) A schematic of the experiments and representative TEM images of GNR@Ag and etched GNR@Ag. (B) UV/Visible absorbance of GNR, GNR@Ag, and etched GNR@Ag. (C) Bacterial counts showing the bactericidal action of etched GNR@Ag. *MRSA* (OD=0.1) was treated with GNR@Ag (2 μM Ag^{+}), GNR@Ag (2 μM Ag^{+}) with 1 mM $[Fe(CN)_6]^{3-}$, 1 mM $[Fe(CN)_6]^{3-}$ (etchant only), and a $AgNO_3$ solution (2 μM Ag^{+}; free Ag^{+} ions), respectively. Error bars represent s.d. (D) The growth inhibition of Gram-positive *MRSA* and Gram-negative *E. coli*, evaluated by bacterial colony counts (log CFU *vs* concentration of Ag^{+}; error bars, s.d.). (E) B-mode ultrasound (gray scale) and photoacoustic (red) images of subcutaneously injected GNR@Ag (bottom) and GNR@Ag with successive addition of etchant (top). The spectral analysis (from Fig. E) of GNR@Ag (with and without AgNPs etching) and the background host tissues.

SESSION TITLE: Late Breaking Session 09: Basic Biology - New Probe Concepts

CONTROL ID: 2805172

TITLE: Ultra-small zwitterionic tantalum oxide nanoparticles for spectral photon-counting computed tomography

PRESENTER: Johoon Kim

AUTHORS (FIRST NAME, LAST NAME): Johoon Kim[1, 2], Daniel Bar-Ness[3, 4], Jessica C. Hsu[1, 2], Peter Chhour[1, 2], Philippe C. Douek[3, 4], David Cormode[1, 2]

INSTITUTIONS (ALL):

1. Department of Radiology, University of Pennsylvania, Philadelphia, PA, United States.
2. Department of Bioengineering, University of Pennsylvania, Philadelphia, PA, United States.
3. Radiology Department, Hospices Civils de Lyon, Lyon, France.
4. CREATIS, UMR CNRS 5220, Inserm U1044, University Lyon1 Claude Bernard, Lyon, France.

ABSTRACT BODY:

Abstract Body: INTRODUCTION: Tantalum has been demonstrated to be highly biocompatible heavy metal element with potential for use as a computed tomography (CT) contrast agent. Tantalum is more than ten-fold cheaper than gold and has been reported to produce contrast that is comparable to that of gold, making it an appealing element for nanoparticle contrast agent development. We have examined the potential of ultra-small tantalum oxide nanoparticles (TaONP) as contrast agent in photon-counting CT, a novel CT modality that has been garnering significant interest due to its ability to specifically detect contrast media, eliminating the need for pre-injection imaging and lowering radiation dose exposure.

METHODS AND RESULTS: Ultra-small (~5nm) TaONP were synthesized via a reverse micelle approach with tantalum(V) ethoxide, Igepal CO-520, sodium hydroxide, and cyclohexane. The resulting nanoparticles were capped with 2-(carbomethoxy)ethyltrimethoxysilane and 3-(trimethoxysilyl)propyl-N,N,N-trimethylammonium chloride for stability in PBS and biological media and were purified via centrifugation (Fig. A). The core size of the surface coated nanoparticles is 4.9 nm in diameter as determined from TEM (Fig. B). The TaONP were further characterized with DLS, which indicated a hydrodynamic diameter of 9.4 nm. Zeta potential measurements revealed the surface charge to be -9 mV (Fig. B). The biocompatibility of TaONP was evaluated with the MTS assay. Three cell lines – HepG2 (hepatocytes), SVEC4 (endothelial), and Renca (kidney epithelial) – were incubated with TaONP treated media for 8 hours. Cell viability was not reduced even at a dose of 1 mg/ml, indicating good biocompatibility (Fig. C). TaONP were also encapsulated in larger polyphosphazene nanoparticles in pursuit of developing a blood pool agent with prolonged circulation time (Fig. D). To evaluate the potential of TaONP as a multispectral CT contrast agent, a prototype spectral photon-counting scanner (Philips Healthcare, Haifa, Israel) was used to scan a range of concentrations of TaONP from 0 mg/ml to 12 mg/ml. Analysis of the phantom images shows comparable measurements between TaONP and gold chloride solutions in both attenuation rate and CNR (Fig. E). K-edge imaging of tantalum (k-edge = 67.4 keV) also demonstrate the tantalum discriminating capabilities of the scanner and linear correlation between the TaONP concentration and signal (Fig. F).

CONCLUSION: We have synthesized ultra-small, zwittorionic tantalum oxide nanoparticles. These nanoparticles are highly biocompatible with strong contrast generation in photon-counting CT scanner, demonstrating their potential as contrast agent in multispectral CT.

(No Image Selected)

SESSION TITLE: Poster Session 01

CONTROL ID: 2715231

TITLE: An Osteoadsorptive Fluorogenic Substrate of Cathepsin K for Imaging Osteoclast Activity and Migration

PRESENTER: Eric Richard

AUTHORS (FIRST NAME, LAST NAME): Eric T. Richard[1, 4], Kimberly Hui[1], Boris A. Kashemirov[1], Kenzo Morinaga[2], Akishige Hokugo[2, 3], Ichiro Nishimura[2], Charles E. McKenna[1]

INSTITUTIONS (ALL):

1. Chemistry, University of Southern California, Los Angeles, CA, United States.
2. Weintraub Center for Reconstructive Biotechnology, UCLA School of Dentistry, UCLA, Los Angeles, CA, United States.
3. Division of Plastic Surgery, David Geffen School of Medicine, UCLA, Los Angeles, CA, United States.
4. Center for Craniofacial Molecular Biology, University of Southern California, Los Angeles, CA, United States.

ABSTRACT BODY:

Abstract Body: Cathepsin K is a protease central to bone diseases including osteoporosis, osteonecrosis of the jaw, and arthritis [1, 2]. Expressed mainly in osteoclast cells, it degrades type I collagen during bone resorption. Molecular probes of cathepsin K activity in vivo and in vitro are valuable for understanding the enzyme's role in skeletal disorders as well as for studying the biology of osteoclasts. Commercially-available fluorogenic substrates of cathepsin K are employed for assays in vitro and as molecular probes for in vitro and in vivo imaging. Available probes have tissue half-lives of up to 1.5 days [3] and are not tissue specific in their uptake. In the case of cathepsin K imaging, uptake in bone is usually desired. Our group sought to extend tissue half-life and improve bone uptake by incorporating the 1,1-bisphosphonate moiety that is known to lead to strong bone binding. This property has been used previously to make targeted prodrugs [4] and imaging reagents [5, 6].

We report the synthesis of OFS-1, an osteoadsorptive fluorogenic substrate of cathepsin K and verification of its performance with enzyme cleavage experiments, in vitro osteoclast imaging, and ex vivo imaging of resorptive activity. This is the first report of a bone-targeted protease sensor. OFS-1 consists of a cleavable fluorophore-quencher pair linked by a cathepsin K peptide substrate and tethered to a bisphosphonate. The probe is cleaved by purified cathepsin K with K_{cat} = 0.2 ± 0.03 s^{-1} and K_m = 1.7 ± 0.2 μM (37 deg. C pH 5.5). Timelapse fluorescence microscopy of monocyte-derived human osteoclasts on a calcium phosphate substrate showed fluorescent labeling of the substrate in response to resorption. Osteoclast migration could be visualized as trails of increased fluorescence. This unique and striking observation is attributed to persistent binding of the activated probe. In a first-in-animal experiment, 5 nmol of OFS-1 was administered to mice. 3 d later a maxillary molar was extracted to stimulate a local increase in resorptive activity. 10 d after administration, increased imaging signal near the site of the extraction was observed. An "always on" control probe lacking the quencher labeled the entire maxilla, demonstrating that the increased fluorescence was due to probe activation, not simply increased uptake.

Unlike existing probes that are rapidly cleared in vivo, OFS-1 allows for monitoring bone resorption over the course of longer experiments with a single dose.

1. Novinec M, Lenarčič B (2013) Biological Chemistry 394:1163–1179.
2. Connor JR, LePage C, Swift BA, et al (2009) Osteoarthritis and Cartilage 17:1236–1243.
3. Kozloff KM, Quinti L, Patntirapong S, et al (2009) Bone 44:190–198.
4. Arns S, Gibe R, Moreau A, et al (2012) Bioorganic & Medicinal Chemistry 20:2131–2140.
5. Kashemirov BA, Bala JLF, Chen X, et al (2008) Bioconjugate Chem 19:2308–2310.
6. Sun S, Blazewska KM, Kadina AP, et al (2016) Bioconjugate Chem 27:329–340.

(No Image Selected)

SESSION TITLE: Poster Session 01

CONTROL ID: 2726454

TITLE: Development of HOPO analogues for conjugation to antibodies and positron emission tomography: synthesis and radiolabeling with Zr-89

PRESENTER: Mian Alauddin

AUTHORS (FIRST NAME, LAST NAME): Sandun Perera[3], Bhasker Radaram[1], David Piwnica-Worms[2], Mian M. Alauddin[1]

INSTITUTIONS (ALL):

1. Cancer Systems Imaging, UT MD Anderson Cancer Center, Houston, TX, United States.
2. Cancer Systems Imaging, University of Texas MD Anderson Cancer Center, Houston, TX, United States.
3. Moffits Cancer center, Tampa, FL, United States.

ABSTRACT BODY:

Abstract Body: Objectives: Zirconium-89 is attractive for use in antibody-based immuno-PET due to its half-life compatible with the biological half-life of antibodies. DFO is commonly used as a chelating agent for this purpose,[1] however, DFO-chelated ^{89}Zr can suffer from in vivo stability.[2] A new chelating agent, 3,4,3-(LI-1,2-HOPO) (HOPO), has demonstrated efficient binding of ^{89}Zr with high stability.[3] We have synthesized three analogues of HOPO that show higher in vitro stability with ^{89}Zr.

Methods: Synthesis of ligands: N-protected amino-alkyl iodides of three different carbon chain length were prepared and reacted with spermine. The mono-substituted spermine derivatives were reacted with HOPO acid chloride to get substituted spermine-HOPO derivatives. The protecting groups from the spermine-HOPO derivatives were removed by acid hydrolysis and the amino-alkyl-spermine-HOPO reacted with phenyl-di-isothiocyante to obtain p-SCN-phenyl-alkyl-spermine-HOPO.

Conjugation and radiolabeling: Chelating agents, p-SCN-phenyl-alkyl-spermine-HOPO, were conjugated with bovine serum albumin and one antibody, purified and the conjugated proteins were radiolabeled with ^{89}Zr-oxalate. After purification on a PD-10 column, the products were analysed and tested for in vitro stability.

Results: Reaction of spermine with N-protected amino-alkyl iodides produced mono-substituted spermine derivatives in 70-75% yields. Reaction between the monosubstituted spermine and HOPO acid chloride produced N-protected amino-alkyl spermine-HOPO in 25% yield. Hydrolysis of the protecting groups followed by reaction with phenyl-di-isothiocyanate produced the desired products in 58% yields, with an overall yield of 10%. Figure 1 depicts the scheme for synthesis of the C5-HOPO analogue.

Conclusion: Syntheses of p-SCN-phenyl-alkyl-spermine-HOPO with three different carbon chain lengths has been achieved in four steps with overall good yields. Initial radiolabeling and in vitro stability results suggest that these chelating agents may be highly useful for radiolabeling antibodies with Zr-89 and immuno-PET; further studies in tumor-bearing mice are warranted.

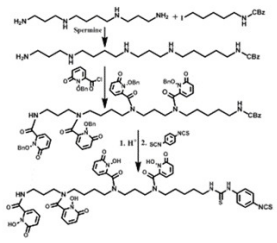
Spermine
1. H+
2. SCN
NCS

IMAGE CAPTION:

SESSION TITLE: Poster Session 01

CONTROL ID: 2726848

TITLE: Theranostic applications using biodegradable nitrogen-doped carbon nanodots

PRESENTER: Changho Lee

AUTHORS (FIRST NAME, LAST NAME): Changho Lee[1], Woosung Kwon[4], Songeun Beac[3], Donghyun Lee[2], Sei Kwang Hahn[3], Shi-Woo Rhee[4], Chulhong Kim[2]

INSTITUTIONS (ALL):

1. Department of Nuclear Medicine, Chonnam National University Medical School, Hwasun, Korea (the Republic of).
2. Creative IT Engineering, Pohang University of Science and Technology, Pohang, Korea (the Republic of).
3. Department of Materials and Science Engineering, Pohang University of Science and Technology (POSTECH), Seoul, Korea (the Republic of).
4. Department of Chemical and Biological Engineering, Sookmyung Women's University, Seoul, Korea (the Republic of).

ABSTRACT BODY:

Abstract Body: Multifunctional nanomaterials are attracting attention as a new class of theranostic contrast agent due to its various capabilities that contributed to the development of biomedical applications including molecular imaging, cancer treatment, drug delivery, etc. Light sensitive nanomaterials have played an important role in the theranostic field, especially based on the ability to generate heat by photon irradiation. Unfortunately, although these light sensitive nanomaterials have been extensively studied, photostability and safety issues remain, as critical drawbacks of practical clinical implementation and commercialization. In this research, a new type of theranostic agent, nitrogen-doped carbon nanodots (N-CNDs) were designed and fabricated by adjusting the nitrogen-doped content for strong light absorption in the near infrared region, superior photostability, and good biodegradability. Controlled N-CNDs enable to use as a sensitive photoacoustic imaging (PAI) agent as well as an excellent photothermal therapy (PTT) agent due to their strong optical absorption in specific wavelengths. To demonstrate the performance of N-CNDs as the theranostic agent, we conducted noninvasive in vivo/ex vivo PAI of sentinel lymph nodes in rat and tested PTT for removing melanoma cancer tumor with N-CNDs. Finally, the analyzed PAI result for bladder and a degradation test demonstrated N-CNDs’s biodegradation and renal clearance.

(No Image Selected)

SESSION TITLE: Poster Session 01

CONTROL ID: 2728213

TITLE: Real-time optical sectioning of ErbB2 expression in breast tumor xenografts

PRESENTER: Zhenghong Gao

AUTHORS (FIRST NAME, LAST NAME): Zhenghong Gao[1], Thomas Wang[1]

INSTITUTIONS (ALL):

1. University of Michigan, Ann Arbor, MI, United States.

ABSTRACT BODY:

Abstract Body: Real time detection of ERBB2 (ERBB2, or HER2/neu, or HER2) status in early breast cancer metastases may be used for image-guided surgery and tumor staging. We aim to demonstrate a NIR-labeled peptide that can be used to visualize ERBB2 overexpressed by human breast cancer cells. We labeled the target and scrambled (control) peptide with a NIR fluorophore (LiCOR IR800CW) to maximize tissue imaging depth. We assessed peptide pharmacokinetics in a mouse xenograft breast tumor model using photoacoustic imaging. We used a handheld dual axes confocal endomicroscope to collect real time optical sections in the vertical plane with a large field-of-view of 1000×430 mm^2. We demonstrate specific peptide binding to the surface of human breast cancer cells in vitro using confocal microscopy, competition, siRNA knockdown, and co-localization studies. Using photoacoustic imaging, we found the peak target-to-background ratio of 2.608±0.436 and 1.447±0.538 the target and control peptides, respectively, at 1 hour post-injection. Real time imaging with a handheld dual axes confocal endomicroscope revealed a peak target-to-background ratio of 2.556±0.899 and 1.619±0.522 for the target and control peptides, respectively. We have demonstrated a peptide that can be used to visualize ERBB2 expression in human breast tumors cells in vivo.

(No Image Selected)

SESSION TITLE: Poster Session 01

CONTROL ID: 2729305

TITLE: New Manganese-Based Chelates Enable Biochemically Responsive MRI Contrast With Exceptional Dynamic Range

PRESENTER: Eric Gale

AUTHORS (FIRST NAME, LAST NAME): Eric Gale[1], Huan Wang[1], Chloe M. Jones[1], Ian Ramsay[1], Christian T. Farrar[2], Peter Caravan[3]

INSTITUTIONS (ALL):

1. Radiology, MGH/ Harvard Medical School, Charlestown, MA, United States.
2. Radiology, Massachusetts General Hospital, Charlestown, MA, United States.
3. Radiology, Massachusetts General Hospital, Harvard Medical School, Charlestown, MA, United States.

ABSTRACT BODY:

Abstract Body: We developed new class of manganese (Mn) based, biochemically responsive MRI contrast agent that provides up to 9-fold relaxivity change in the presence of biochemical stimuli. This large and unprecedented relaxivity change is reversibly acheived via toggling between the Mn(3+) and Mn(2+) oxidation states. Switching between oxidation states is facilitated by a "Janus" ligand that isomerizes between binding modes that favor the Mn(3+) and Mn(2+) oxidation states. It is the only ligand that will support both oxidation states in biological media. Oxidation state change is mediated by peroxidase activity (oxidation) and cysteine (reduction). We report the synthesis and biophysical characterization of the new biochemically responsive agents, and structure-activity relationships dictating agent reactivity.

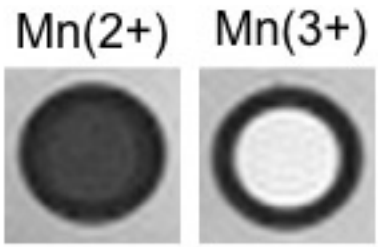
Mn(2+)
Mn(3+)

IMAGE CAPTION:

SESSION TITLE: Poster Session 01

CONTROL ID: 2731937

TITLE: Synthesis and evaluation of ^{68}Ga-labelled DOTA-6′′-deoxy-6′′-maltotrioseamine as a PET tracer for imaging bacterial infection

PRESENTER: Mohammad Namavari

AUTHORS (FIRST NAME, LAST NAME): Mohammad Namavari[1], Gayatri Gowrishankar[1], Ananth Srinivasan[1], Sanjiv S. Gambhir[1]

INSTITUTIONS (ALL):

1. Radiology, Stanford University, Stanford, CA, United States.

ABSTRACT BODY:

Abstract Body: Purpose: To test the possibility of using ^{68}Ga-labelled maltotriose as an imaging agent for bacterial infections, we have synthesized ^{68}Ga-labelled DOTA-6′′-deoxy-6′′-maltotrioseamine. The goal of this study is to use a ^{68}Ga-labelled DOTA-6′′-deoxy-6′′-maltotrioseamine as positron emission tomography (PET) tracer to visualize and monitor the therapeutic response to bacterial infections. There have been several publications on the use of ^{18}F-labelled maltose and maltohexose as PET probes for imaging bacterial infections (Gowshankar et al, PLOS one 2014 and Ning et al, Angew. Chem. Int. 2014) based on specificity of the maltose transporter only being present in bacteria not mammalian cells. We have designed, successfully prepared and evaluated [^{68}Ga] DOTA-6′′-deoxy-6′′-maltotrioseamine as a bacterial infection PET imaging agent.

Method: [^{68}Ga] DOTA-6′′-deoxy-6-′′maltotrioseamine (2) was synthesized from DOTA-6′′-deoxy-6′′- amino-maltotriose (1) and $^{68}GaCl_3$). Escherichia-coli uptake was evaluated in bacterial culture.

Results: We have successfully synthesized [^{68}Ga] DOTA-6′′-deoxy-6′′-maltotrioseamine in 76 % radiochemical yield (decay corrected) with 96 % chemical and radio-chemical purities with specific activity of 227 mCi/mg. Total synthesis time was 75 min. Preliminary bacteria uptake experiments showed that E-coli accumi\ulated [^{68}Ga] DOTA-6′′-deoxy-6′′-maltotrioseamine. However, competition assay indicated that the accumulation was not blocked by co-incubation with 1 mM of cold maltose blocking, (Fig 1), the natural substrate of the maltose transporter. This observation is shows that ^{68}Ga-labelled DOTA-6′′-deoxy-maltotrioseamine is not being recognized and transported by the bacteria in a manner similar to maltose. Likely, the negative charges on the surface of the bacteria membrane attached to the positively charges of ^{68}Ga and showed the oserved results. Also, the biodistribution in mice (N=3) showed that tracer appeared to be retained in the infected muscle, this could be because the positive charge of ^{68}Ga adheres to the negative charge of the bacterial membrane. Similar observations for ^{68}Ga-maltotriose were noticed.

Conclusion: We have synthesized ^{68}Ga- DOTA-6′′-deoxy-6′′-maltotrioseamine by a direct reaction of a DOTA protected 6′′-maltotriosamine precursor with [^{68}Ga] $GaCl_3$. Preliminary bacterial uptake and competition assay experiments in E-coli suggest that ^{68}Ga-labelled DOTA-6′′-deoxy-maltotrioseamine is not being recognized by the maltose transporter and is therefore not transported in to the bacteria.

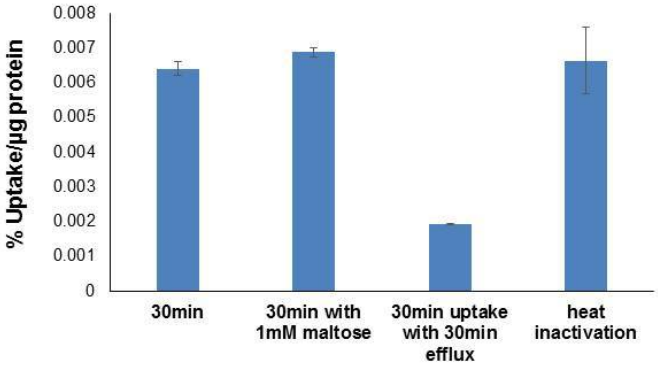

Fig 1. ^{68}Ga-maltotriose bacteria uptake:
Uptake could not be blocked by co-incubation of maltose.
Efflux showed 30% retention in bacterial cells.
Heat inactivation does not abolish uptake of ^{68}Ga-maltotriose indicating that the tracer is sticking to Bactria non-specifically.

IMAGE CAPTION:

SESSION TITLE: Poster Session 01

CONTROL ID: 2732605

TITLE: De novo design of a genetically-encoded T_2-relaxive MRI reporter protein

PRESENTER: Molly Sheehan

AUTHORS (FIRST NAME, LAST NAME): Molly M. Sheehan[1], Brian Y. Chow[1]

INSTITUTIONS (ALL):

1. Bioengineering, University of Pennsylvania, Philadelphia, PA, United States.

ABSTRACT BODY:

Abstract Body: We have previously established de novo far-red fluorescent proteins (dFP), a new class of optogenetic tools created by first principles of protein design, which outperform bacteriophytochrome-derived fluorescent proteins in cellular brightness in mammalian cells. The biliverdin-binding dFP scaffold, a de novo four helix bundle, is a robust platform that can be remodeled to bind a variety of cofactors for other functionalities. To acquire whole-body images using genetically-encoded tags, we accordingly re-engineered the scaffold to create a paramagnetic heme center and facilitate rapid water exchange to enhance T_2* relaxation for magnetic resonance imaging (MRI). Thus, here we present a mammalian cell-expressible and genetically-encoded de novo magnetic resonance contrast protein (dMP). Previous genetically-encoded heme-binding proteins, including natural hemoglobin variants[1], have poor heme affinity, so lose heme, leading to toxic oxidative damage. The de novo platform here was designed to have a tight heme-binding pocket with a globin-like bis-histidine ligation; it has a heme b (protoporphryn IX) K_D of <200pM, better than previously described de novo scaffolds[2]. This affinity resulted in superior heme retention, even compared to hemoglobin, retaining heme for weeks at 37°C.

The dMP exterior was engineered to have extensive intra-helical hydrogen-bonding to both increase its protein stability and inter-helical dynamics. dMP was highly thermostable (T_m>95°C), without sacrificing the necessary dynamics for rapid water exchange, enabled by the movement between helices. Water exchange improves potential relaxivity by exposing the paramagnetic heme center to more water. The protons closest to the heme center, whether protein protons or structured waters, become dephased due to the varied magnetic field, and then exchange hydrogens or placement with bulk water, bringing in new protons to be consequently dephased. This high level of dephasing will result in a signal that cannot be rephased with the next 180° pulse, and thus the loss of T_2 signal arises from T_2* contrast enhancement.

Such MR contrast enhancement requires a highly paramagnetic heme center. A high spin Fe^{3+} heme center was rationally engineered in a pentacoordinate-ligated form with low ligand field splitting energy (LFSE) and 5 unpaired electrons. dMP had a T_2* relaxivity of 3.4 $mM^{-1}s^{-1w}$ with no significant T_1 relaxivity observed. T_2* contrast enhancement was evident in a tube bundle titration at all concentrations over 80μM protein in PBS. While these high concentrations may not be achievable in mammalian cells with endogenous heme binding to dMPs, which express well in mammalian cells, further engineering of cofactor binding is underway. Ongoing work includes dMPs engineered for improved relaxivity through kinetically enhanced dephasing of exchanged waters, and the optical and NMR spectroscopy to mechanistically establish a visit-based model of T_2* shortening.

1. Vandegriff, K. D. et al. Biochem J 399, 463 (2006).

2. Farid, T. A. et al. Nature Chemical Biology 9, 826–833 (2013).

(No Image Selected)

SESSION TITLE: Poster Session 01

CONTROL ID: 2733916

TITLE: Detection of DT-diaphorase Enzyme with a ParaCEST MRI Contrast Agent

PRESENTER: Iman Daryaei

AUTHORS (FIRST NAME, LAST NAME): Iman Daryaei[1], Kyle Jones[3], Mark D. Pagel[2]

INSTITUTIONS (ALL):

1. Chemistry and Biochemistry, University of Arizona, Tucson, AZ, United States.
2. Medical Imaging, University of Arizona, Tucson, AZ, United States.
3. Biomedical Imaging, University of Arizona, Tucson, AZ, United States.

ABSTRACT BODY:

Abstract Body: Introduction: Yb-DO3A-oAA have been reported as a paramagnetic CEST (paraCEST) agent that produces a CEST signal from a proton of the amide functional group connecting the aniline ring to the DO3A chelate, and a second CEST signal from the protons of the amine group on the aniline ring.[1] The reaction of Yb-DO3A-oAA with nitric oxide created a larger ligand that caused conformational changes in the agent, which resulted in a loss of one or both CEST signals.[2]

We hypothesized that attaching a larger ligand with a quinone functional group to the aniline ring of the paraCEST agent would eliminate the CEST signal from the protons of the amine group of the aniline ring. Consequently, reduction of the quinone functional group to a hydroquinone group, followed by intramolecular disassembly, would release the CEST agent and produce a CEST signal from the amine group (Scheme 1). We designed this strategy to detect DT-diaphorase enzyme (DTD) that is a biomarker for hypoxic tumors.[3]

Methods: The cloaked paraCEST agent was synthesized in 8 steps with an overall isolated yield of 6%. Activation of the probe was monitored in different combinations of the cloaked agent, DTD enzyme, β-nicotinamide adenine dinucleotide (NADH), and glutathione (GSH) under anaerobic and aerobic conditions at 37°C. The CEST signals were measured at clinically relevant saturation conditions of 6 uT for 4 seconds using a 7 T Bruker Biospec MRI scanner. CEST spectra were fit with Lorentzian line shapes.

Results: Only one CEST signal at -9 ppm was observed from the solution of the cloaked CEST agent in PBS. Incubation of the cloaked CEST agent with DTD enzyme, NADH, and GSH resulted in detecting a CEST signal at +9 ppm, which indicated release of the CEST agent (Figure 1). The additional CEST studies and mass spectroscopy analyses confirmed that Yb-DO3A-oAA was released from the cloaked CEST agent only with DTD, NADH, and GSH. No signal at +9 ppm from the released CEST agent was observed when NADH or GSH were not added to the solution. Analysis of the enzyme reaction under anaerobic condition showed the same results, including a reaction with no GSH.

Conclusion: We have developed a new responsive CEST MRI agent that detects DTD enzyme activity. The agent can change CEST signals in the presence of DTD, NADH and GSH. In addition, the enzyme is stable under reducing conditions, which may aid in detecting hypoxic tumors.

References:

V. R. Sheth, Y. Li, L. Q. Chen, C. M. Howison, C. A. Flask, and M. D. Pagel, Magn. Reson. Med. 2012, 67, 760-768.
G. Liu, Y. Li, and M. D. Pagel, Magn. Reson. Med. 2007, 58, 1249-1256.
Ma, Y., J. Kong, G. Yan, X. Ren, D. Jin, T. Jin, L. Lin, Z. Lin, BMC Cancer 2014, 14, 414-423.

(No Image Selected)

SESSION TITLE: Poster Session 01

CONTROL ID: 2733990

TITLE: Fluorescent NV-Center Nanodiamonds for In Vitro and In Vivo Imaging Applications.

PRESENTER: Arfaan Rampersaud

AUTHORS (FIRST NAME, LAST NAME): Isaac Rampersaud[1], Adam Dalis[2], David Albertson[1], Charles Moritz[1], Timothy Dumm[2], Arfaan A. Rampersaud[1]

INSTITUTIONS (ALL):

1. Columbus NanoWorks, Columbus, OH, United States.
2. Sandvik-Hyperion, Columbus, OH, United States.

ABSTRACT BODY:

Abstract Body: Fluorescent nanodiamonds are a next-generation platform of nanomaterials for biomedical imaging with distinct advantages over existing reagents. Unlike quantum dots, they are biocompatible, do not exhibit intermittent fluorescence emission (blinking), and their fluorescence does not depend on their size. Unlike organic dyes, fluorescent nanodiamonds are infinitely photostable, (even under intense laser excitation), and have very little overlap between their excitation and emission wavelengths, (large Stokes shift). Nanodiamond themselves are stable to nearly all environmental extremes, and have excellent potential for surface modification.

Nanodiamonds that contain nitrogen-vacancy (NV) centers produce non-quenching fluorescence in the near-infrared region, following excitation with a green laser light. An NV-center is essentially a molecular impurity within the diamond crystalline lattice in which a nitrogen atom is adjacent to a carbon vacancy. We prepare nanodiamonds containing NV-centers, (hereafter FNDs), by electron irradiation of micron-sized diamonds to first create vacancy defects. Irradiated diamonds are then annealed to mobilize the vacancies close to the nitrogen atoms. This process creates hundreds, if not thousands, of NV-centers within a diamond crystal and accounts for the brightness of the particles. The diamonds are then milled to the nanoscale and thoroughly cleaned.

FNDs can be repeatedly excited over long periods of time without loss in fluorescence. Thus, they are useful for real-time imaging of cellular processes, such as in-vivo and in-vitro cell tracking. They have also been used for related bio-imaging applications, such as fiducial markers during long term super resolution microscopy studies. Additionally, FNDs can act as remarkable, optically readable sensors to measure physical properties with high precision, including magnetic fields, electric fields, temperature, and ion concentrations. For imaging, we have taken advantage of their NIR fluorescence to image FNDs through approximately 1 cm of chicken breast using a CRI Maestro in-vivo fluorescent imaging device.

Unconjugated FNDs can be readily taken up by a macrophage cell line, which can be cultured for several days with no toxic effects. We have also developed several routes for attaching peptides, proteins, and small molecules to the FND surface for targeting studies. Briefly, the nanodiamonds are conjugated with short-chain polyethylene glycol (PEG) having terminal alcohol groups. These are then converted into reactive NHS-esters, and used for bioconjugation reactions. For most antibodies, conjugation can be confirmed by ELISA assays as well as a catalytic assay that uses secondary antibody-Horse Radish Peroxidase (HRP) conjugate.

Figure 1. Brightfield (left) and fluorescence images (right) of colloidal, *NV-center* nanodiamonds. Their fluorescence was collected using a 532nm laser and 650 nm long-pass filter. Images were captured on a Maestro *in vivo* imaging system.

IMAGE CAPTION:

SESSION TITLE: Poster Session 01

CONTROL ID: 2734252

TITLE: Fluorescence Fingerprinting of Aldehydes for Blood-based Detection of Disease & Injury

PRESENTER: Adam Shuhendler

AUTHORS (FIRST NAME, LAST NAME): Caitlin Lazurko[3], Scott Foster[1], Mojmir Suchy[4], Adam Shuhendler[1, 2]

INSTITUTIONS (ALL):

1. Chemistry and Biomolecular Sciences, University of Ottawa, Ottawa, ON, Canada.
2. University of Ottawa Heart Institute, Ottawa, ON, Canada.
3. Chemistry & Biomolecular Sciences, University of Ottawa, Ottawa, ON, Canada.
4. Chemistry & Biomolecular Sciences, University of Ottawa, Ottawa, ON, Canada.

ABSTRACT BODY:

Abstract Body: The production of reactive carbonyls, especially aldehydes, is a nearly ubiquitous response to cell stress induced by disease or injury[1]. Aldehydes have previously been shown to possess the potential to serve as early diagnostic biomarkers for chemical or physical stress-associated conditions: malondialdehyde as a marker for positive tumor response to chemotherapy[2], 3-aminopropanal and malondialdehyde for severity of brain damage following trauma or concussion[3], 3-aminopropanal as a marker of brain ischemia-reperfusion injury[4], catecholamine-aldehydes (e.g. DOPAL) in Parkinson's Disease etiology[5], and 4-hydroxynonenal as a marker of neuronal stress across a range of neurodegenerative diseases[6]. While these aldehydes have shown significant elevations in human body fluids, including blood, their detection often requires laborious sample preparation or advanced analytical techniques (e.g. mass spectrometry). In order to realize the diagnostic potential of endogenously generated aldehydes for the diagnosis of a range of diseases and injuries, a rapid and simple point-of-care method of aldehyde identification is needed.

We have developed carboxylic acid or ester-modified N-amino anthranilates (NA[3]) towards a simplified method for aldehyde identification in body fluids. These small molecule hydrazine-derived fluorophores react rapidly (within seconds) ex vivo at room temperature in extracted serum and whole blood, simplifying the derivatization process. The carboxylic acid-based NA[3] was applied for the specific detection of malondialdehyde, as the unique structure of this aldehyde resulted in the formation of a pyrazole ring and 'turn-on' of the NA[3] fluorescence (Fig. 1A), which was not achieved by other endogenous reactive carbonyls. The initial hydrazone formation with malondialdehyde and subsequent cyclization to form the pyrazole ring was monitored by both fluorescence (Fig. 1B) and ^{1}H-NMR. The ester-based NA[3] showed rapid (within ca.1 second at room temperature) and significant spectral changes upon hydrazone formation with a variety of endogenous carbonyls (Fig. 1C). The resulting hydrazones, including those derived from 3-aminopropanal, acetaldehyde, and crotonaldehyde, displayed alterations in their fluorescence excitation-emission matrices (EEM) that were specific to the reactive carbonyl bound (Fig. 1D). These three-dimensional spectra provide a fluorescence fingerprint through which aldehyde identification can be achieved.

Utilizing a simple anthranilic acid-based scaffold present in carboxylic acid or ester-modified NA[3], we are developing a rapid and simple method for reactive carbonyl derivatization and identification. Presented methodology does not require the use of complex analytical instrumentation (e. g. mass spectrometer) and is amenable to point-of-care implementation even in a modest clinical setting. By targeting aldehyde products of endogenous stress processes, our probe chemistry and fluorescence fingerprinting technique could be applied for the expedient monitoring of successful cancer chemotherapy, the detection of neurodegenerative disease onset, and the prognosis following traumatic brain injury.

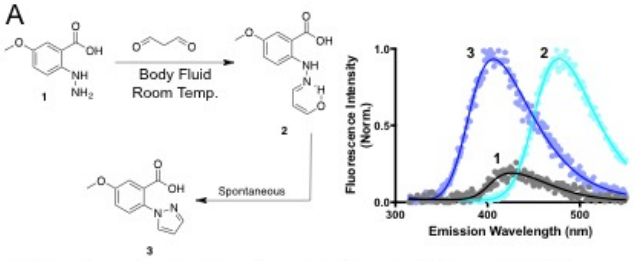

1-A. **N-amino anthranilic acid reacts rapidly with malondialdehyde (MDA) to form a fluorescent pyrazole.** *Left:* Proposed 2-step reaction scheme for the formation of the MDA-derived pyrazole (**3**) from 5-methoxy-N-amino anthranilic acid (**1**). *Right:* Emission spectra of the probe (**1**), the short-lived hydrazone (**2**), and the pyrazole product (**3**).

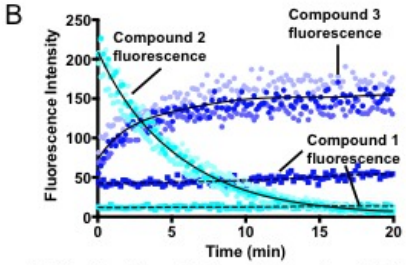

1-B. **Fluorimetric monitoring of the trapping of MDA by the N-amino anthranilic acid probe.** The rapid conversion of **2** to **3** is observed over 10 min at room temperature.

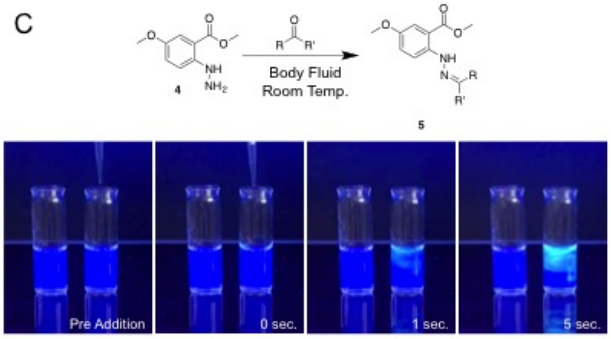

1-C. **N-amino anthranilate methyl ester reacts rapidly with endogenous reactive carbonyls.** *Top:* The reaction of 5-methoxy-N-amino anthranilate methyl ester (**4**) with a reactive carbonyl results in the formation of the hydrazone (**5**) under physiological conditions at room temperature. *Bottom:* The formation of the acetaldehyde-derived hydrazone is demonstrated through time-lapse imaging, with hydrazone formation within 1 second of aldehyde addition to a PBS solution of **4**.

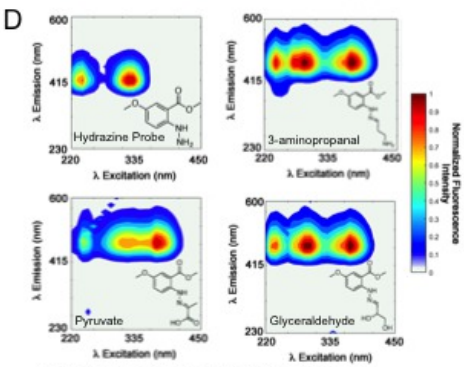

1-D. **Fluorescent fingerprinting of endogenous reactive carbonyls.** Excitation-emission matrices are shown for stress-related (3-aminopropanal) and metabolic (glyceraldehyde, pyruvate) reactive carbonyls.

References: [1] O'Brien PJ et al., Critical Reviews in Toxicology (2005) 35:609-62.
[2] Kumaraguruparan R et al., Clinical Biochemistry (2005) 38:154-58; Amin KA, et al., Journal of Breast Cancer (2012) 15:306-12; Panis C et al., Breast Cancer Research and Treatment (2012) 133:89-97. [3] Wang H-C et al., World Neurosurgery (2016) 87:463-70; Lorente L et al., Journal of Neurotrauma (2015) 32:1-6; Halstrom A et al., Journal of Clinical Neuroscience (2017) 35:104-8.
[4] Wood PA et al., Brain Research (2006) 1122:184-90;Ivanova S. et al., Journal of Experimental Medicine (1998) 188:327-40. [5] Anderson DG et al., Chemical Research in Toxicology (2016) 29:1098-1107; Wood PA et al., Brain Research (2007) 1145:150-6. [6] Di Domenico F et al., Free Radical Biology and Medicine (2016) In Press.

IMAGE CAPTION: References: [1] O'Brien PJ et al., Critical Reviews in Toxicology (2005) 35:609-62.
[2] Kumaraguruparan R et al., Clinical Biochemistry (2005) 38:154-58; Amin KA, et al., Journal of Breast Cancer (2012) 15:306-12; Panis C et al., Breast Cancer Research and Treatment (2012) 133:89-97. [3] Wang H-C et al., World Neurosurgery (2016) 87:463-70; Lorente L et al., Journal of Neurotrauma (2015) 32:1-6; Halstrom A et al., Journal of Clinical Neuroscience (2017) 35:104-8.
[4] Wood PA et al., Brain Research (2006) 1122:184-90;Ivanova S. et al., Journal of Experimental Medicine (1998) 188:327-40. [5] Anderson DG et al., Chemical Research in Toxicology (2016) 29:1098-1107; Wood PA et al., Brain Research (2007) 1145:150-6. [6] Di Domenico F et al., Free Radical Biology and Medicine (2016) In Press.

SESSION TITLE: Poster Session 01

CONTROL ID: 2734337

TITLE: Selectively Targeting M2 Tumor Associate Macrophages by Mannose Conjugated Anti-Biofouling Magnetic Nanoprobes

PRESENTER: Yuancheng Li

AUTHORS (FIRST NAME, LAST NAME): Yuancheng Li[1], Hui Wu[1], yaolin Xu[3], Lily Yang[2], Hui Mao[1]

INSTITUTIONS (ALL):

1. Radiology and Imaging Sciences, Emory University, Atlanta, GA, United States.
2. Surgery, Emory University, Atlanta, GA, United States.
3. Emory University School of Medicine, Atlanta, GA, United States.

ABSTRACT BODY:

Abstract Body: Macrophages play many key roles in host defense as a part of the innate immune system. Increasing evidence has shown that tumor associated macrophages (TAMs, macrophages that infiltrate the tumor stroma) can promote tumor growth.[1] TAMs are also found to be associated with tumor hypoxia, chemo-resistance, and survival rate.[2] TAMs are classified into two major phenotypes: pro-inflammatory M1, which is believed to inhibit tumor growth,[3] and anti-inflammatory M2, which widely distributes in tumor and is responsible for tumor growth.[1] Hence targeted imaging of the subtype of macrophages with specific phenotype is of great interest in understanding and treating cancers, especially with cancer immunotherapies, as well as a broad range of diseases that associate with immune responses, including infectious diseases and cardiovascular diseases.

Magnetic iron oxide nanoparticles (IONPs) are known to be endocytosed by macrophages, and thus have been widely used to develop MRI based molecular imaging probes or fluorescent dye carriers for imaging and tracking macrophages and its activities in vivo. Given their intrinsic physical and imaging properties of nanoparticle probes and their unique interactions with biological systems, the applications of IONPs in imaging TAMs with specific phenotype have received increased attention but been limited by the lack of capability in differentiating M1 and M2 TAMs. IONPs with anti-biofouling coating have been developed to inhibit the non-specific macrophage uptake and formation of protein corona on the surface that may attenuate targeting efficacy.[4] The anti-biofouling IONPs have demonstrated highly specific targeting to selected cancer cells only when the targeting ligands were conjugated. By incorporating mannose as targeting ligand, the developed nanoprobes have shown their capability to specifically target M2 cells in vitro (generated by stimulating Raw264.7 macrophages with interleukin-4), while no M1 cell (generated by stimulating Raw264.7 macrophages with lipopolysaccharide) targeting and little Raw264.7 macrophage targeting by the mannose conjugated anti-biofouling IONPs were observed. The ex vivo immunostaining of the tumor tissue using mannose conjugated anti-biofouling IONPs labeled with fluorescein isothiocyanate (FITC) against M2 TAMs exhibited high consistency with the result from IHC staining using CD206 antibodies (against mannose receptors on M2 TAM surface). For in vivo study, the mannose conjugated IONPs labeled with FITC were injection intravenously to the mice bearing xenograft tumor before tumors were taken for the immunostaining against M2 TAMs. Consistent distributions of M2 cells and mannose conjugated IONPs were observed within tumor. In conclusion, we demonstrated that the developed “anti-fouling” coating polymer and coated nanoparticles allow for selectively targeting the specific subtype of TAMs, which could be applied for imaging immunotherapy responses in the future.

References: [1] Weissleder R. et al., Nat. Mater. 2014, 13, 125. [2] Song M. et al., ACS Nano 2016, 10, 633. [3] Zanganeh S. et al., Nat. Nanotechnol. 2016, 11, 986. [4] Li Y. et al., J. Mater. Chem. B 2015, 3, 3591.

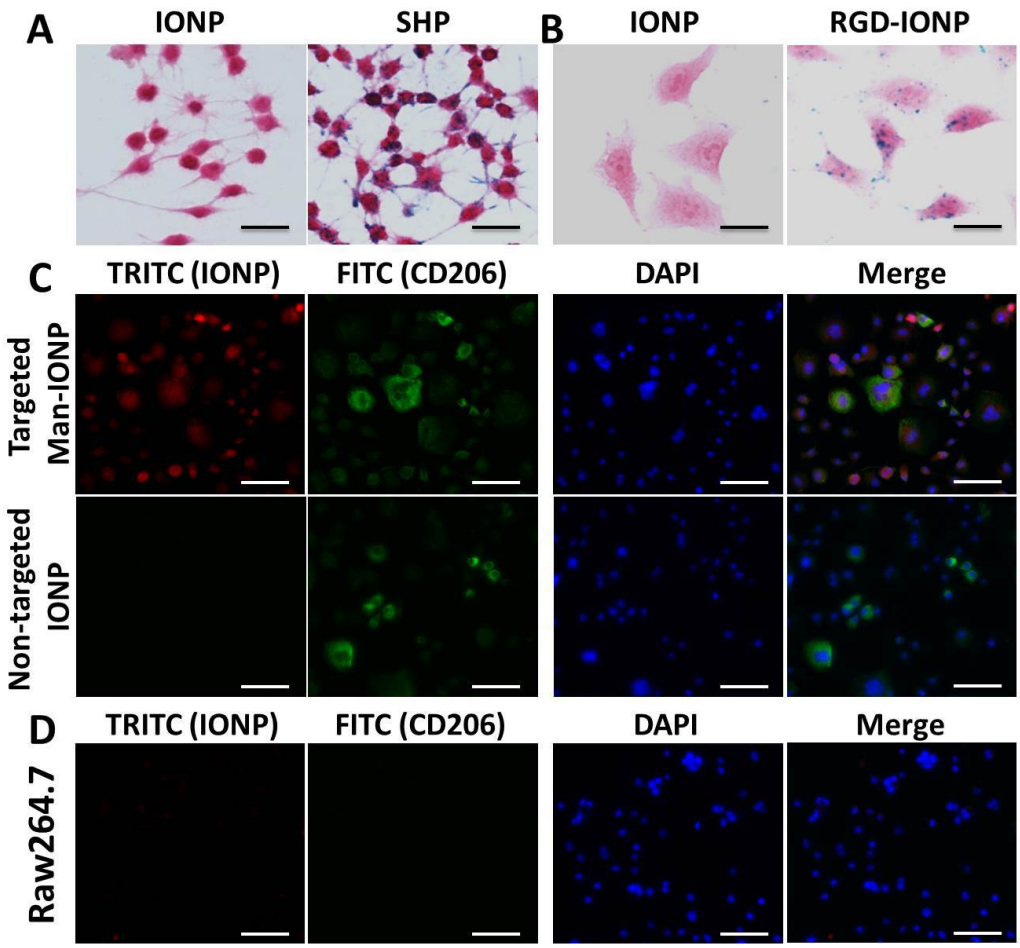

Prussian blue stained images of (A) anti-biofouling IONPs and commercial SHP uptake by Raw264.7 macrophage at Fe concentrations of 0.2 and 0.05 mg/mL, respectively; (B) anti-biofouling IONPs and RGD-conjugated IONPs uptake by U87MG glioblastoma cells. Fluorescence images of (C) M2 cells targeted by mannose conjugated anti-biofouling IONPs and non-targeted IONPs; (D) Raw264.7 macrophages targeted by mannose conjugated anti-biofouling IONPs and non-targeted IONPs. Cells were incubated with IONPs at the Fe concentration of 0.2 mg/mL. Scale Bar 20 μm.

IMAGE CAPTION: Prussian blue stained images of (A) anti-biofouling IONPs and commercial SHP uptake by Raw264.7 macrophage at Fe concentrations of 0.2 and 0.05 mg/mL, respectively; (B) anti-biofouling IONPs and RGD-conjugated IONPs uptake by U87MG glioblastoma cells. Fluorescence images of (C) M2 cells targeted by mannose conjugated anti-biofouling IONPs and non-targeted IONPs; (D) Raw264.7 macrophages targeted by mannose conjugated anti-biofouling IONPs and non-targeted IONPs. Cells were incubated with IONPs at the Fe concentration of 0.2 mg/mL. Scale Bar 20 μm.

SESSION TITLE: Poster Session 01

CONTROL ID: 2734547

TITLE: Near-infrared photoswitchable nanoprobe for supersensitive photoacoustic imaging

PRESENTER: Xianchuang Zheng

AUTHORS (FIRST NAME, LAST NAME): Xianchuang Zheng[1], Steven Chu[2], Jianghong Rao[1]

INSTITUTIONS (ALL):

1. Radiology, Stanford University, Stanford, CA, United States.
2. Physics, Stanford University, Stanford, CA, United States.

ABSTRACT BODY:

Abstract Body: Photoacoustic (PA) imaging has become a powerful, new biomedical imaging modality because it overcomes the depth and resolution limitation of conventional optical imaging. The development of exogenous PA contrast agents, such as organic dyes, gold nanoparticles and carbon nanotubes, has greatly broadened the horizon of PA imaging [1]. However, the high intrinsic background signals from the blood significantly limit the in vivo detection sensitivity of these PA probes. Novel approaches and designs are required to develop new generations of PA probes that potentially break the intrinsic limit on the sensitivity.

Photoswitchable fluorescent probes have been developed to enable super-resolution fluorescence imaging. Similar approach has been realized with a photoswitchable bacterial phytochrome (BphP1) for PA imaging [2]. However, the use of BphP1 requires genetic engineering of cells and tissues, which will not be applicable to cancer imaging and diagnosis in clinics. Here we present photoswitchable nanoparticles for super-sensitive PA imaging.

The photoswitchable PA nanoprobes can be reversibly switched between PA inactive and PA active states by light. PA imaging can be first taken with the probe in its inactive state. Then the probe can be switched to PA active state using light (λ_1) followed by another PA imaging. The subtraction of the two PA images can produce the differential image which presents only the probe signal. Then, the probe can be switched back to the inactive state using light (λ_2) to start the next cycle of PA imaging. By adding the differential images together, the background signal can be greatly suppressed and the imaging sensitivity can be improved.

We have prepared the photoswichable PA imaging nanoprobe and successfully demonstrated the reversible switching ON/OFF of the PA signal of the nanoprobe. The nanoprobe can be switched ON to the PA active state or switched OFF to the PA inactive state totally by NIR light with an ON/OFF signal ratio of ten (Fig. 1). In a phantom imaging experiment, the nanoprobe was mixed with hemoglobin and first imaged at the OFF state, then NIR light was used to switch ON the nanoprobe for another PA imaging. The probe signal could be extracted by subtracting the OFF PA image (corresponding to the strong background from hemoglobin) from the ON PA image (Fig. 2). The probe signal from one single cycle was quite weak at the low probe concentration (0.5 nM), but the PA imaging contrast could be significantly enhanced by increasing the switching-imaging cycle number. For instance, the signal-to-noise ratio (SNR) was improved by one order of magnitude after ten cycles of photoswitchable PA imaging (Fig. 3).

This photoswitchable PA nanoprobe may be further funcationalized for targeted imaging. It can also used to label cells of interest for in vivo cell tracking through PA imaging. With the photoswitching capability, the PA imaging sensitivity is expected to significantly improve.

References:

[1] Science 2012, 335, 1458.

[2] Nat. Methods 2016, 13, 67.

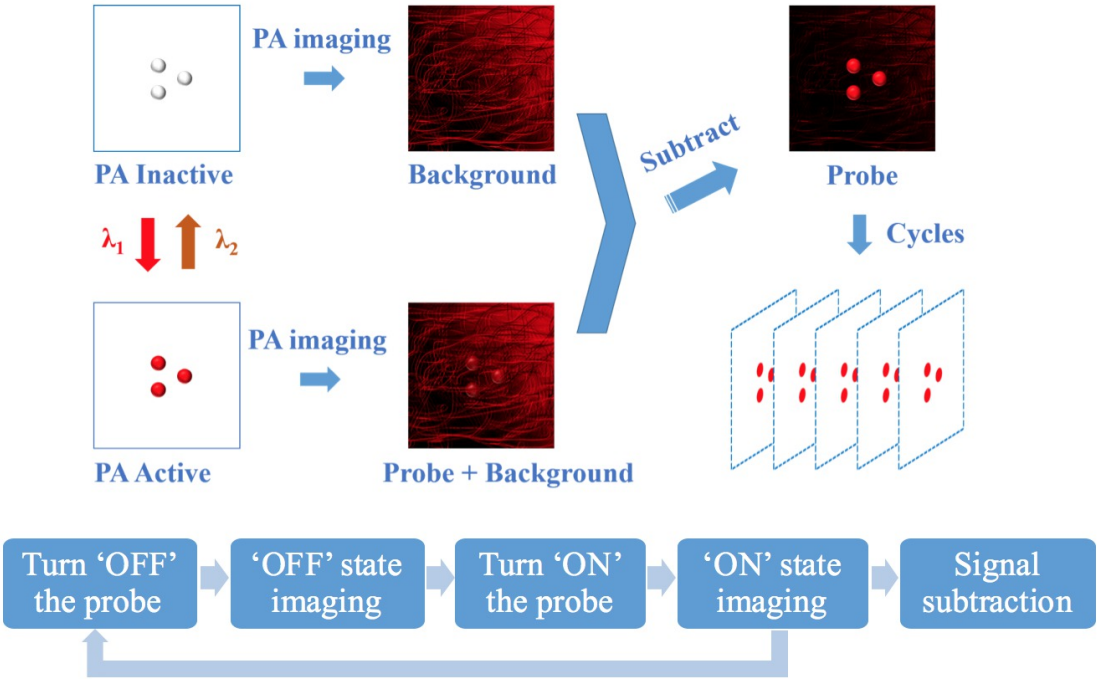

Basic principle of the photoswitchable PA imaging.

IMAGE CAPTION: Basic principle of the photoswitchable PA imaging.

SESSION TITLE: Poster Session 01

CONTROL ID: 2734711

TITLE: Novel Molecularly Engineered Gaussia Luciferase Reporters for Enhanced Intracellular and Extracellular Biosensor Applications

PRESENTER: Aarohi Bhargava-Shah

AUTHORS (FIRST NAME, LAST NAME): Ramasamy Paulmurugan[1], Shuchi Gaur[1], Aarohi Bhargava-Shah[1], Sharon S. Hori[2], Rayhaneh Afjei[3], Sekar V. Thillai[1], Sanjiv S. Gambhir[1], Tarik F. Massoud[3]

INSTITUTIONS (ALL):

1. Radiology, Stanford University, Palo Alto, CA, United States.
2. Radiology, MIPS, Stanford Univ-Geophysics Dept, Stanford, CA, United States.
3. Radiology and MIPS, Stanford University School of Medicine, Palo Alto, CA, United States.

ABSTRACT BODY:

Abstract Body:

Gaussia luciferase (GLUC) is a secretory bioluminescent reporter of increasing importance in molecular imaging. It has much greater sensitivity in vitro and in vivo over its competitor, secreted alkaline phosphatase. Unfortunately, the advantages afforded by the secretory nature of GLUC also limit its usefulness for many more possible intracellular applications. Hence, to widen the gamut of potential applications of GLUC, we developed variants that could increase its intracellular retention through modifying the N-terminal secretory signal peptide, or by tagging additional sequences to its C-terminal region. We validated the use of these new variants in two novel cellular biosensor applications.

We constructed GLUC variants in a lentiviral vector system and then engineered Ln229 and MDA-MB231 cells to stably carry equal numbers of cDNA copies after viral transduction and selection through FACS sorting. We identified specific GLUC variants preferentially retained inside the cells, and then used these to construct biosensors for measuring endoplasmic reticulum stress and caspase 3 activation in response to different drugs.

We observed that 95% of expressed wtGLUC was secreted extracellularly. We tested a truncated version of GLUC by removing the N-terminal secretory signal peptide (amino acids 1-16) and found that more protein was retained intracellularly but with significantly lower levels of luciferase activity; the secretory signal peptide was also crucial for proper GLUC folding. Conversely, modifying the C-terminal of GLUC by tagging endoplasmic reticulum targeting peptide (KDEL) in multiple repeats significantly improved its intracellular retention, with little impact on enzymatic activity. We validated this new intracellular GLUC variant, firstly by treating cells with tunicamycin, an endoplasmic reticulum stressor, and found that more of the KDEL-tagged GLUC protein released extracellularly compared to control cells. We then engineered an apoptotic sensor using modified variants of GLUC containing a four amino acid caspase substrate peptide (DEVD) between GLUC and three KDEL repeats [GLUC-DEVD-$(KDEL)_3$]. Again there was increased GLUC secretion extracellularly when cells were treated with the chemotherapeutic drugs doxorubicin, paclitaxel, and carboplatin. Immunoblot analysis confirmed enhancement in the cleavage of GLUC-DEVD-$(KDEL)_3$ by caspase in drug treated cells.

The N-terminal secretory signal peptide of GLUC is critical for its proper folding, in addition to its known secretory function. We successfully engineered a new variant GLUC possessing C-terminal KDEL multimers that significantly improve intracellular retention of GLUC and further expand its repertoire and applications in designing highly sensitive biosensors for imaging cellular functions, e.g. for measuring caspase activation induced by chemotherapy, and for monitoring the effects of drugs inducing endoplasmic reticulum stress. Availability of this newly engineered variant GLUC reporter could have far-reaching applications in biological research, including in translational cancer cell biology and therapy, and in vivo molecular imaging.

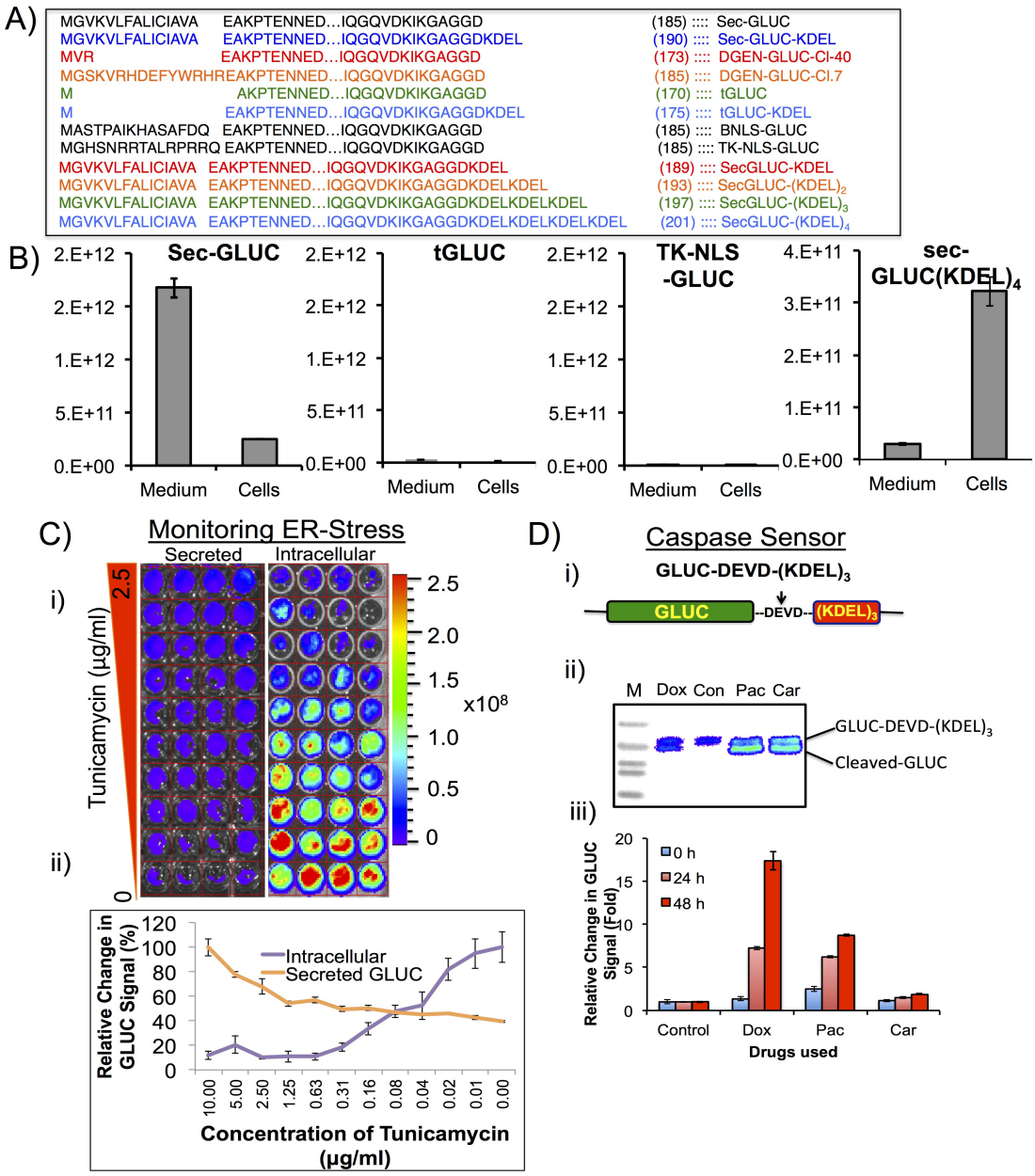

Figure 1: *Developing GLUC variants to improve its intracellular retention for cellular biosensor applications*. (**A**) Amino acid sequences of different GLUC variants developed with N-terminal and C-terminal modifications. **(B)** Comparison of GLUC signal from different variants for their intracellular and secretory signals. **(C)** Endoplasmic reticulum stress measured by the GLUC variant in response to the treatment of different doses of tunicamycin, a known ER-stressor, in MDA-MB231 cells stably expressing the constructs [(i) Optical bioluminescence imaging of GLUC activity in cells and in the medium of cells treated with tunicamycin; (ii) Quantitative graph of signal measured from images in (i)]. **(D)** Schematic figure of lentiviral construct showing caspase 3 sensors (i), its cleavage in cells treated with anticancer drugs by immunoblot analysis (ii), and time and dose dependent secretion of GLUC protein in the medium of cells treated with chemotherapeutic drugs (iii).

IMAGE CAPTION: Figure 1: *Developing GLUC variants to improve its intracellular retention for cellular biosensor applications*. (**A)** Amino acid sequences of different GLUC variants developed with N-terminal and C-terminal modifications. **(B)** Comparison of GLUC signal from different variants for their intracellular and secretory signals. **(C)** Endoplasmic reticulum stress measured by the GLUC variant in response to the treatment of different doses of tunicamycin, a known ER-stressor, in MDA-MB231 cells stably expressing the constructs [(i) Optical bioluminescence imaging of GLUC activity in cells and in the medium of cells treated with tunicamycin; (ii) Quantitative graph of signal measured from images in (i)]. **(D)** Schematic figure of lentiviral construct showing caspase 3 sensors (i), its cleavage in cells treated with anticancer drugs by immunoblot analysis (ii), and time and dose dependent secretion of GLUC protein in the medium of cells treated with chemotherapeutic drugs (iii).

SESSION TITLE: Poster Session 01

CONTROL ID: 2734749

TITLE: Molecular Imaging Biosensors Imaging Specific Interaction of Chromodomains with Histone Lysine Methylation Marks within the Chromatin of Intact Cells Through Protein Stabilization

PRESENTER: Sekar Thillai

AUTHORS (FIRST NAME, LAST NAME): Sekar V. Thillai[1], Ramasamy Paulmurugan[1]

INSTITUTIONS (ALL):

1. Radiology, Stanford University, Palo alto, CA, United States.

ABSTRACT BODY:

Abstract Body: Lysine methylation is one among many covalent modifications in histone proteins that controls the structure and function of chromatin. Methylation to specific lysine in the N-terminal tails of histone proteins alters chromatin structure by recruiting regulatory proteins with specific structural motifs (chromodomain, tudor-domain, or WD40-repeat domains). We recently developed split reporter protein complementation and degron-protease blockade imaging sensors for real-time imaging of methylation status of different histone lysine marks in live cells and small animal models. To further improve the sensitivity and to create a library approach to simultaneously measure the methylation status of various marks in a given time, in this study we developed Renilla luciferase based degron protease sensor with structural domains derived from various regulatory proteins. We evaluated these sensors in cells in response to the treatment of drugs, which modulate methyltransferase enzymes and siRNAs that silence specific methyltransferases. We constructed various plasmid vectors coding for red shifted Renilla luciferase variant with C-terminal attachment of Chromo- or tudor- domain followed by degron sequence of mouse ornithine decarboxylase (RLuc8.6-Chromo/tudor domain-C-terminal Degron) (Figure 1b). The principle behind this sensor relies on blocking the degron-mediated action of protease enzyme on reporter protein (RLuc8.6). When chromo- or tudor- domain binds to specific methylated histone target, a conformational change induced by this interaction blocks sensor protein from degradation and resulting in higher signal yield; conversely, reporter protein is degraded by protease action when there is no binding of chromo/tudor domains with the chromatin (Figure 1a).

Plasmid vectors expressing sensor fusion proteins with chromodomains and tudordomains derived from different regulatory proteins [Suv39H1, Heterochromatin protein 1 (HP1), Polychrome 2 (PC2), JMJD2A, 53BP1, PHF19, SMN] in transfected HEK293T cells showed significant level of luciferase signal as independently measured by IVIS Lumina imaging, and Luminometer. Methylation-assisted luciferase signal level varied from 5 to 220 folds ($2.1x10^5 \pm 9.3x10^4$ to $8.9x10^6 \pm 4.1x10^5$ RLU) with all 7 different sensors constructed with different structural domains when compared to sensor protein containing only the linker sequence before degron ($4.0x10^4 \pm 1.9x10^3$ RLU) (Figure 1c). Further evaluation by immunoblot analysis using RLuc specific antibody showed a correlation with the results observed in luminometer and IVIS intact cell imaging assays (Figure 1d). We developed stable cell lines of different cancer types (Ln229: glioma; MDA MB231: breast cancer cells, etc.) expressing all seven sensors and the control sensor for in vivo imaging applications and for drug evaluation studies. These degron blockade sensors would be potentially used for the identification, and preclinical validation of small molecule compounds that can modulate methylation level of various histone methylation marks, which are currently identified as promising therapeutic targets for various diseases.

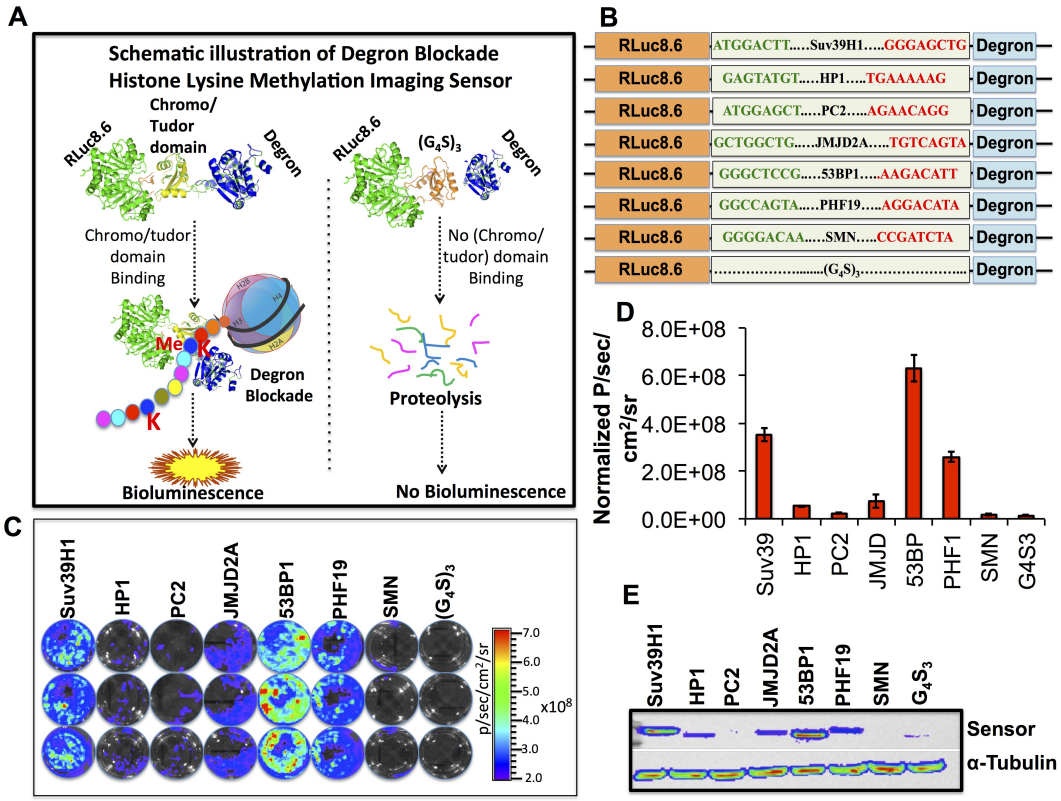

Figure 1: A, Schematic illustration of the principle of protease blockade methylation imaging sensor; **B,** Schematic of plasmid vector constructs express fusion proteins with different structural domains and control vector used for imaging histone methylation in cells; **C,** Optical bioluminescence imaging of HEK293T cells transfected with plasmid vectors expressing sensor fusion proteins with different structural motifs by IVIS-optical CCD camera; **D,** Quantitative graph showing the methylation mediated normalized luciferase (Fluc) signal measured from figure shown in **'C'** ; **E,** Immunoblot analysis showing the level of sensor fusion proteins stabilized in HEK293T cells transfected with different vector constructs.

IMAGE CAPTION: Figure 1: A, Schematic illustration of the principle of protease blockade methylation imaging sensor; **B,** Schematic of plasmid vector constructs express fusion proteins with different structural domains and control vector used for imaging histone methylation in cells; **C,** Optical bioluminescence imaging of HEK293T cells transfected with plasmid vectors expressing sensor fusion proteins with different structural motifs by IVIS-optical CCD camera; **D,** Quantitative graph showing the methylation mediated normalized luciferase (Fluc) signal measured from figure shown in **'C'** ; **E,** Immunoblot analysis showing the level of sensor fusion proteins stabilized in HEK293T cells transfected with different vector constructs.

SESSION TITLE: Poster Session 01

CONTROL ID: 2734796

TITLE: Fluorinated Senor for Monitoring Zn^{2+} by ^{19}F-CEST MRI

PRESENTER: Deva Nishanth Tirukoti

AUTHORS (FIRST NAME, LAST NAME): Deva Nishanth Tirukoti[2, 1], Alona Bar-on[1], Liat Avram Biton[1], Amnon Bar-Shir[1]

INSTITUTIONS (ALL):

1. Organic Chemistry, Weizmann Institute of Science, Rehovot, Israel.
2. organic chemistry, Weizmann Institute of science, Rehovot, Israel.

ABSTRACT BODY:

Abstract Body: Introduction

Zinc (Zn^{2+}) is the second most abundance metal ion in the human body playing a crucial role in the biology of heath and diseases[(1)]. Hence, the ability to noninvasively detect, quantify and map the distribution of Zn^{2+} is important. ^{19}F-based sensors for MRI applications show several advantages [(2)]. Here we show the rational design of ^{19}F-modified dipicolylamine derivatives as potential MRI-based sensors for specific detection of Zn^{2+} ions using the ion CEST (iCEST)[(2)] approach that combines CEST and ^{19}F-MRI for the detection of low ion concentrations.

Methods

^{19}F-CEST experiments were performed on 9.4 T (i.e. 376 MHz for ^{19}F-nuclei) NMR spectrometer in order to determine the chemical shift between Zn^{2+}-bound chelate and free chelate (Dw) and evaluating the CEST characteristics. For iCEST MRI experiments, phantom composed of 5mM of NIS-2 with (i) no ions (ii-iv) 100 μM of Zn^{2+}, Ca^{2+} or Mg^{2+} was used. MRI experiments were performed on 9.4T MRI scanner equipped with dual ^{1}H/^{19}F rf coil. For ^{19}F-CEST a modified RARE sequence (TR/TE=6000/3.64 ms, Rare factor=16, 8mm slice, FOV=4.8x4.8cm, matrix size=32x32, resolution=1.5x1.5 mm, NA=160, saturation pulse=2.5 μT/2 s), was used to acquire ^{19}F-CEST MRI images.

Results

A library of ^{19}F-modified dipicolylamine derivatives was synthesized. Two compounds showed large Dw between free and Zn2+-bound 19F-dipicolylamine (Fig:1a,1b) with high specificity to Zn^{2+} over Ca^{2+} or Mg^{2+}. While no ^{19}F-CEST was obtained with NIS-1 (Fig: 1c), a significant effect was detected with NIS-2, i.e., 25% CEST effect at 60 μM Zn^{2+} (Fig: 1d). Fig: 1e shows 19F-CEST MRI without or with Zn^{2+}, Ca^{2+}, Mg^{2+}. ^{19}F-CEST map was obtained at the frequency of Zn^{2+} bound NIS-2 (Dw=5 ppm) and overlaid on 1H image. CEST effect was observed only in the presence of Zn^{2+}.

Conclusions

The ^{19}F-modified dipicolylamine with ^{19}F-atom at the 5-position showed the largest Δw at the ^{19}F-NMR spectrum between free and Zn^{2+}-bound ^{19}F-dipicolylamine. Introducing methyl group to the 6 position of 5-fluoro-dipicolylamine improve dramatically the ^{19}F-CEST performances and allowed the detection of low concentrations of Zn^{2+} ions.

References

1. Frederickson CJ, et al. Nat Rev Neurosci. 2005;6(6):449-62.

2. Bar-Shir A, et al. J Am Chem Soc. 2013;135(33):12164-7.

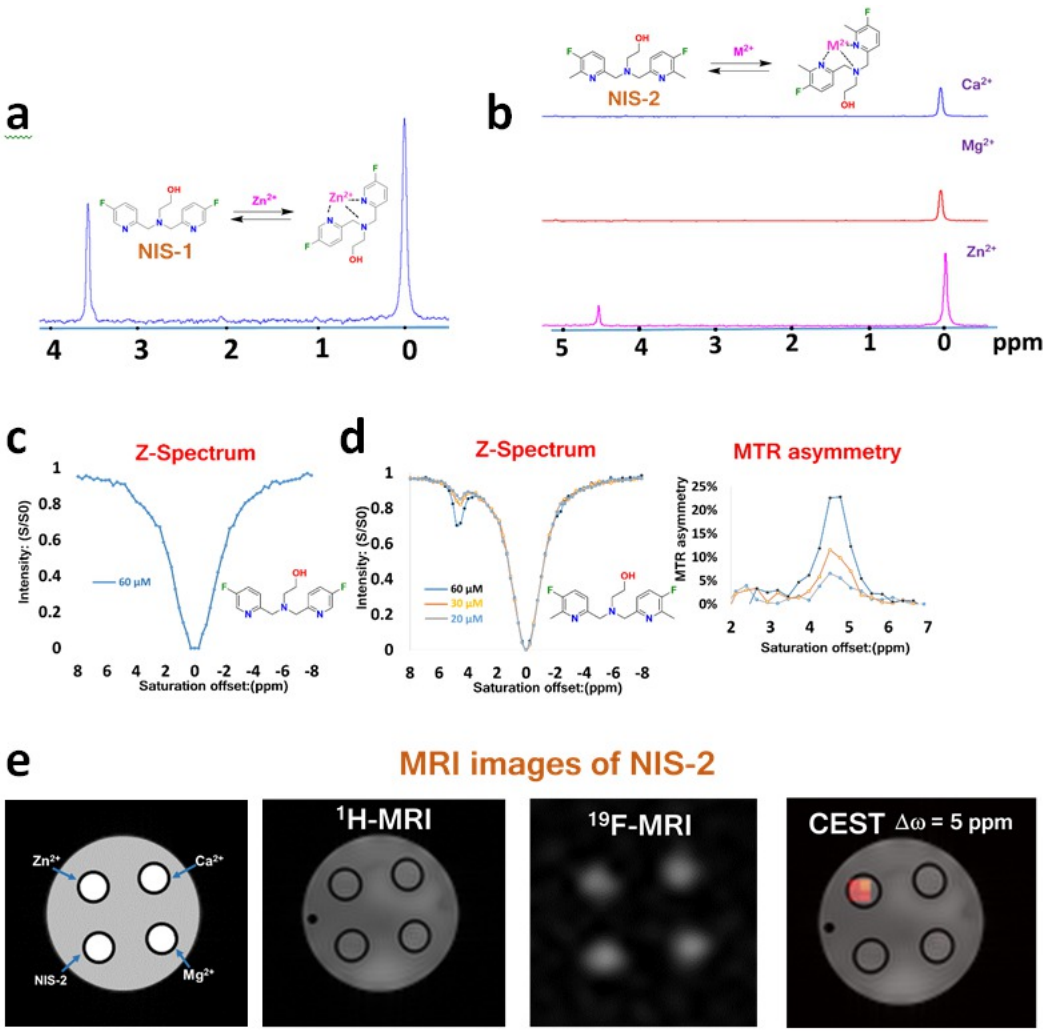

Figure 1:
(a) ^{19}F-NMR spectrum of NIS-1 in the presence of Zn^{2+}. (b) ^{19}F-NMR spectra of NIS-2 in the presence of Zn^{2+}, Ca^{2+} or Mg^{2+}. (c) Z-spectrum of NIS-1 in the presence of Zn^{2+}. (d) iCEST data of NIS-2. (e) iCEST MRI obtained for NIS-2.

IMAGE CAPTION: Figure 1:
(a) ^{19}F-NMR spectrum of NIS-1 in the presence of Zn^{2+}. (b) ^{19}F-NMR spectra of NIS-2 in the presence of Zn^{2+}, Ca^{2+} or Mg^{2+}. (c) Z-spectrum of NIS-1 in the presence of Zn^{2+}. (d) iCEST data of NIS-2. (e) iCEST MRI obtained for NIS-2.

SESSION TITLE: Poster Session 01

CONTROL ID: 2734799

TITLE: Multimodality imaging of non small-cell lung cancer using folate-targeted perfluorocarbon nanoparticles

PRESENTER: Xiuan Xu

AUTHORS (FIRST NAME, LAST NAME): Xiuan Xu[1], Lina Wu[1], Xilin Sun[1], Baozhong Shen[2]

INSTITUTIONS (ALL):

1. Molecular Imaging Research Center (MIRC), Harbin Medical University, Harbin, China.
2. Molecular Imaging Research Center (MIRC), Harbin Medical University, Harbin, China.

ABSTRACT BODY:

Abstract Body: Purpose:

Lung cancer is one of the most prevalent pulmonary diseases and leading cause of oncologic mortality in the world, with bad diagnostic and therapeutic effect. One of the main reasons for the dismal prognosis of lung cancer is related to late diagnosis of this pathology[1]. Molecular imaging of tumor can reveal the biology and pathobiology process of alive tissue in vitro and in vivo with high sensitivity and specifity[2]. In this study, we explore the Folate receptor(FR) specific imaging of non small-cell lung cancer(NSCLC) by integrating ^{1}H MR, ^{19}F MR and fluorescent imaging, employing two types of animal models (carcinoma in situ and subcutaneous).

Materials and Methods:

Perfluoro-15-crown-5-ether was encapsuled with phosphorilipid monolayer, and decorated with Gd,rodamine and folate as affiliative part for improving the ability to target FR over-expressing tumors. The control group of PFC NPs is basically the same but without folate. MTT assay was used to test the toxicity of the nanoparticles.Four NSCLC cell lines including H460,H520,HCC827 and A549 were selected. Western blotting was used to test the FR expression. Flow cytometry and confocal laser scanning microscope were taken on for cell-uptake after co-incubated with perfluorocarbon nanoparticles. Subcutaneous and in situ tumor bearing nude mice models were setted up. In order to verify the effectiveness of the stragety, multi-model and multi-nucleus imaging was used. The major organs and tumor were isolated and subjected to ex vivo optical imaging.

Results:

The diameter of the nanoparticles was 140 nm with uniform distribution. The size is stable in wide pH range. The FR expression level was measured to be in the order of H460>H520>HCC827 >A549. In vitro targeted effectiveness experiments showed approximately 60 % fluorescence intensity of the H460 cells incubated with the targeted PFC, obviously higher than others($p < 0.05$). In vivo imaging results showed that H460 targeted group had high signal intensity in optical and MR imaging compared with other groups, especially at 24h after nanoparticles injection. Most of the nanoparticles were aggregated in liver,spleen and lung from the tissue biodistribution.

Conclusion:

These folate targeted nanoparticles were successfully delivered into FR-positive tumor xenograft models and showed significantly enhanced signal intensities of ^{1}H-MRI and fluorescence imaging in the tumor area.This nanoparticles have a great potential to serve as a useful targeted agent for the difference of FR positive or negative tumor.

Keywords:

folate recepter, perfluorocarbon, ^{19}F MR,cancer

References:

1. A. B, et al. Targeting and in vivo imaging of non-small-cell lung cancer using nebulized multimodal contrast agents. Proceedings of the National Academy of Sciences of the United States of America 111, 9247-9252 (2014).
2. B. Z. Shen. Systems Molecular Imaging: Right Around the Corner. Nano Biomed. Eng. 2014, 6(1), 1-6.

(No Image Selected)

SESSION TITLE: Poster Session 01

CONTROL ID: 2735020

TITLE: SWIR in vivo Imaging with Gold Nanoclusters

PRESENTER: Yue Chen

AUTHORS (FIRST NAME, LAST NAME): Yue Chen[2], Oliver T. Bruns[1], Moungi Bawendi[3]

INSTITUTIONS (ALL):

1. Chemistry, MIT, Cambridge, MA, United States.
2. Chemistry, Massachusetts Institute of Technology, Cambridge, MA, United States.
3. Chemistry, MIT, Cambridge, MA, United States.

ABSTRACT BODY:

Abstract Body: The use of visible/NIR -emitting gold nanoclusters (Au NCs), previously proposed for in vivo imaging, has been limited to some extent by low quantum yields (QYs) and the limited penetration of visible light in tissue. Here we report short wavelength infrared (SWIR, λ=1-2 μm) emitting Au NCs with a good photoluminescence QY for this wavelength range (0.6% to 3.8% for λ_{em}=1,000 to 900 nm), and excellent stability under physiological conditions. We show that surface ligand chemistry is critical to achieving these properties. We demonstrate the potential of these SWIR-emitting Au NCs for in vivo imaging in mice. The Au NCs have a hydrodynamic diameter (HD) that is small (~5 nm) enough that they exhibit a rapid renal clearance, and images taken in the SWIR region show better resolution of the blood vessels than in the NIR region.

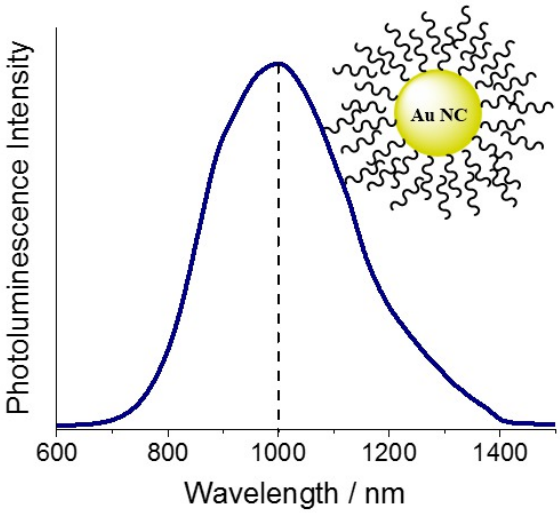
Photoluminescence Intensity
Au NC
600
800
1000
1200
1400
Wavelength / nm

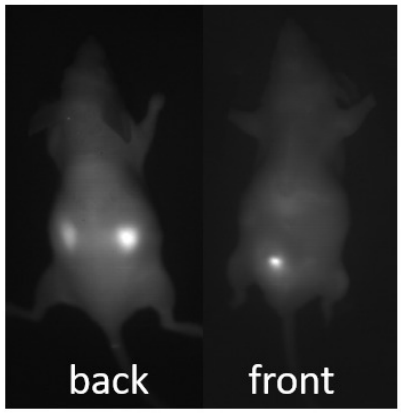
back
front

IMAGE CAPTION:

SESSION TITLE: Poster Session 01

CONTROL ID: 2735025

TITLE: Shortwave Infrared Fluorescence Imaging with Clinically Accessible Near-Infrared Dyes

PRESENTER: Daniel Franke

AUTHORS (FIRST NAME, LAST NAME): Daniel Franke[2], Jessica A. Carr[3], Rakesh Jain[4], Moungi Bawendi[1], Oliver T. Bruns[1]

INSTITUTIONS (ALL):

1. Chemistry, MIT, Cambridge, MA, United States.
2. Chemistry, Massachusetts Institute Of Technology, Cambridge, MA, United States.
3. Chemistry, Massachusetts Institute of Technology, Cambridge, MA, United States.
4. Massachusetts General Hospital, Boston, MA, United States.

ABSTRACT BODY:

Abstract Body: Fluorescence imaging is a method of real-time molecular tracking in vivo which has enabled revolutionary clinical technologies, especially for image-guided surgery. Imaging in the shortwave infrared region (SWIR, 1-2 μm) promises higher contrast, sensitivity, and penetration depths compared to conventional visible and near-infrared (NIR) fluorescence imaging. However, adoption of SWIR imaging in clinical settings has been limited, due in part to the lack of FDA-approved fluorophores with peak emission in the SWIR. Here, we show that commercially available NIR dyes, including the FDA approved contrast agent indocyanine green (ICG), exhibit excellent optical properties for in vivo SWIR fluorescence imaging. Despite the fact that their emission peaks outside of the SWIR, these dyes can be imaged non-invasively in vivo in the SWIR spectral region, even beyond 1500 nm. We demonstrate real time fluorescence angiography at wavelengths beyond 1300 nm using ICG at clinically relevant doses. Furthermore, we show tumor-targeted SWIR imaging with trastuzumab labeled with IRDye 800CW, a NIR dye currently being tested in multiple phase II clinical trials. Surprisingly, these findings indicate that high-contrast SWIR fluorescence imaging can be easily implemented alongside existing imaging modalities, simply by switching the detection from conventional silicon-based NIR cameras to emerging indium gallium arsenide (InGaAs) SWIR cameras. Using ICG in particular opens the possibility of immediate translation of SWIR fluorescence imaging to human clinical applications.

(No Image Selected)

SESSION TITLE: Poster Session 01

CONTROL ID: 2735055

TITLE: Intracellular Self-Assembly of Theranostic Nanoparticles for CEST MR Imaging and Cancer Therapy

PRESENTER: Yue Yuan

AUTHORS (FIRST NAME, LAST NAME): Yue Yuan[1], Xiaoliang Qi[1], Xiaolei Song[1], Mike McMahon[1, 2], Jeff W. Bulte[1, 2]

INSTITUTIONS (ALL):

1. The Russell H. Morgan Department of Radiology and Radiological Science; Cellular Imaging Section, Institute for Cell Engineering, The Johns Hopkins University, Baltimore, MD, United States.
2. F.M. Kirby Center for Functional Brain Imaging, Kennedy Krieger Institute, Baltimore, MD, United States.

ABSTRACT BODY:

Abstract Body: Introduction: Chemical exchange saturation transfer magnetic resonance imaging (CEST MRI) holds great promise for biomedical applications and molecular diagnostics. There is, however, a lack of enzyme-activatable probes for cancer-specific imaging. Furin is a proprotein convertase that activates many cancer development-related substrates such as growth factors, growth factor-receptors, adhesion molecules, and matrix degrading enzymes, and is overexpressed in malignant tumor cells[1]. We report here on a new molecular probe RRVR-Olsa (Fig. 1a), in which the exchangeable hydroxyl protons in olsalazine provide CEST contrast with the cell-penetrating peptide RVRR acting as a specific substrate for furin. After the RRVR-Olsa enters furin-expressing cells, the RRVR peptide is cleaved by furin, initiating a condensation reaction between the GSH-induced 1,2-aminothiol group and the cyano group of the 2-cyanobenzothiazole motif, resulting in the formation of olsalazine nanoparticles (Olsa-NPs) as CEST polymers. As it has been reported that cancer cells can be killed by intracellular accumulation of olsalazine[2], we investigated whether intracellular assembly of Olsa-NP could represent a new theranostic approach.

Methods: CEST imaging: Furin-overexpressing HCT 116 human colon cancer cells and furin-deficient (control) LoVo human colon cancer cells were incubated with or without RRVR-Olsa (5 mM) for 24 h, and then cells were collected in 5 mm NMR tubes after washing. Cells were mixed with 2% agarose to prevent sedimentation. A modified RARE sequence (TR/TE=6,000/5 ms, RARE factor=32, 5 mm slice thickness, FOV=14×17 mm, matrix size=64×64, resolution=0.22×0.27 mm, NA=2 and a saturation pulse B_1=5.9 μT/4 s) was used. Cell viability: The number of HCT116 cells was counted after the incubation of different concentration (125, 250, and 500 μM) of RRVR-Olsa, olsalazine, and 5-aminosalicylic acid (5-ASA) for 48 h. Cell viability was calculated as a percentage of control (untreated) set at 100%. Data are expressed as means ± SD from three independent experiments.

Results: Fig. 1b shows an enhanced CEST MRI contrast for furin-overexpressing HCT 116 cells compared to furin-deficient LoVo cells, indicating that the furin-catalyzed intracellular formation of olsalazine nanoparticles is accountable for signal enhancement. Significant cytotoxicity was observed at 125 μM RRVR-Olsa, with no cytotoxicity at 500 μM olsalazine or 5-ASA. For the latter two compounds, a comparable cytotoxicity could only be observed when the drug concentration increased to 2.5 mM (Fig. 1c). These results suggest that RRVR-Olsa accumulation in tumor cells exhibits a potent anti-tumor effect.

Conclusion: Furin-induced intracellular formation of olsalazine nanoparticles using the new theranostic probe RRVR-Olsa may have potential for cancer-specific imaging and therapy.

Acknowledgements: This project was supported by the Pearl and Yueh-Heng Yang Foundation.

References: [1]Bassi, D. E. et al. Mol. Carcinogen. 2001, 31, 224. [2]Brown, W. A. et al. Digest. Dis. Sci. 2000, 45, 1578.

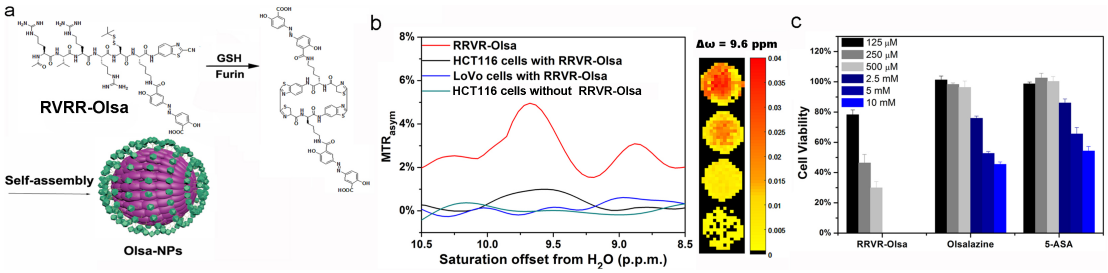

Figure 1. (a) Chemical structure of RVRR-Olsa and schematic illustration of intracellular furin-controlled self-assembly of Olsa-NPs. (**b**) MTR_{asym} curves and CEST MRI (from top to bottom) of 5 mM RRVR-Olsa reference standard, HCT 116 cells treated with 5 mM RRVR-Olsa, LoVo cells treated with 5 mM RRVR-Olsa, and untreated HCT 116 cells. (**c**) Cell viability of HCT116 cells incubated with different concentrations of RRVR-Olsa, olsalazine, and 5-ASA for 48 h.

IMAGE CAPTION: Figure 1. (a) Chemical structure of RVRR-Olsa and schematic illustration of intracellular furin-controlled self-assembly of Olsa-NPs. (**b**) MTR_{asym} curves and CEST MRI (from top to bottom) of 5 mM RRVR-Olsa reference standard, HCT 116 cells treated with 5 mM RRVR-Olsa, LoVo cells treated with 5 mM RRVR-Olsa, and untreated HCT 116 cells. (**c**) Cell viability of HCT116 cells incubated with different concentrations of RRVR-Olsa, olsalazine, and 5-ASA for 48 h.

SESSION TITLE: Poster Session 01

CONTROL ID: 2735400

TITLE: SYNTHESIS OF [^{18}F]SIFA-TETRAZINE FOR PRETARGETED PET APPLICATONS

PRESENTER: Sofia Otaru

AUTHORS (FIRST NAME, LAST NAME): Sofia Otaru[1], Outi M. Keinänen[1], Dave Lumen[1], Kristiina Wähälä[2], Anu J. Airaksinen[1]

INSTITUTIONS (ALL):

1. Department of Chemistry, Radiochemistry, University of Helsinki, Helsinki, Finland.
2. Medicum, University of Helsinki, Helsinki, Finland.

ABSTRACT BODY:

Abstract Body:

Objectives: Inverse electron demand Diels-Alder (IEDDA) between tetrazine and trans-cyclooctene is an efficient bioorthogonal reaction type that can be utilized in imaging and therapeutical applications. The aim was to develop an optimally lipophilic ^{18}F-labeled tetrazine for pretargeted PET-applications via one-step synthesis route.
Methods: The precursor, (E,Z)-N-[4-(1,2,4,5-tetrazin-3-yl)benzyl]-2-{[(4-di-tert-butyl(fluorosilyl)benzylidene]aminooksi}acetamide (SiFa-tetrazine) was synthesized via a multistep synthesis sequence. The radiolabeled product was synthesized utilizing one-step and two-step labeling methods in a semiautomatic synthesis unit. In the one-step method the [^{18}F]SiFa-tetrazine was synthesized by labeling the precursor with [^{18}F]fluoride via isotopic exchange. In the two-step method, first a prosthetic group 4-(di-tert-butylfluorosilyl)benzaldehyde (SiFa) was labeled by isotopic exchange after which it was reacted with an aminooxy functionalized tetrazine precursor leading to oxime bond formation and to desired product. The radiolabeled prosthetic group [^{18}F]SiFa and the final product [^{18}F]SiFa-tetrazine were characterized with HPLC (UV-, radio-) and radio-TLC analysis methods. The structures of all intermediates were verified with NMR-analysis. The structure of the precursor was verified using 1D- and 2D-NMR analysis, ESI-TOF MS and HPLC-methods.
Results: The aim was to develop a method for synthesizing a ^{18}F-labeled tetrazine for pretargeted PET applications via a one-step synthesis route. However radiolabeling the precursor in one step resulted in loss of starting material because of the subsequent cleavage of the oxime bond. A two-step fluorination was applied and [^{18}F]fluorination of the prosthetic group SiFa via isotopic exchange resulted in 78 % degree of labeling (NON-DCY) of the total fluorine within minutes (analyzed with radio-TLC). The method produced two minor ^{18}F-labeled side-products and 4 % of free fluorine. The oxime formation between and the aminooxy functionalized precursor was completed at rt. within 10 min. and the total overall radiochemical yield of the HPLC purified final product was 16 % DCY to EOB.
Conclusions: Our effords for optimizing the reaction conditions for the one-step radiosynthesis procedure of [^{18}F]SiFa-tetrazine were not successful. However an efficient two-step ^{18}F-labeling method was demonstrated providing the ^{18}F-labeled tetrazine in high enough activities for further evaluations. First results of the biological evaluation of [^{18}F]SiFa-tetrazine will be presented.
References: [1] O. Keinänen, X-G Li, N. K. Chenna, D. Lumen, J. Ott, C. F. M. Molthoff, M. Sarparanta, K. Helariutta, T. Vuorinen, A. D. Windhorst, A. Airaksinen, ACS Med. Chem. Lett. 2016, 7 (1), s. 62–66. [2] V. Bernard-Gauthier, J. J. Bailey, Z. Liu, B. Wängler, C. Wängler, K. Jurkschat, D. M. Perrin, R. Schirrmacher, Bioconjugate Chem., 2016, 27 (2), pp 267–279.
(No Image Selected)

SESSION TITLE: Poster Session 01

CONTROL ID: 2735486

TITLE: Accelerating High Resolution Hyperpolarized C-13 Quantitative T_2 Mapping Using a Local Low Rank plus Sparse Reconstruction

PRESENTER: Eugene Milshteyn

AUTHORS (FIRST NAME, LAST NAME): Eugene Milshteyn[1, 2], Galen D. Reed[3], Cornelius von Morze[1], Zihan Zhu[1, 2], Jeremy W. Gordon[1], Daniel Vigneron[1, 2]

INSTITUTIONS (ALL):

1. Radiology and Biomedical Imaging, UCSF, San Francisco, CA, United States.
2. UC Berkeley-UCSF Graduate Program in Bioengineering, University of California, San Francisco and University of California, Berkeley, CA, San Francisco, CA, United States.
3. HeartVista Inc., Los Altos, CA, United States.

ABSTRACT BODY:

Abstract Body: Purpose: New advances in probe development for hyperpolarized ^{13}C imaging has enabled monitoring of various physiological processes, such as metabolism and perfusion, of a variety of diseases[1]. Quantitative T_2 values of hyperpolarized probes can provide unique parameters informing on both normal tissues and changes with pathologies. T_2 mapping using the balanced steady-state free precession (bSSFP) sequence has provided high spatial resolution maps for multi-exponential fitting of several compounds, including [^{13}C]urea, [^{13}C,$^{15}N_2$]urea, [2-^{13}C]pyruvate, and [1-^{13}C]lactate[2,3]. However, conventional T_2 mapping acquisitions are slow and would benefit from acceleration methods such as compressed sensing to provide improvements in both spatial resolution and temporal resolution. In this study, we demonstrated 2-fold acceleration of in vivo bSSFP T_2 mapping using a local low rank plus sparse (LLR+S) reconstruction that provided significant spatiotemporal improvements over existing methods.

Methods: The initial in vivo studies were performed using HP001 (bis-1,1-(hydroxymethyl)-[1-^{13}C]cyclopropane-d_8), [^{13}C,$^{15}N_2$]urea, [2-^{13}C]pyruvate, and [1-^{13}C]lactate in 3-4 different Sprague-Dawley rats per compound. The acquisition and multi-exponential fitting was performed as described in Reed et al[2]. Acceleration via compressed sensing was implemented by selecting a different 50% undersampling variable-density pattern for each time-point, and used to achieve 0.25-1 mm^2 in-plane resolution. Additionally, 1-2.5 mm isotropic 3D T_2 maps of [^{13}C,$^{15}N_2$]urea were acquired using 75% undersampling. Accelerated acquisitions were reconstructed using the LLR+S algorithm as described previously[4].

Results and Discussion: The prospectively reconstructed T_2 maps were in good agreement as evidenced by the ratio maps of the fully sampled and accelerated acquisitions for [^{13}C,$^{15}N_2$]urea and HP001, which had an average value of 0.87±0.06 in the kidneys and vasculature. The urea acquisition demonstrates the capability of sub-millimeter in-plane resolution acquisitions for HP probes with sufficient acceleration. The average value in the kidneys for the [2-^{13}C]pyruvate acquisition, 0.77±0.018, agreed well with previously acquired, lower resolution T_2 maps[3], while also allowing ~6-fold improvement in resolution. Additionally, both [1-^{13}C]lactate (~2.43s in kidneys) and 3D [^{13}C,$^{15}N_2$]urea T_2 maps (~4.84s in kidneys) matched up well with literature values[2,3].

Conclusion: We demonstrated the ability to acquire undersampled T_2 mapping data of various HP probes that correlated well with both fully sampled acquisitions and literature values. Further development of the method, such as increasing the amount of undersampling, may improve multi-exponential fitting via detection of short-lived components, potentially allow for 3D T_2 mapping of hyperpolarized probes, and be translated to the clinic to optimize current HP acquisitions and provide new quantitative assessments of normal values and changes with disease.

References: 1) Kurhanewicz et al., Neoplasia 2011. 2) Reed et al., Tomograhy 2016. 3) Milshteyn et al., MRI 2017. 38. 4) Milshteyn et al., ISMRM 24 (2016), #2329.

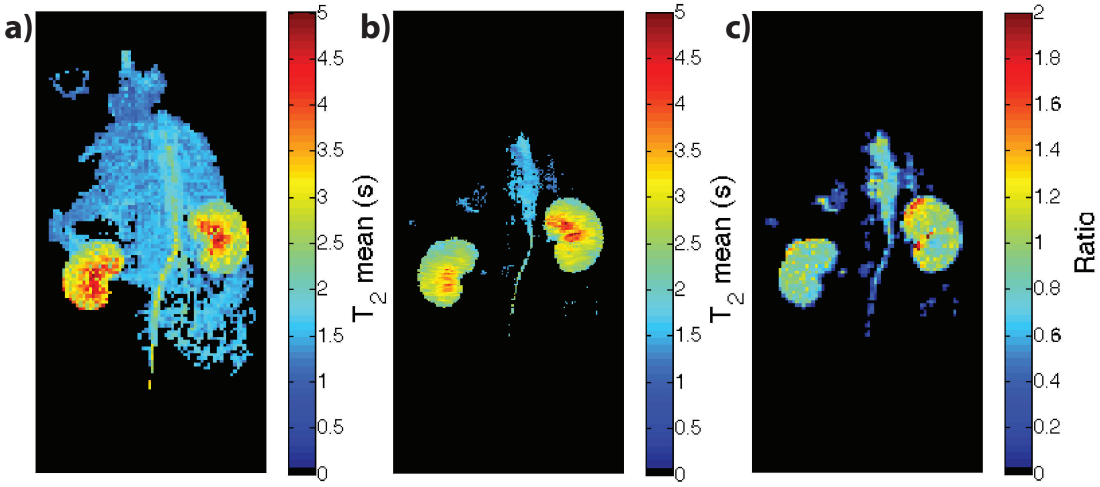

Example T_2 maps of the prospective fully sampled (1 mm^2 in-plane resolution) (a) and 2-fold accelerated (0.25 mm^2 in-plane resolution) (b) acquisitions of [^{13}C,$^{15}N_2$]urea can be seen here. The differences in biodistribution between the maps are due to SNR thresholding of the pixels as part of the fitting algorithm. Furthermore, the accelerated acquisition T_2 map has 4-fold higher spatial resolution than the fully sampled acquisition. Nevertheless, the ratio map had an average of 0.89 ± 0.21 (mean±intra-image standard deviation) within the kidneys and vasculature, showing the calculated T_2 values are in good agreement between both acquisitions.

IMAGE CAPTION: Example T_2 maps of the prospective fully sampled (1 mm^2 in-plane resolution) (a) and 2-fold accelerated (0.25 mm^2 in-plane resolution) (b) acquisitions of [^{13}C, $^{15}N_2$]urea can be seen here. The differences in biodistribution between the maps are due to SNR thresholding of the pixels as part of the fitting algorithm. Furthermore, the accelerated acquisition T_2 map has 4-fold higher spatial resolution than the fully sampled acquisition. Nevertheless, the ratio map had an average of 0.89 ± 0.21 (mean±intra-image standard deviation) within the kidneys and vasculature, showing the calculated T_2 values are in good agreement between both acquisitions.

SESSION TITLE: Poster Session 01

CONTROL ID: 2735492

TITLE: Structural modeling and ligand discovery of ASCT2 targeted theranostics utilizing in silico methodology

PRESENTER: Shannon Smith

AUTHORS (FIRST NAME, LAST NAME): Shannon T. Smith[1]

INSTITUTIONS (ALL):

1. Vanderbilt University Institute of Imaging Science, Vanderbilt University Medical Center, Nashville, TN, United States.

ABSTRACT BODY:

Abstract Body: Shannon T. Smith[1], Michael L. Schulte[1], H. Charles Manning[1]

[1]Vanderbilt University Medical Center, Nashville, Tennessee, 37232

In order to maintain rapid rates of division, cancer cells demonstrate altered metabolic activities. In addition to an increased influx of metabolites such as glucose, cancer cells also exhibit an increased uptake of the amino acid glutamine(1). Targeting specific glutamine transporters has been shown to be a promising approach for cancer treatment and may also represent innovative targets for molecular imaging. One such target is the glutamine transporter, ASCT2 (gene symbol SLC1A5)(2). Despite its prevalence in oncology, the structure of ASCT2 is relatively unstudied. By improving upon a model of ASCT2 using in silico methods, we have generated promising leads for novel molecular imaging probes and drug development. Additionally, these models are used as supporting evidence in substrate affinity studies, such as our novel ASCT2 inhibitor, V-9302.

ASCT2, a member of the alanine-serine-cysteine transport (ASC) protein family, is a homotrimeric, sodium-dependent neutral amino acid transporter. Due to the lack of crystallographic information, structural models of ASCT2 were generated using in silico comparative tools. Homology protocols utilized the crystallized 3D structure of an archaeal sodium-dependent aspartate transporter, GltPh, in complex with an aspartate derivative inhibitor (PDBID: 2NWW)(3). In addition to simple homology, extensive loop and symmetry protocols were performed in order to further enhance the accuracy of the ASCT2 model. After acquiring a more precise model, in silico ligand docking studies were performed in order to determine likely binding poses of particular substrates. Potential substrates of interest are extensions of amino acids primarily derived from glutamine, tyrosine and proline. One compound in particular, V-9302, has shown preferable binding in silico as supporting evidence to both in vitro and in vivo assays. These docking studies show the zwitterion of the amino acid derivatives forming hydrogen bonds with multiple serines and aspartate sidechains. Despite these polar interactions, the majority of residues in the active site residues contain primarily hydrophobic sidechains. Likely due to this significant hydrophobicity within the pocket, docking simulations demonstrate pose variation suggesting significant mobility of the substrate sidechain within the active site. In the case of V-9302, however, docking data suggest a more pronounced, less-mobile binding pose potentially being a major factor in substrate affinity.

As the docking studies suggest, V-9302 successfully inhibited the uptake of glutamine in cancer cells, resulting in decreased tumor size(4). Further improvement of ASCT2 models and docking simulations will help further optimize the design of glutamine inhibitors and molecular imaging probe development. References: 1) Pochini, L., et. al., Front. Chem., 2014. 2) Fuchs, BC., et. al., Semin Cancer Biol., 2005, 15(4): 254-66. 3) Albers T., et. al. Mol. Pharmacol. 2012. 81(3): 356-65. (4) Schulte, M.L., et. al. In Press.

(No Image Selected)

SESSION TITLE: Poster Session 01

CONTROL ID: 2735588

TITLE: Core-shell structured gold nanorod/mesoporous silica/gadolinium oxide carbonate hydrate nanoparticles as novel contrast agents for MRI, CT and photoacoustic imaging

PRESENTER: Ying Zhao

AUTHORS (FIRST NAME, LAST NAME): Ying Zhao[1, 2], Fei Ye[3], Ramy El-Sayed [1], Mamoun Muhammed[3], Moustapha Hassan[1, 2]

INSTITUTIONS (ALL):

1. Division of Experimental Cancer Medicine, Department of Laboratory Medicine (LABMED) , karolinska institutet, Huddinge, Sweden.
2. Clinical Research Center, Karolinska University Hospital-Huddinge, Stockholm, Sweden.
3. Division of Functional Materials (FNM), Department of Materials and Nanophysics, Royal Institute of Technology (KTH), Stockholm, Sweden.

ABSTRACT BODY:

Abstract Body: The rapid development of personalized medicine and the need for improving diagnostic tools have increased the demand on multimodality imaging. The development of novel contrast agents that can be detected by multiple imaging techniques is of high significant importance. Such development may greatly improve therapy, diagnosis and hence benefit patient's clinical outcome.

In the present study, we report the synthesis of gold nanorod/mesoporous silica/gadolinium oxide carbonate hydrate core/shell nanoparticles (AuNR@mSiO2@Gd2O(CO3)2H2O NPs) and the application as a trimodal contrast agent for magnetic resonance imaging (MRI), X-ray computed tomography (CT), and photoacoustic (PA) imaging.

The synthesis of core-shell structured composite NPs as contrast agent is illustrated in Scheme 1. The NPs compose gold nanorod (NR)/mesoporous silica (mSiO2)/Gd2O(CO3)2H2O core-shell particles with a polyethylene glycol (PEG) coating. The morphological structure of the composed NPs was characterized by transmission electron microscopy (TEM) and high-angle annular dark-field−scanning transmission electron microscopy (HAADF−STEM). In vitro biocompatibility evaluation of the NPs on A549 cells suggested low toxicity and good biocompatibility, which make the NPs suitable for clinical applications.

In phantom examination that was preformed in vitro, we studied the composite NPs coated with ca. 2 nm, 8 nm, and 15 nm shell-thickness of Gd2O(CO3)2H2O. In MRI imaging, the NPs were able to generate MR contrast on both T1- and T2-weighted images. The magnetic relaxivities r1 and r2 were estimated 42.5 s-1 mM-1 and 64.0 s-1 mM-1 of the Gd coating, respectively, which is more than 7-8 times higher than those of a clinical contrast agent Gadovist. For CT imaging, both gold NRs and gadolinium in the coating layers contribute to CT contrast. The attenuation of the composite particles, containing 2 mM Au and 42 mM Gd, was Hounsfiled unit (HU) 342 HU, higher than the value of commercial CT contrast agent of Visipaque with the same concentration of Iodine (188 HU). Under a tunable laser source (680-970 nm), the NPs showed strong, stable and a broad wavelength range of photoacoustic (PA) signal with peak absorbance at 830 nm. After systemic administration in mice, the composited NPs showed significant contrast enhancement under PA imaging in various organs, for example liver and spleen. The dynamic biodistribution of the composited NPs was successfully exanimated in albino C57/BL6 mice up to 48 hours post injection.

In conclusion, our in vitro and in vivo data demonstrated the AuNR@mSiO2@Gd2O(CO3)2H2O NPs have high potency as contrast agents for three imaging modalities, MRI / CT / PA, as well as being biocompatible.

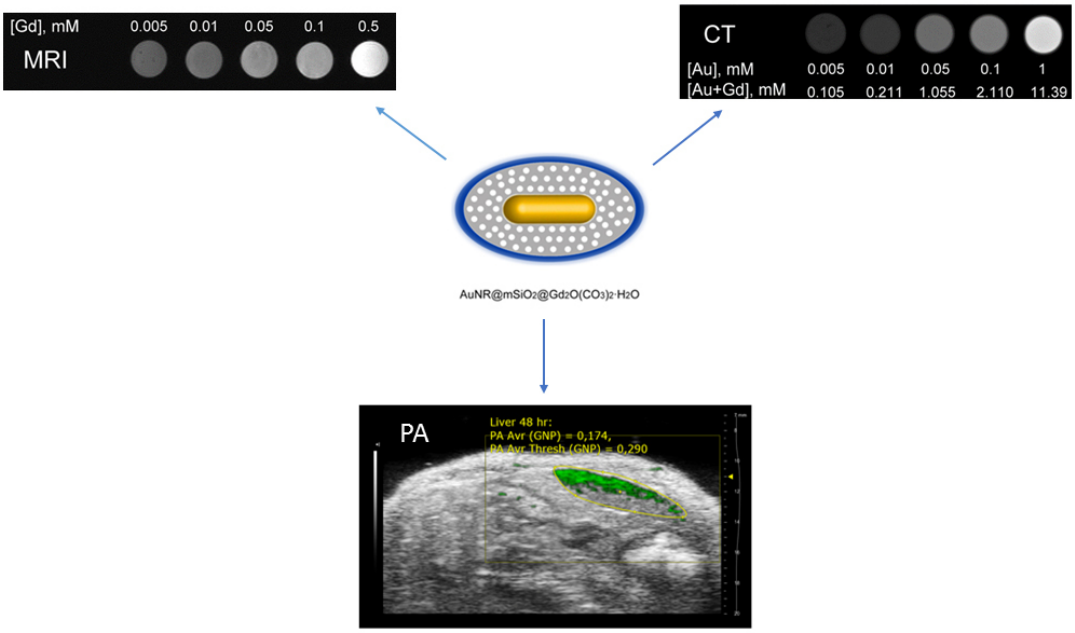
[Gd], mM
0.005
0.01
0.05
0.1
0.5
MRI
CT
[Au], mM
0.005
0.01
0.05
0.1
1
[Au+Gd], mM
0.105
0.211
1.055
2.110
11.39
AuNR@mSiO2@Gd2O(CO3)2·H2O
PA
Liver 48 hr:
PA Avr (GNP) = 0,174,
PA Avr Thresh (GNP) = 0,290

IMAGE CAPTION:

SESSION TITLE: Poster Session 01

CONTROL ID: 2735603

TITLE: Toward Single-Color Carbon Nanotube Fluorescence Microscopy

PRESENTER: Rachel Langenbacher

AUTHORS (FIRST NAME, LAST NAME): Rachel Langenbacher[4], J. Budhathoki-Uprety [1], D. Roxbury[1], Prakrit V. Jena[1], Jackson Harvey[3], Daniel A. Heller[2]

INSTITUTIONS (ALL):

1. Molecular Pharmacology, Memorial Sloan Kettering Cancer Center, New York, NY, United States.
2. Molecular Pharmacology and Chemistry, Memorial Sloan Kettering Cancer Center, New York, NY, United States.
3. Pharmacology, Weill Cornell, New York, NY, United States.
4. Pharmacology, Weill Cornell Medicine, New York, NY, United States.

ABSTRACT BODY:

Abstract Body: The properties of single-walled carbon nanotubes make them well-suited for potential uses in imaging and sensing applications. Their environmentally-sensitive, photostable emission does not exhibit the blinking phenomenon observed with other nanostructures such as quantum dots, and they emit in the near-infrared where tissue autofluorescence is low, making them ideal for imaging in tissue or cells. Due to the large number of optically distinct emitters, nanotube-based probes could potentially be developed for extensive multiplexed imaging applications. Although single-walled carbon nanotubes are synthesized as a heterogeneous mixture of many different chiralities, aqueous two-phase extraction methods allow enrichment of single nanotube chiralities to the purities needed for imaging applications. We developed hyperspectral microscopy instrumentation and techniques to distinguish between 17 optically distinct nanotube chiralities, each with a narrow and distinguishable near-infrared emission band. We are also developing polymeric materials to facilitate probe development. Polycarbodiimides are helical polymers which allow for highly modular derivitization. Polycarbodiimides can non-covalently encapsulate carbon nanotubes to enable optical modulation and diverse surface functionalization. We will discuss how polycarbodiimide-nanotube complexes can be developed for near-infrared imaging applications.

(No Image Selected)

SESSION TITLE: Poster Session 01

CONTROL ID: 2735666

TITLE: Breast Cancer Targeting Peptide: A New Method
To Deliver Imaging Agents For Breast Cancer Detection?

PRESENTER: Irene Evans

AUTHORS (FIRST NAME, LAST NAME): Irene M. Evans[2], Callie J. Donahue[2], Aflah Hanafiah[2], Norfatini A. Omar[2], Elizabeth A. Pattie[2], A. K. Embong[2], Hans F. Schmitthenner[1], Kamaljit Kaur[3]

INSTITUTIONS (ALL):

1. School of Chemistry and Materials Science , Rochester Institute of Technology, Rochester , NY, United States.
2. The Thomas H. Gosnell School of Life Sciences, Rochester Institute of Technology, Rochester, NY, United States.
3. Chapman University School of Pharmacy, Chapman University , Irvine, CA, United States.

ABSTRACT BODY:

Abstract Body: Post-metastatic and primary cancers are often very difficult to both detect and treat and delayed detection and inefficient treatment methods lead to higher patient mortality. Targeted Molecular Imaging Agents (TMIAs) are small molecules that preferentially bind to receptors that may be overexpressed on cancer cells, presenting more effective techniques for both detecting and treating a primary cancer or a cancer after metastasis has occurred. A 10mer peptide targeting molecule has been found to effectively bind multiple types of breast cancers, including triple-negative breast carcinomas[1,2]. This 10mer peptide has been conjugated with the near infra-red Cy5.5 fluorophore and used to assess binding to various cell types. We have termed the Cy5.5 fluorophore 10mer peptide conjugate, M1. TMIA M1 receptor binding and cancer-type specificity is being investigated by observing binding and endocytosis of the M1 agent via confocal laser microscopy. M1 was applied to both breast cancer cell lines MCF-7 and triple-negative line MDA-MB-231 to determine binding to breast cancer cells. To determine cancer specificity, binding of M1 to lung and prostate cancer cell lines and non-cancerous endothelial cells was performed to examine cell-specificity and targeting. Due to specificity and targeting to breast cancer, M1 should prove useful for delivery of imaging agents and chemotherapeutic drugs to detect and treat breast cancer.

(No Image Selected)

SESSION TITLE: Poster Session 03

CONTROL ID: 2759015

TITLE: Balancing passive and active tumor targeting using fluorescent, riboflavin-functionalized multi-arm PEG drug carriers

PRESENTER: Fabian Kiessling

AUTHORS (FIRST NAME, LAST NAME): Tsvetkova Yoanna[1], Nataliia Beztsinna[2], Maike Baues[1], Dionne Klein[3], Anne Rix[1], Susanne Golombek[1], Wa'el Al Rawashdeh[1], Felix Gremse[1], Srinivas Banala[1], Wiltrud Lederle[1], Twan Lammers[1], Fabian Kiessling[1]

INSTITUTIONS (ALL):

1. Experimental Molecular Imaging, RWTH Aachen University, Aachen, Germany.
2. Institute of Chemistry & Biology of Membranes & Nano-objects, Bordeaux University , Pessac, France.
3. 3)Institute for Molecular Cardiovascular Research , RWTH Aachen University, Aachen, Germany.

ABSTRACT BODY:

Abstract Body: Active targeting Is often assumed to be able to improve drug delivery to tumors. However, active targeting of larger (>100 nm) nanomedicines has often been shown to only marginally improve tumor accumulation and sometimes even decreases the accumulated amount. Since the advantage of active targeting is rather the improvement of tumor retention and cellular internalization than of accumulation, ideal tumor targeting may be achieved by balancing effects from “enhanced permeability and retention (EPR)” and active targeting. For example, this is given for IgG antibodies with sizes of around 15-20 nm, which represent the main natural targeting agents in the human body. Therefore, we generated fluorescent, branched PEG polymers of 5 nm (10 kDa) and 15 nm (40 kDa), and actively targeted them to tumors using riboflavin derivatives. Riboflavin (RF), vitamin B2, is crucial for cellular metabolism, growth and development. It is taken up by cells through a specific pathway involving three riboflavin transporters. Besides tumor cells, activated endothelial cells and tumor macrophages show an enhanced riboflavin uptake, which enables a multi-compartmental tumor targeting.

Using µCT-FMT as well as fluorescence microscopy, the biodistribution and target site accumulation of the polymers were investigated in mice bearing angiogenic squamous cell carcinoma (A431) and prostate cancer (PC3) xenografts. The non-targeted and targeted 10 kDa PEG polymers were renally excreted and showed a short blood half-life. Their tumor accumulation was characterized by rapid inter-compartmental exchange and was clearly dependent on active targeting with RF. In contrast, the non-targeted and targeted 40 kDa PEGs circulated in the blood over several hours and strongly accumulated in tumors via EPR four times more efficiently than the small polymers. However, Rf-targeting showed no significant effect on accumulation of the 40 kD PEG over the examination period of 72 h although RF-targeting improved the cellular internalization of both polymers in both tumor models. In this context, it is noteworthy that the nanocarriers’ cell uptake in tumors was not directly correlated with the extent of accumulation. Furthermore, the size of the polymers had a strong influence on their preferential uptake by different tumor cells that are located in different tumor compartments. For instance, the highest amount of 10 kDa RF-PEG was found in the cancer cell compartment, while the highest uptake of the 40 kDa RF-PEGs was observed in tumor-associated macrophages.

In summary, using µCT-FMT imaging and fluorescence microscopy we highlight the potential of RF-mediated tumor targeting and show that drug carriers with sizes in the range of therapeutic antibodies show balanced properties with respect to passive accumulation, tissue penetration and active targeting. It is indicated that active Rf-targeting clearly improves cellular uptake but also that strong tumor accumulation does not automatically mean high cellular uptake. Furthermore, it is demonstrated that small changes in polymer size can strongly influence the compartment and the type of tumor cell being targeted.

(No Image Selected)

SESSION TITLE: Poster Session 03
CONTROL ID: 2760807
TITLE: Designing an Optimal Naphthalocyanine Based Photoacoustic Probe
PRESENTER: Mitchell Duffy
AUTHORS (FIRST NAME, LAST NAME): Mitchell Duffy[1, 2], Andreas Faust[1, 2], Oriol Planas[3], Sven Hermann[1, 2], Michael Schäfers[1, 2, 4], Santi Nonell[3], Cristian Strassert[5]
INSTITUTIONS (ALL):
1. European Institute for Molecular Imaging, Westfälische Wilhelms Universität Münster, Münster, Germany.
2. Cells in Motion (CiM) Cluster of Excellence, Westfälische Wilhelms Universität Münster, Münster, Germany.
3. Photochemistry, Instituto Quimico de Sarria, Barcelona, Spain.
4. Nuclear Medicine, Universitätsklinikum Münster, Münster, Germany.
5. Physical Institute and Center for Nanotechnology (CeNTech), Westfälische Wilhelms Universität Münster, Münster, Germany.
ABSTRACT BODY:
Abstract Body: Introduction

In order to create photoacoustic probes with properties tailored for in vivo imaging (high signal generation, peak absorption wavelength near 800nm where in vivo background is lowest, small molecule, able to be modified, low photobleaching, low quantum yields of fluorescence and singlet oxygen production and low toxicity) [1] we screened four naphthalocyanines (Nc) with varied substitution patterns and central metal ions.[2,3]
This led to a design for a contrast agent which we believe will be easily translatable and is currently being characterized in its water soluble form.

Methods

Naphthalocyanines CuNc, NiNc, SiNc and VNc were tested at 5μM by performing standard absorption spectroscopy and photoacoustic spectroscopy (PAS). To measure singlet oxygen phosphorescence kinetics was used. Using a Xe lamp and repeated absorption measurments we characterized how the photobleach. Using the MSOT photoacoustic system we were able to perform PAS, using serial diultion of the Ncs to corroborate our data.

Results

NiNc produced around two times the signal of CuNc, SiNc and VNc solubilized in toluene. Results were found to be similar in a Cremophor EL solution, except for VNc which exhibited low signal because of low solubility. SiNc, as an unsubstituted Nc, had a signal maximum (λ_m) at 774nm. CuNc and NiNc have a λ_m at 850nm(±2nm) due to their axial substitution. Distally substituted VNc exhibited an optimal λ_m at 808nm. Only SiNc produced significant fluorescence or triplet state quantum yields, 0.07 and 0.29 respectively. PAS results were confirmed by MSOT spectroscopy and the limit of detection for the Ncs could be inferred to be between 50 and 200nM.

Conclusions

To design a small molecule contrast agent tuned for translatable, in vivo photoacoustic imaging must take into consideration many properties of excited state molecules. This screen has identified Nickel(II) as the optimal central metallic ion both in terms of signal production but also generating negligible fluorescence and singlet oxygen. A distally substituted structure, meanwhile, would allows us to shift the excitation maximum into a window optimal for spectral unmixing in vivo.
A water soluble molecule combining these two properties is currently being characterized and tested in vivo.

References

[1]Weber, Beard, Bohndiek. 2016. Nature Methods

[2]Zhang, Lovell. 2016. Nanomed. Nanobiotechnol.
[3]Beziere, Ntziachristos. 2014. J. Nucl. Med
(No Image Selected)

SESSION TITLE: Poster Session 03

CONTROL ID: 2761286

TITLE: A novel highly-efficient, site-specific, and directional antibody crosslinking method for the rapid production of bispecific antibodies and the attachment of “armed” protein scaffolds to antibodies for imaging and radioimmunotherapy applications.

PRESENTER: Brian Agnew

AUTHORS (FIRST NAME, LAST NAME): Brian J. Agnew[1], Robert Aggeler[2], Shanhua Lin[3], Terry Zhang[3]

INSTITUTIONS (ALL):

1. Licensing and Commercial Supply, Thermo Fisher Scientific , Eugene, OR, United States.
2. Biosciences Division, Thermo Fisher Scientific , Eugene, OR, United States.
3. Chromatography and Mass Spectrometry Division , Thermo Fisher Scientific , San Jose, CA, United States.

ABSTRACT BODY:

Abstract Body: Bispecific antibodies have been recently used in molecular imaging for pre-targeting applications or as companion diagnostics for evaluating bispecific drug targeting. Bispecific antibodies are produced by a number of different recombinant strategies but production using these methods can be time consuming and costly, especially for preliminary screening of multiple antibody pairs. Chemical approaches have been developed which exploit the reactivity of antibody lysine or cysteine residues but result in the production of highly crosslinked unwanted species, difficult time-consuming characterization and purification of the desired products, and the lack of site-specificity of conjugation which can destroy mAb binding affinity.

Here we present a novel site-specific, directional antibody crosslinking method. Specifically, we show application in producing bispecific antibodies that contain a single crosslink between the antibody Fc glycosylation sites. The yield of the desired dimeric singly-crosslinked species is greater than 80% without purification, which is unprecedented when compared to any other in vitro chemical crosslinking technologies. We extend this method to the site-specific crosslinking of antibodies with a 25 kD IgG Fc protein used as a scaffold that can be loaded with multiple different payloads including fluorescent dyes and PET chelators ensuring preservation of antigen binding avidity.

The method involves three main steps. First, the Fc glycans are cleaved with endoglycosidase S2 leaving single core GlcNAc residues at the core glycosylation sites. Second, the core GlcNAcs are azide-activated with a mutant GalT enzyme that transfers a galactose-azide sugar onto the core GlcNAc. Thirdly, each of the antibodies in the pair is activated with one of two Diels-Alder functional groups, transcyclooctyne (TCO) or methytetrazine (Tzn). Once activated, the mAb pairs can be mixed and matched in equal molar amounts to yield site-specifically, directionally-conjugated bispecific pairs. In our second application, one of the antibodies is replaced with an IgG Fc protein and used as a scaffold for payload loading.

In preliminary studies we used the NISTmAb monoclonal antibody as a model for bispecific antibody production. Gel and enzymatic analyses of the TCO/Tzn-crosslinked antibodies confirm site-specific crosslinking at the antibody Fc glycosylation sites and demonstrate a high yield of the desired ~300 kD tetravalent bispecific species (>80%). Mass spec analyses confirms a single crosslink between the 2 antibodies. We expanded the application to demonstrate the formation of multiple bispecific pairs using 5 different existing therapeutic antibodies with high reproducibility and yield. Finally, the TCO/Tzn-functionalized NISTmAb was crosslinked to a Tzn/TCO functionalized human IgG Fc protein that was loaded with multiple fluorescent dyes yielding a ~175 kD site-specifically labeled, highly-fluorescent antibody, ensuring preservation of the IgG antigen binding domain while still carrying a high load of dyes. The antibody-Fc scaffold can be armed with any payload including dyes or chelators for use in imaging or radioimmunotherapy applications.

(No Image Selected)

SESSION TITLE: Poster Session 03

CONTROL ID: 2773082

TITLE: A Thiol Sensing Probe Based on a Caged Luciferin

PRESENTER: Mayu Hemmi

AUTHORS (FIRST NAME, LAST NAME): Mayu Hemmi[1], Yuma Ikeda[1], Yutaka Shindo[1], Shigeru Nishiyama[1], Kotaro Oka[1], Daniel Citterio[1], Koji Suzuki[1]

INSTITUTIONS (ALL):

1. Faculty of Science and Technology, Keio University Graduate School, Yokohama, Tokyo, Japan.

ABSTRACT BODY:

Abstract Body: Thiols are indispensable biomolecules associated with diseases including diabetes and cancers. Therefore, the simple and sensitive detection of biothiols in vivo is desirable. While conventional fluorescent probes for thiols allow simple and noninvasive detection, they suffer from setbacks such as autofluorescence, hence limiting their uses in bioimaging.[1] In contrast, bioluminescence has gained wide attention for its high sensitivity and biocompatibility[2,3]; more specifically, the substrate “luciferin” required for the enzymatic light-emitting reaction by the firefly is known for its high quantum yield and has been applied to various bioluminescent probes. Therefore, this research focuses on the development of a selective probe for thiols, which allows dual detection in both fluorescence and bioluminescence.

In 2014, a highly selective fluorescent probe for thiols was reported, which possesses a sulfonate ester that can be cleaved only by thiols to release the fluorophore.[4] We anticipated that this mechanism can be applied to bioluminescence by attaching this ligand to the 6’-position of firefly luciferin, which affects the luciferase-substrate reaction and thus exhibits no luminescence.

Probe 1 was successfully synthesized in a total of 6 steps. To assess its reactivity with thiols, probe 1 was incubated with increasing concentrations of cysteine, a model compound for thiols, and its changes in fluorescence and bioluminescence were observed. A linear calibration curve was obtained for the thiol concentration-dependent fluorescence emission ratio values of probe 1 (428 nm) and the free luciferin (533 nm), and the LOD was calculated to be 0.33 μM. This ratiometric fluorescence output allows for a valid quantification of cysteine within its intracellular concentrations. Furthermore, while probe 1 hardly emitted bioluminescence, increasing concentrations of cysteine resulted in the generation of a new peak at 564 nm, therefore confirming the release of D-luciferin from this reaction.

Next, probe 1 was incubated with various biothiols as well as other biological nucleophiles such as amino acids and disulfides to assess its selectivity. The addition of thiols such as GSH and cysteine resulted in over 100-fold increase in bioluminescence, whereas no significant increase in both fluorescence and bioluminescence was observed for other analytes including disulfides.

Finally, to examine the applicability of probe 1 towards visualization of intracellular biothiols, probe 1 was incubated with HeLa cells for 30 min. and its change in fluorescence (533 nm) was monitored. Bright fluorescence was observed, presumably due to the generation of D-luciferin from the thiol-dependent reaction. Furthermore, the addition of NEM, a known thiol scavenger, elicited a sharp decrease in fluorescence.

In summary, the reactivity of probe 1 towards biothiols as well as its cell permeability was evaluated and confirmed and we anticipate the application of this probe for future uses in vivo.

References:

1) T. Troy, Mol. Imaging, 2004, 2, 9. 2) G. Van de Bittner, PNAS, 2010, 50, 21316. 3) B. Ke, Anal. Chem., 2015, 87, 9110. 4) S. Malwal, Chem. Commun., 2014, 50, 11533.

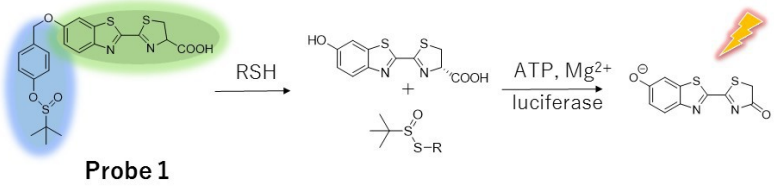

Fig. 1 Reaction mechanism of Probe 1

IMAGE CAPTION:

SESSION TITLE: Poster Session 03

CONTROL ID: 2784827

TITLE: Near-Infrared Emitting Lanthanide(III)-Based Molecules, Macromolecules and Nanomaterials: New Generation of Probes for in vitro Optical Imaging

PRESENTER: Ivana Martinic

AUTHORS (FIRST NAME, LAST NAME): Ivana Martinic[1, 2], Svetlana V. Eliseeva[1], Regis Delatouche[5], Tu N. Nguyen[4], David Gosset[1], Tianyi Luo[6], Sylvain Routier[5], Nathaniel Rosi[6], Vincent . Pecoraro[4], Franck Suzenet[5], Stephane Petoud[1, 3]

INSTITUTIONS (ALL):

1. Centre de Biophysique Moléculaire, CNRS, UPR 4301, Orleans, France.
2. SATT Grand Centre, Clermont-Ferrand, France.
3. Department of Inorganic, Analytical and Applied Chemistry, University of Geneva, Geneva, Switzerland.
4. Department of Chemistry, University of Michigan, Ann Arbor, MI, United States.
5. Institute of Organic and Analytical Chemistry, Orleans, France.
6. Department of Chemistry, University of Pittsburgh, Pittsburgh, PA, United States.

ABSTRACT BODY:

Abstract Body: Background: Fluorescence optical imaging is a highly sensitive technique which requires extremely small amount of probes. Imaging in the near-infrared (NIR) region or in the biological diagnostic window attracts particular attention due to the minimal autofluorescence and reduced light scattering. Most of the commercial fluorescent probes rely on organic dyes or quantum dots which exhibit drawbacks. Lanthanide(III) (Ln^{3+})-based probes (LPs) possess unique optical properties e.g. sharp emission bands, large differences between excitation and emission wavelengths and strong resistance toward photobleaching. The low absorbance of free Ln^{3+} requires the use of appropriate chromophores for sensitization of their luminescence.[1] We present here the synthesis, characterization and in vitro fluorescence imaging with several families of LPs.

Methods: $Yb^{3+}[Zn(II)MC_{pyzHA}]$ was synthesized by the reaction of pyrazinehydroxamic acid (H_2pyzHA) with Zn^{2+} and Yb^{3+} triflates. The $L1Nd^{3+}$ complex was obtained by interaction between the ligand L1 and Nd^{3+} nitrate in a 1:1 ratio. AQ1,nOH-Yb@PS/PEG (n= 4, 8) nanoparticles were obtained by encapsulation of 1,4- or 1,8-dihydroxyanthraquinones and Yb^{3+} triflates in the NH_2-functionalized 100 nm polystyrene beads (PS/NH_2) followed by further functionalization of their surface with polyethylene glycol (PEG). (Ln_8-)G3P-(aza-BODIPY)$_n$ (n= 16, 32; Ln= Yb^{3+}, Nd^{3+}) were synthesized via peptide coupling of aza-BODIPY with NH_2-functionalized generation-3 polyamidoamine (G3P) dendrimers, and further treatment with a 8-time excess of Yb^{3+} or Nd^{3+} nitrates. Absorption/excitation/emission spectra, luminescence lifetimes, quantum yields and photostability were measured. Uptake of LPs by HeLa cells was analyzed by confocal and epifluorescence microscopies in the visible/NIR and by flow cytometry. Cytotoxicity was evaluated by Alamar Blue assay.

Results: Novel LPs have been designed and successfully used for visible/NIR in vitro imaging and their advantages over the current fluorescent probes have been demonstrated. In particular, (i) non-permeable and photostable polymetallic metallacrown (MC) complexes, $Yb^{3+}[Zn(II)MC_{pyzHA}]$, demonstrated their applicability for labelling of cell necrosis[2]; (ii) monometallic $L1Nd^{3+}$, the first LP with excitation and emission wavelengths within the biological diagnostic window, demonstrated a deeper penetration through tissues of different origins and a more sensitive detection; (iii) polymetallic AQ1,nOH-Yb@PS/PEG nanoparticles represent a major breakthrough in the design of LPs with improved properties by simplifying screening of efficient chromophores, and (iv) polymetallic G3P dendrimers, (Ln_8-)G3P-(aza-BODIPY)$_n$, demonstrated possibility for tuning of photophysical properties, photostability and cellular uptake by changing the number of chromophores on their periphery and by the presence and/or nature of Ln^{3+}.

Conclusions: The reported LPs due to the number of advantageous properties represent significant breakthroughs toward the creation of new generation of optical imaging probes.

References: 1. Martinić I.,et al., J.Lumin. 2017, 189, 19.

2. Martinić I.,et al., JACS, 2017, DOI: 10.1021/jacs.7b01587

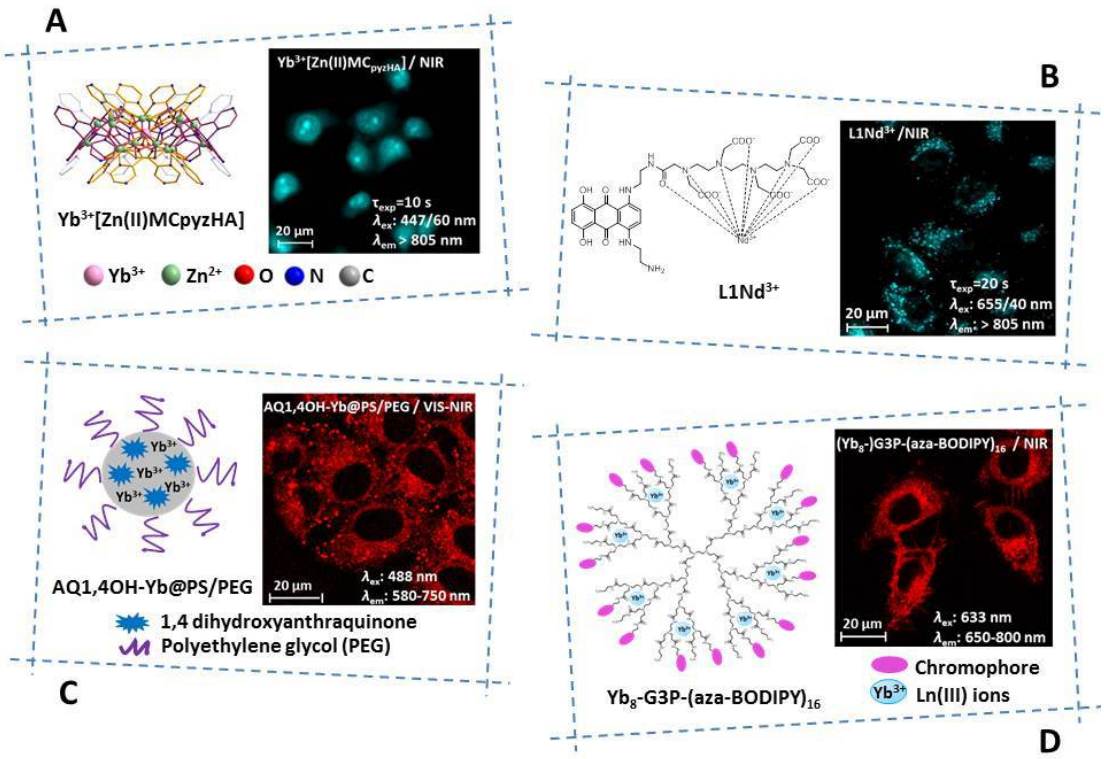

Crystal structure of $Yb^{3+}[Zn(II)MC_{pyzHA}]$ (A, left). Schematic representations of: $L1Nd^{3+}$ (B, left), AQ1,4OH-Yb@PS/PEG nanoparticle (C, left) and Yb_8-G3P-(aza-BODIPY)$_{16}$ dendrimer (D, left). Epifluorescence microscopy of: necrotic HeLa cells incubated with 45 µM $Yb^{3+}[Zn(II)MC_{pyzHA}]$ during 15 min (λ_{ex}: 447nm/60nm, λ_{em}> 805nm, τ_{exp} : 10s) (A, right) and viable HeLa cells incubated with 5 µM $L1Nd^{3+}$ during 3 h (λ_{ex}: 655nm/40nm; λ_{em}> 805nm, τ_{exp}: 20 s) (B, right). Confocal microscopy of HeLa cells incubated with: 250 µg/mL of AQ1,4OH-Yb@PS/PEG during 3h and 30 min (λ_{ex}: 488nm; λ_{em}: 580–750nm) (C, right) and 1.5 µM Yb_8-G3P-(aza-BODIPY)$_{16}$ during 30 min (λ_{ex}: 633nm; λ_{em}: 650-800nm) (D, right).

IMAGE CAPTION: Crystal structure of Yb^{3+}[Zn(II)MC_{pyzHA}] (A, left). Schematic representations of: $L1Nd^{3+}$ (B, left), AQ1,4OH-Yb@PS/PEG nanoparticle (C, left) and Yb_8-G3P-(aza-BODIPY)$_{16}$ dendrimer (D, left). Epifluorescence microscopy of: necrotic HeLa cells incubated with 45 μM Yb^{3+}[Zn(II)MC_{pyzHA}] during 15 min (λ_{ex}: 447nm/60nm, λ_{em} > 805nm, τ_{exp}: 10s) (A, right) and viable HeLa cells incubated with 5 μM $L1Nd^{3+}$ during 3 h (λ_{ex}: 655nm/40nm; λ_{em} > 805nm, τ_{exp}: 20 s) (B, right). Confocal microscopy of HeLa cells incubated with: 250 μg/mL of AQ1,4OH-Yb@PS/PEG during 3h and 30 min (λ_{ex}: 488nm; λ_{em}: 580–750nm) (C, right) and 1.5 μM Yb_8-G3P-(aza-BODIPY)$_{16}$ during 30 min (λ_{ex}: 633nm; λ_{em}: 650-800nm) (D, right).

SESSION TITLE: Poster Session 03

CONTROL ID: 2787780

TITLE: Development and Assessment of Multifunctional Molecular Probe for Fluorescence and Photoacoustic Imaging

PRESENTER: Hyeon Sik Kim

AUTHORS (FIRST NAME, LAST NAME): Hyeon Sik Kim[1], Sung-Hwan You[1], hee seung yoon[1], jung-joon min[1]

INSTITUTIONS (ALL):

1. Nuclear Medicine, Chonnam national university medical school, Gwangju, Korea (the Republic of).

ABSTRACT BODY:

Abstract Body: Purpose: Dual-modular imaging approaches by combining NIR fluorescence (FLI) and photoacoustic imaging (PAI) demands suitable contrast agents enabling dual-modular signal production. The current study focused on exploiting small molecules for dual-modular PA and NIR fluorescence imaging. Herein, we introduce novel squaraine (SQ), based agent (JJ25), dyes for this purpose and report the rational preparation and conjugation with cyclic RGD (cRGD), JJ25-RGD. Materials and methods: Human cancer cell lines (M21 and M21L) were harvested and suspended in 100 μL of PBS prior to subcutaneous injection into the right thigh in five nude mice. Animals were sacrificed after 1 day, and the tumor and other organs were excised for ex vivo experiments. For the NIR fluorescence experiments, the JJ25 or JJ25-RGD were administered intravenously (i.v.) into the tail vein. Optical data acquisition and analysis were conducted using the Maestro 2.0 in vivo imaging system. PA signals were obtained by a Nexus 128 (ENDRA). The JJ25 or JJ25-RGD was injected into tumor-bearing mouse through the tail vein. The PA signals of the mouse tumors were acquired pre-injection (0 h) and at 1, 2, 4, and 6 hr at 680, 750, and 900 nm wavelengths. Results: JJ25 showed intense absorption and fluorescence properties above 650 nm in aqueous conditions, with a maximum absorption at 665 nm, and emission at 680 nm. PA signal scanning experiments also showed the maximum signal intensity in the range of the 680-700 nm. For an active-targeting ability, JJ25 was conjugated with cRGD to target $\alpha_v\beta_3$ integrin that is overexpressed in numerous cancer cells and angiogenic cells. A series of in vitro, in vivo and ex vivo fluorescence imaging studies showed that JJ25-RGD stained and targeted $\alpha_v\beta_3$ overexpressing tumor cells and xenografts, which was clearly imaged by FLI and PAI. Conclusion: we demonstrated the feasibility and future potential of a SQ-based imaging agent for hybrid PA and NIR dual-imaging of cancer. JJ25-RGD has the ability to specifically detect the $\alpha_v\beta_3$ target in living animals while maintaining its NIR fluorescence and PA signals.

(No Image Selected)

SESSION TITLE: Poster Session 03

CONTROL ID: 2790417

TITLE: Development of coelenterazine derivative for cysteine detection

PRESENTER: Nanako Nomura

AUTHORS (FIRST NAME, LAST NAME): Nanako Nomura[1], Ryo Nishihara[1], Sung Bae Kim[2], Naoko Iwasawa[1], Daniel Citterio[1], Shigeru Nishiyama[1], Koji Suzuki[1]

INSTITUTIONS (ALL):

1. Applied Chemistry, Keio University, Yokohama-shi, Japan.
2. National Institute of Advanced Industrial Science and Technology, Tsukuba-shi, Japan.

ABSTRACT BODY:

Abstract Body: Cysteine (Cys), one of the biothiols along with homocysteine (Hcy) and glutathione (GSH), is an indicator of various types of diseases. Elevated levels of Cys are related to neurotoxicity and cardiovascular diseases, on the other hand, Cys deficiency is involved in liver damage, skin lesions and weakness. In addition, Cys and GSH play essential roles in biological redox homeostasis as antioxidant reservoir to regulate the level of ROS. These biothiols are closely related. For example, Cys deficiency results in perturbation of the GSH redox state, because Cys is required for the synthesis of GSH.

Various detection methods such as HPLC and colorimetry have been reported. However, these methods are destructive to tissues and cells. Recently, our research group has been focusing on a bioluminescent system for cysteine detection to achieve real time imaging. Bioluminescence is based on an enzymatic reaction, offering a noninvasive approach to the study of biological phenomena.

There have been numerous reports about various bioluminescent substrates. Coelenterazine (CTZ), the bioluminescent substrate of Renilla, is widely used for biological analysis because it does not require cofactors for the luminescence reaction. This research mainly focuses on the development of a cysteine probe by modifying the CTZ structure. The C3-position of CTZ was modified and a conventional ligand reacting with Cys by Michael addition was attached (CysOMeCTZ). Even though CTZ is unstable in aqueous media, modification at the C-3 position inhibits its degradation and increases its stability.

First, it was confirmed by HPLC analysis that CysOMeCTZ showed high reactivity with Cys, confirming its suitability as a sensitive Cys detection reagent. Next, the bioluminescence intensity of CysOMeCTZ in the presence of Cys was measured. In the absence of Cys, no luminescence was observed, while the intensity gradually increased following the addition of Cys. Furthermore, a linear response in the bioluminescence intensity was obtained up to 100 μM for the Cys concentration-dependent calibration curve. The limit of detection was 4.7 μM. Thus, CysOMeCTZ is suitable for the detection of Cys, which is present at an intracellular concentration of about 100 μM. Moreover, the selectivity against other amino acids was measured and a high selectivity for Cys was successfully confirmed.

When evaluating selectivities against other biothiols including Hcy and GSH, highest reactivity of the probe was observed to Cys, while also showing a response to GSH. This trend of selectivity differed from earlier reported fluorescent probes modified by the same ligand. Finally, the reactivity towards other thiol compounds was investigated. Ligand elimination was also observed for thiol compounds lacking the amino functional group. Therefore, CysOMeCTZ can detect GSH. In conclusion, the characteristics of CysOMeCTZ indicate its suitability to investigate the relationship between Cys and GSH, for example their ability as antioxidant biomarkers.

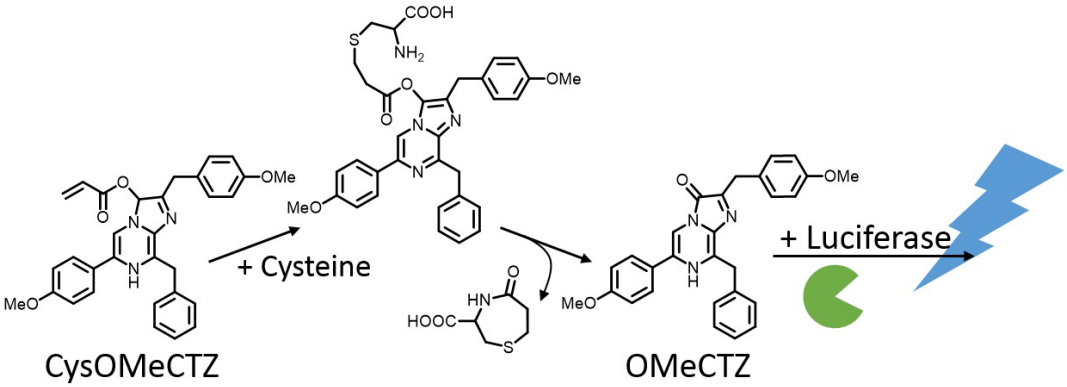
COOH
NH2
S
OMe
MeO
+ Cysteine
HN
HOOC
S
+ Luciferase
CysOMeCTZ
OMeCTZ

IMAGE CAPTION:

SESSION TITLE: Poster Session 03

CONTROL ID: 2803454

TITLE: Hyperpolarized [^{13}C, ^{15}N]Xanthine as a probe for evaluating Xanthine oxidase activity in vivo

PRESENTER: Valentina Di Gialleonardo

AUTHORS (FIRST NAME, LAST NAME): Valentina Di Gialleonardo[1], Roozbeh Eskandari[1], Kayvan R. Keshari[1]

INSTITUTIONS (ALL):

1. radiology, memorial sloan kettering cancer center, New York , NY, United States.

ABSTRACT BODY:

Abstract Body: Xanthine oxidase (XO) in an enzyme present ubiquitously in nearly all mammalian cells. In several pathological conditions, such as in cancer and a series of inflammatory process where reactive oxygen species (ROS) are involved, intracellular and plasmatic XO is increased. XO oxidizes xanthine (XA) to uric acid (UA) using superoxide (O_2^-) as a cofactor. In this study, a new probe [2-^{13}C,1,3-$^{15}N_2$]3,7-dihydro-1H-purine-2,6-dione ([^{13}C, $^{15}N_2$]XA) has been developed to evaluate XO activity in vitro and in vivo using hyperpolarized MRI (HP MRI). Methods: [^{13}C, $^{15}N_2$]XA was synthesized using previously published methods. For hyperpolarization experiments, a preparation containing 0.2 M [^{13}C, $^{15}N_2$]XA and the OX063 radical was hyperpolarized using a SPINlab hyperpolarizer. T_1 measurements were performed using 1T Magritek Spectrometer. For the acquisition of HP spectra, data were acquired with a 5 s repetition time and 15° excitation for a total of 45s. In vitro enzymatic experiments to evaluate the activity of XO were performed using 100 mg of mouse liver extract together with a PMS/NADH+ system to generate $O2^-$. ^{13}C spectra were acquired using a 14.1 T NMR spectrometer. Western blots for XO and XA transporter were performed using 20 ng of protein extract from 14 cell lines. In vitro fluorescent microscopy using CellROX green was performed in U251 cells to evaluate intracellular ROS and the effect of XA as an ROS scavenger. Results: HP [^{13}C, $^{15}N_2$]XA was synthesized from double labeled Urea (^{13}C, ^{15}N urea) with overall yield of 30%. The chemical shift between [^{13}C, $^{15}N_2$]XA and [^{13}C, $^{15}N_2$]UA was of 0.8 ppm. As expected, splitting of the ^{13}C carbon was observed due the nitrogen labeling (Fig. 1A). [^{13}C, $^{15}N_2$]XA was hyperpolarized and after dissolution the spectra were then fit to a mono-exponential decay function, correcting for flip angle, to determine the spin-lattice relaxation time. A T_1 of 77 ± 1.4 s was measured (Fig. 1B). Additional in vitro NMR experiments demonstrated that XA could be oxidized in less than 10 minutes to UA in liver extracts in the presence of O_2^- (Fig. 1C). 14 different cancer cell lines from renal, sarcoma, lung, prostate, breast, pancreatic, oral, epithelial cancer were screened to evaluate expression of XA transporter and XA oxidase. In all the cells a high expression of XO was observed, whereas XA transporter was variable between the cell lines, with the largest expression in U251 cells (Fig. 1D). Therefore, this cell line was used for further in vitro fluorescence experiments. Figure 1E shows a panel of fluorescent images, using CellRox as an indicator of oxidative stress, treatment with menadione dramatically increases oxidative stress and this can be reduced using co-incubation with XA for 45 min, demonstrating that XA can rapidly participate in this enzymatically catalyzed antioxidant system. Conclusions: A novel redox probe, ([^{13}C, $^{15}N_2$]XA has been successfully synthesized. This probe has a long T_1 and differential chemical shift, which is necessary for future imaging in vivo. Furthermore, this work demonstrates the potential for HP [^{13}C, $^{15}N_2$]XA to probe an enzymatically catalyzed antioxidant system, which is specific to O2-.

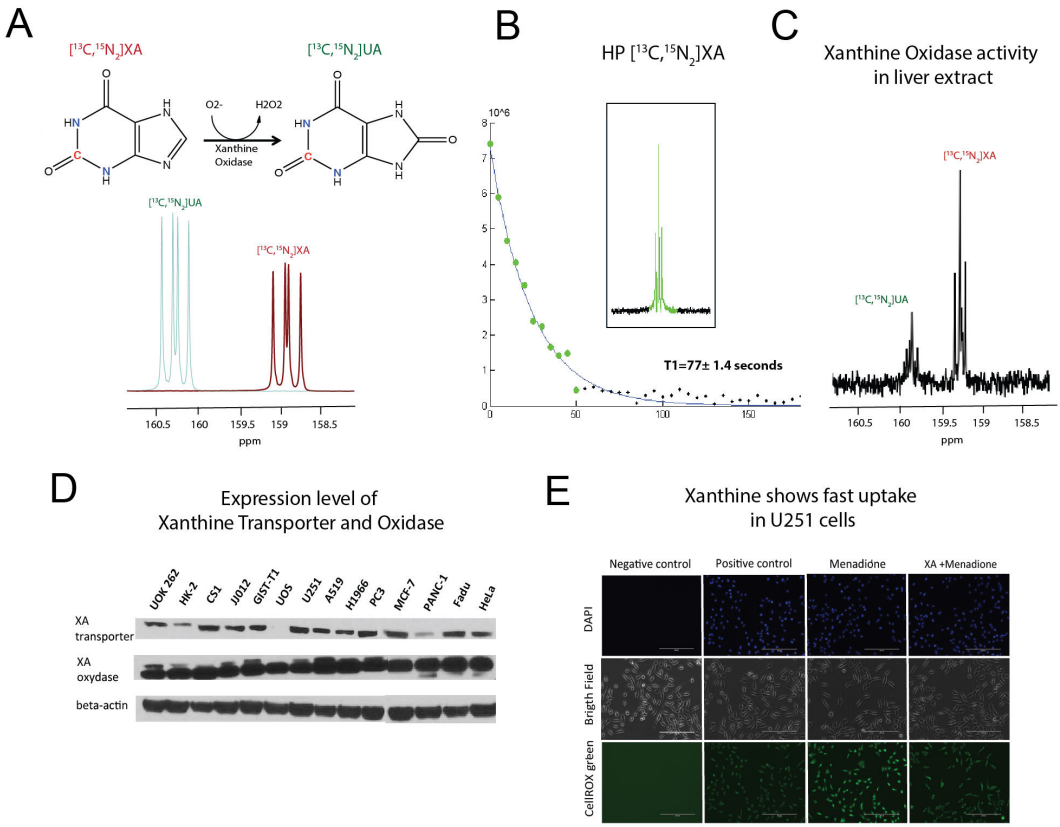

Figure 1. A) Chemical structure and chemical shift between [^{13}C, $^{15}N_2$]XA and [^{13}C, $^{15}N_2$]UA . **B)** Hyperpolarized HP [^{13}C, $^{15}N_2$]XA and T_1 measurement. **C)** [^{13}C, $^{15}N_2$]XA conversion to [^{13}C, $^{15}N_2$]UA in liver extract in presence of O_2-. **D)** Expression level of Xanthine transporter and Xanthine oxidase in several cell lines. **E)** Fluorescece microscopy and uptake study of [^{13}C, $^{15}N_2$]XA in U251 cells.

IMAGE CAPTION: Figure 1. A) Chemical structure and chemical shift between [^{13}C, $^{15}N_2$]XA and [^{13}C, $^{15}N_2$]UA . **B)** Hyperpolarized HP [^{13}C, $^{15}N_2$]XA and T_1 measurement. **C)** [^{13}C, $^{15}N_2$]XA conversion to [^{13}C, $^{15}N_2$]UA in liver extract in presence of O_2-. **D)** Expression level of Xanthine transporter and Xanthine oxidase in several cell lines. **E)** Fluorescece microscopy and uptake study of [^{13}C, $^{15}N_2$]XA in U251 cells.

SESSION TITLE: Poster Session 03

CONTROL ID: 2803459

TITLE: Development of a multimodality molecular imaging probe for the in vitro and in vivo evaluation of a cellulose nanocrystal drug delivery system

PRESENTER: SURACHET IMLIMTHAN

AUTHORS (FIRST NAME, LAST NAME): SURACHET IMLIMTHAN[2], Alexandra M. Correia[1], Dave Lumen[2], Vimalkumar Balasubramanian[1], Marko J. Vehkamäki[2], Mauri A. Kostiainen[3], Hélder A. Santos[1], Anu J. Airaksinen[2], Mirkka Sarparanta[2]

INSTITUTIONS (ALL):

1. Division of Pharmaceutical Chemistry and Technology, University of Helsinki, Helsinki, Finland.
2. Department of Chemistry, University of Helsinki, Helsinki, Finland.
3. Department of Bioproducts and Biosystems, Aalto University, Espoo, Finland.

ABSTRACT BODY:

Abstract Body: Background: Single-photon emission computed tomography (SPECT) is a noninvasive imaging widely available and used in clinic for obtaining quantitative information on tissue biochemistry. ^{111}In is a radioactive isotope for SPECT with its relatively long physical half-life (2.80 days) suitable for tracking nanoscale drug delivery in vivo within the time frame of biological interactions such as tumor accumulation, elimination and passage through the gastrointestinal tract. A multimodality probe is generated by adding fluorescence dye, allowing the use of the same imaging probe to observe events that beyond SPECT spatial resolution. Cellulose nanocrystal (CNC) shows potential as a nanocarrier in drug delivery. [1,2] CNC has a reactive surface that allow the incorporation of a wide range of functional groups, labels and therapeutic payloads. Herein, we aim to prepare a CNC-installed DOTA for labeling with ^{111}In and fluorescent dye in order to study cytotoxicity, biocompatibility and behavior of CNC in vitro and in vivo.

Methods: DOTA hydrazide precursor was synthesized via methylester and hydrazinolysis reactions of 1,4,7,10-Tetraazacyclododecane-1,4,7-tris-tert-butyl acetate-10-acetic acid. The DOTA hydrazide and Cyanine5 hydrazide were selectively bonded with the aldehyde on CNC reducing end and hydroxyl activated CDI in dried DMSO at 60 °C under argon. The labeled CNC were characterized by zeta potential and electron microscopy. The cytotoxicity and cellular uptake were investigated in murine RAW 264.7 macrophages. The cells were incubated 24 hours with unmodified CNC, DOTA-CNC, and Cy5-CNC at 5, 25, and 100 µg/ml for cytotoxicity and Cy5-CNC at 100 µg/ml for cellular uptake assays. A LIVE/DEAD® cytotoxicity assay was used for the determination of cell viability. Both cell viability and Cy5-labeled CNC uptake were studied with confocal fluorescence microscopy. Experiments to optimize the ^{111}In-labeled DOTA-Cy5-CNC construct and biodistribution studies in CD-1 mice are underway.

Result: The ^{1}H and ^{13}C NMR, and mass spectrometry revealed the success of the DOTA hydrazide synthesis. The zeta potential was not significantly altered in presence of CNC surface modification in comparison to the unmodified CNC and the average size of CNC was 5 nm in diameter and 200 nm in length. Both unmodified and modified CNC showed good biocompatibility in RAW 264.7 cells after 24 hours incubation together with an interaction between the CNC nanoparticles and macrophages in vitro warranting in vivo evaluation.

Conclusions: The multimodal CNC developed herein can be used for the evaluation of the suitability of the material for the construction of molecular imaging probes and drug delivery systems in vitro and in vivo with SPECT and fluorescence imaging, a key step in advancing the biomedical applications of nanocrystalline cellulose.

Acknowledgements: Financial support from the Academy of Finland (decision no. 278056 and 298481) and the University of Helsinki is gratefully acknowledged.

References:

(1) Rajalaxmi, D. et al. RSC Advances 2012, 2, 3403 – 3409

(2) Klemm, D. et al. Angewandte Chemie International Edition 2011, 50, 5438–5466.

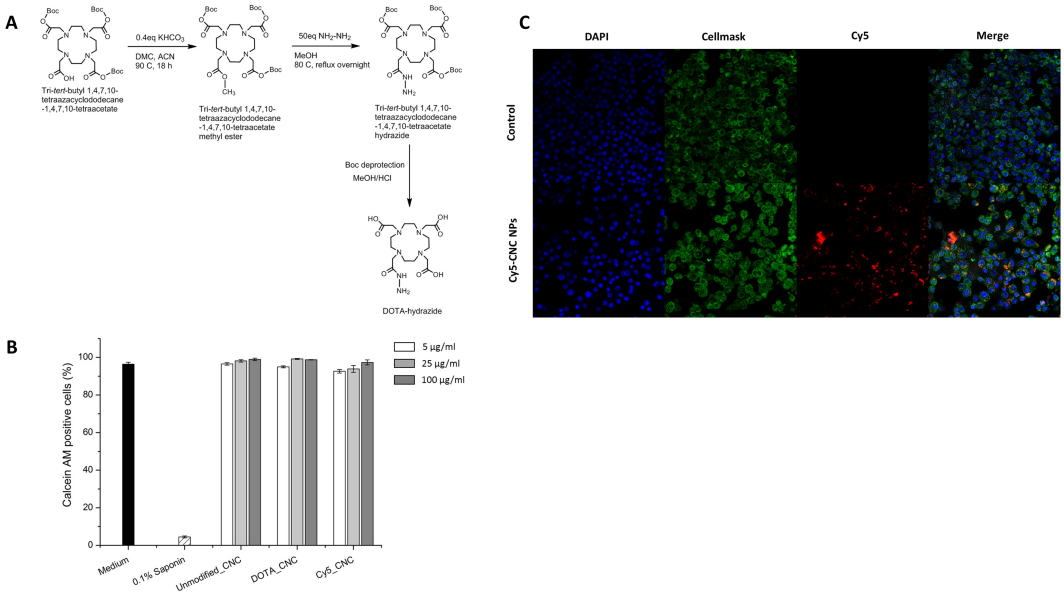

Figure 1. (A) The synthesis scheme of DOTA hydrazide **(B)** *In vitro* cytotoxicity study in RAW 264.7 macrophages of unmodified-CNC, DOTA-CNC, and Cy5-CNC at 5, 25, and 100 µg/ml for 24 hours **(C)** *In vitro* confocal microscopy study of cellular uptake of Cy5-CNC at 100 µg/ml for 24 hours in RAW 264.7 macrophages

IMAGE CAPTION: Figure 1. (A) The synthesis scheme of DOTA hydrazide **(B)** *In vitro* cytotoxicity study in RAW 264.7 macrophages of unmodified-CNC, DOTA-CNC, and Cy5-CNC at 5, 25, and 100 µg/ml for 24 hours **(C)** *In vitro* confocal microscopy study of cellular uptake of Cy5-CNC at 100 µg/ml for 24 hours in RAW 264.7 macrophages

SESSION TITLE: Poster Session 03

CONTROL ID: 2804320

TITLE: Engineering of monobody conjugates for human EphA2-specific optical imaging

PRESENTER: Min-A Kim

AUTHORS (FIRST NAME, LAST NAME): Min-A Kim[1, 2], Hee Seung Yoon[3, 2], Seung-Hwan Park[4], Dong-Yeon Kim[3], Ayoung Pyo[3], Hyeon Sik Kim[3], Jung-Joon Min[3], Yeongjin Hong[1]

INSTITUTIONS (ALL):

1. Department of Microbiology, Chonnam National University Medical School, Gwangju, Korea (the Republic of).
2. Department of Molecular Medicine (BK21Plus), Chonnam National University Medical School, Gwangju, Korea (the Republic of).
3. Department of Nuclear Medicine, Chonnam National University Medical School, Gwangju, Korea (the Republic of).
4. Biological Resource Center, Korea Research Institute of Bioscience & Biotechnology (KRIBB), Jeongeup, Korea (the Republic of).

ABSTRACT BODY:

Abstract Body: In a previous study, we developed an E1 monobody specific for the tumor biomarker hEphA2 [PLoS ONE (2015) 10(7): e0132976]. E1 showed potential as a molecular probe for in vitro and in vivo targeting of cancers overexpressing hEphA2. In the present study, we constructed expression vectors for E1 conjugated to optical reporters such as Renilla luciferase variant 8 (Rluc8) or enhanced green fluorescent protein (EGFP) and purified such recombinant proteins by affinity chromatography in E. coli. E1-Rluc8 and E1-EGFP specifically bound to hEphA2 in human prostate cancer PC3 cells but not in human cervical cancer HeLa cells, which express hEphA2 at high and low levels, respectively. These recombinant proteins maintained >40% activity in mouse serum at 24 h. In vivo optical imaging for 24 h did not detect E1-EGFP signals, whereas E1-Rluc8 showed tumor-specific luminescence signals in PC3 but not in HeLa xenograft mice. E1-Rluc8 signals were detected at 4 h, peaked at 12 h, and were undetectable at 24 h. These results suggest the potential of E1-Rluc8 as an EphA2-specific optical imaging agent.

(No Image Selected)

SESSION TITLE: Poster Session 03

CONTROL ID: 2804894

TITLE: A Novel Engineered Small Protein for PET Imaging of Human Programmed Death-1 Ligand (PD-L1) in a Mouse Model

PRESENTER: Arutselvan Natarajan

AUTHORS (FIRST NAME, LAST NAME): Arutselvan Natarajan[1], Sindhuja Ramakrishnan[1], Sanjiv S. Gambhir[1, 2]

INSTITUTIONS (ALL):

1. Radiology, Stanford University, Stanford, CA, United States.
2. 2Bioengineering, Materials Science & Engineering, Stanford University, Stanford, CA, United States.

ABSTRACT BODY:

Abstract Body: Purpose: PET imaging at early time points is desirable for effective patient management compared to antibody based immunoPET. The aim of this research was to engineer and evaluate a small protein targeted against programmed death-1 ligand (PD-L1) present on tumor cells. The engineered protein is a 12 kDa human fibronectin type 3 domain (FN3) scaffold. PET imaging was performed with ^{64}Cu-FN3$_{PD-L1}$ in NSG mice with tumors of human (h) PD-L1+, hPD-L1-negative, and hPD-L1+ blocking groups.

Materials and Methods: The engineered ^{64}Cu-FN3$_{PD-L1}$ was produced in E. coli cells at >5 mg/L. This protein binder was tested for an affinity assay by *in vitro* live cell (hPD-L1stably expressing on CT26) binding and conjugated to NHS-DOTA (Do). The conjugated Do-FN3$_{PD-L1}$ was labeled with ^{64}Cu and tracer quality assays of purity, specific activity, and immunoreactivity were performed. This tracer was further evaluated for targeting of hPD-L1+ cells that were xenografted subcutaneously in a NSG mouse. Four groups of mice (n=3) were tested: hPD-L1+ tumors of non-blocking, and blocking (control)]; hPD-L1 negative, and Nblk-dual tumor [hPD-L1+ (left) and hPD-L1-neg (right)]. The blocking group received 1 mg of unconjugated FN3$_{PD-L1}$ two hours prior to radiotracer injection. Each mouse received ^{64}Cu-FN3$_{PD-L1}$ (3.7 MBq/7 µg of Do-FN3 in 200 µL PBS) via the lateral tail vein. Small animal PET/CT imaging was performed at 1, 2, 4, 18, and 24 h post-injection.

Results: The in vitro assay demonstrated that FN3 binds to hPD-L1 with 1.8 ± 0.9 nM affinity on hPD-L1 positive cells. FN3 radiotracer quality demonstrated >70% yield and >90% purity. The ^{64}Cu-FN3$_{PD-L1}$ imaging showed clear, contrast visualization of hPD-L1+ tumor in the Nblk mice group as early as 1 hour post-injection (1.4 ± 0.4 %ID/g) and exhibited a tumor-to-muscle ratio of 12-fold by 4 h (Figure 1, supplementary MIP image). At 4h the Nblk-tumor signal was 9-fold greater, when compared to the (P = 0.001) blocking mice group.

Conclusion: The ^{64}Cu-Do-FN3$_{PD-L1}$ radiotracer represents a novel, small, high affinity binder for imaging hPD-L1 on tumor cells. These data support further exploration and clinical translation of this novel engineered peptide which may be well suited to select potential patients who may be responders to immune checkpoint therapy.

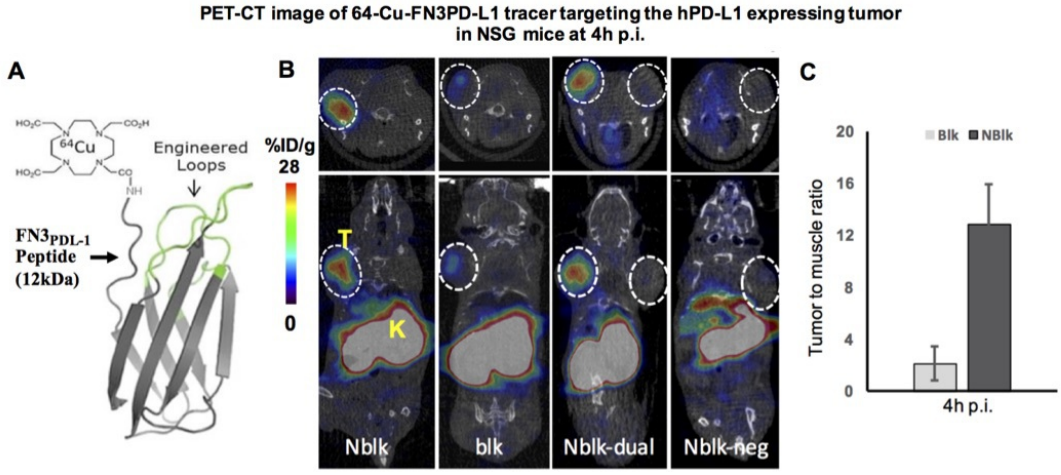

Figure 1. Small animal PET/CT images show the ^{64}Cu-Do-FN3$_{PD\text{-}L1}$ **(A)** tracer specifically targeted on hPD-L1+ tumor mice (left tumor) compared to hPD-L1 negative tumor of Raji cells (right tumor). The PET/CT co-registered images **(B)** on top and bottom rows are transverse and coronal views respectively. PET images were obtained at 4 h time points after tail-vein injection of ^{64}Cu-Do- FN3$_{PD\text{-}L1}$ tracer (3.7 MBq). Non-blocking (Nblk) mice received tracer alone. Blocking (blk) mice were pre-blocked with 1mg of unconjugated FN3 $_{PD\text{-}L1}$ 2 h prior to tracer injection. Left tumor (hPD-L1+) and kidney is indicated by the yellow fonts of T and K, respectively. Nblk-dual and Nblk-neg mice on the right side are hPD-L1 negative tumors, marked with a white circle, with extremely low PET signal. The histogram **(C)** indicates the ROI computation of PET signal from PET/CT images. It shows comparison of tumor-to-muscle ratio of blk and Nblk mice groups (9-fold greater; $P = 0.001$) after 4h p.i.

IMAGE CAPTION:

SESSION TITLE: Poster Session 03

CONTROL ID: 2804918

TITLE: Solubilization and Functionalization of Upconverting Nanoparticles with Janus-Dendrimers

PRESENTER: MIRNA EL KHATIB

AUTHORS (FIRST NAME, LAST NAME): MIRNA EL KHATIB[1], Shane Plunkett[1], Ikbal SENCAN[2], Joshua Collins[3], Sava Sakadzic[2], Sergei A. Vinogradov[1]

INSTITUTIONS (ALL):

1. University of Pennsylvania, Philadelphia, PA, United States.
2. Massachusetts General Hospital, Boston, MA, United States.
3. Intelligent Material Solutions, Princeton, NJ, United States.

ABSTRACT BODY:

Abstract Body: Lanthanide-based upconverting nanoparticles (UCNP's) are able to efficiently convert near infrared excitation energy into visible or higher energy near infrared light, thereby presenting an attractive platform for construction of biological imaging agents. However, lack of solubility and difficulty in their surface modifications hampered development of UCNP's as general imaging agents. Previously, we have demonstrated that shape-persistent polyglutamic dendrimers, exhibiting multiple carboxylate groups as their termini, are of tight bind to UCNP surfaces, thus stabilizing them in aqueous solutions and converting them into bio-compatible imaging probes.[1] However, solubility imparted by polycarboxylates was found to be negatively impacted by the presence of divalent metal cations and various macromolecules (proteins, lipids etc), which are abundant in biological systems. In this work, we report extension of our approach using Janus-type dendrimers, in which one half of the dendrimer surface features carboxylates for binding to UCNP surfaces and another is highly hydrophilic, but neutral as a result of extensive PEG-ylation. The new dendritic UCNP's proved to have superior stability and biocompatibility and allowed high-resolution imaging of brain vasculature in mice up to 1 mm deep into the cortex by means of multiphoton microscopy with continuous-wave infrared excitation sources. The synthesis of PEGylated Janus-dendrimers as well as the method of dendrimerization of UCNP's has been optimized and scaled up, thus presenting a new generally applicable methodology.

References

[1] Esipova, T. V.; Ye, X.; Collins, J. E.; Sakadzic, S.; Mandeville, E. T.; Murray, C. B.; Vinogradov, S. A. Proc. Natl. Acad. Sci. U.S.A. 2012, 109, 20826.

Support of the NIH grant EB018464 is gratefully acknowledged.

(No Image Selected)

SESSION TITLE: Poster Session 03

CONTROL ID: 2804921

TITLE: Innovation of New Luciferin Analog for in vivo Optical Imaging

PRESENTER: Ryohei Saito

AUTHORS (FIRST NAME, LAST NAME): Ryohei Saito[1], Masahiro Kiyama[1], Nobuo Kitada[1], Rika Obata[2], Rei Morimitsu[1], takashi hirano[1], Shojiro Maki[1]

INSTITUTIONS (ALL):

1. Dept. of Engineering Science, The University of Electro-Communications, Chohu, Tokyo, Japan.
2. Keio University, Hiyoshi, Kanagawa, Japan.

ABSTRACT BODY:

Abstract Body: We are innovating new imaging technologies by using organic chemistry. For making advanced medicinal technology, in vivo optical imaging is needed. So, we have been developing luciferin analogues suitable for deep in vivo optical imaging.

It is very difficult for deep in vivo optical imaging to be absorbed and scattered light in living tissue. But, it is well known that the light in the near infrared region (NIR) has high permeability for the living tissue. It is a challenge to visualize in vivo deep optical imaging by developing an imaging material that has NIR emission. We have got structure-activity relationship data on the firefly luciferin luciferase reaction. According to the structure-activity relationship data on luciferin analogues reacted with Ppy luciferase, we have designed and marked NIR probe “TokeOni, (SIGMA-ALDRICH)”. TokeOni gives a higher brightness compared with the natural firefly luciferin because of high permeability TokeOni in tissue (Kuchimaru, T. et al. Nat. Commun. 2016, 7, 11856.).

Based on the TokeOni structure, new luciferin analogues have designed and synthesized three types.

We made the substances of three new luciferin analogues. One of these emits in the NIR and has high water-solubility in PBS, that is named “seMpai”.

We will apply new probe to the animal for conforming practical ability and discuss these new luciferin analogues for in vivo imaging technology.

(No Image Selected)

SESSION TITLE: Poster Session 03

CONTROL ID: 2804962

TITLE: Characterization and in vivo imaging of mesenchymal stem cells derived exosomes.

1,2,3,4 Cheng-Hsiu Lu1, Chien-Chih Ke1,2, Yi-An Chen3, Chao-Cheng Chen1, and Ren-Shyan Liu1,2,3,4

1. Department of Biomedical Imaging and Radiological Sciences, National Yang- Ming University, Taipei, Taiwan
2. Biomedical Imaging Research Center, National Yang-Ming University, Taipei, Taiwan
3. Institute of Clinical Medicine, National Yang-Ming University, Taipei, Taiwan
4. Department of Nuclear Medicine and National PET/Cyclotron Center, Taipei Veterans General Hospital, Taipei, Taiwan

PRESENTER: Cheng-Hsiu Lu

AUTHORS (FIRST NAME, LAST NAME): Cheng-Hsiu Lu[1], Chien-Chih Ke[1], Yi-An Chen[1], Chao-Cheng Chen[1], Ren-Shyan Liu[1]

INSTITUTIONS (ALL):

1. Department of Biomedical Imaging and Radiological Sciences, National Yang- Ming University, Taipei, Taiwan, Taipei, Taiwan.

ABSTRACT BODY:

Abstract Body: Objective: Mesenchymal stem cells (MSCs) are extensively studied adult stem cells which show the great potential in tissue engineering, regenerative medicine and the treatment of various diseases. Several studies have pointed out the most important action by which MSCs exert the therapeutic potential is paracrine effect. Further, exosomes are reportedly the major player mediating the therapeutic and paracrine effects of MSCs. Therapeutics of MSC-derived exosomes have also been demonstrated on injury repair, regulation of immune system and inhibition of tumorigenesis. With the increasing therapeutic significance of MSC-derived exosomes, it is of great importance and interests to discover the fate and in vivo biodistribution of administrated exosomes. In this study, exosomes derived from Wharton's jelly MSCs were isolated, characterized and radiolabeled with 111In-oxine followed by biodistribution study and in vivo γ- scintigraphy.

Methods: Conditioned medium was collected followed by exosome isolation using Exo-Prep kit (Hansa BioMed). Expression of exosomal specific proteins CD63 and HSP70 was verified by western blot. Morphology and size were characterized by transmission electron microscopy (TEM) nanoparticle tracking analysis(NTA). For radiolabeling, exosomes were incubated with 111In-oxine in PBS at 37oc for 1 hr followed by purification and further characterization. Biodistribution and in vivo γ-scintigraphy of 111In-oxine-labeled exosomes were performed at 1, 4, 8, 24, 48 hr after intravenous injection into BALB/c mice.

Results: CD63 and HSP70 expression were observed on exosomes as well as 111In-oxine-exosomes. Radiochemical purity of 111In-oxine-exosomes as higher than 90% and remained stable for at least 48 hours. Result of biodistribution showed that 111In-oxine-labeled exosomes accumulated in liver, spleen, bone marrow, kidney, and cleared rapidly from the circulation as compared to 111In-oxine alone. In vivo γ-scintigraphy showed high accumulation in liver, bone, spleen and liver, but not in brain and circulation.

Conclusion: In this study, we have preliminarily demonstrated the feasibility of in vivo tracking of MSC- derived exosomes labeled with 111In-oxine. Further investigation is still needed and underway to monitor the in vivo fate and behavior of exosomes.

(No Image Selected)

SESSION TITLE: Scientific Session 01: Oncology - Probes Nano 1

CONTROL ID: 2732879

TITLE: DNA Origami assembled with QD655 and gold nanorod working as a novel nanoprobe for fluorescence and optoacoustic dual imaging modality in 4T1 mammary tumor model

PRESENTER: Yang Du

AUTHORS (FIRST NAME, LAST NAME): Yang Du[1], Jie Tian[2]

INSTITUTIONS (ALL):

1. Key laboratory of molecular imaging, Institute of Automation, Beijing, Beijing, China.
2. institute of Automation,CAS, Beijing, China.

ABSTRACT BODY:

Abstract Body: Aims: Fluorescence (FMI) and optoacoustic imaging (OAI) are emerging as important research tools for biomedical studies. OAI offers both strong optical absorption contrast and high ultrasonic resolution and fluorescence molecular imaging provides excellent superficial resolution and high sensitivity. Therefore, combining the imaging information on both modalities can provide comprehensive in vivo physiological and pathological information. However, currently there are limited probes available that can realize both FMI and OAI imaging. DNA origami nanostructures exhibited great potential application in molecular imaging, targeted payload delivery due to their programmability, uniform structures, and their intrinsic biocompatibility as delivery vehicles. The aim of this study is to create a novel FMI and OAI nanoprobe by assembling QD655 and gold nanorod (AuNR) onto the surface of DNA origami delivery system, which may facilitate a more efficient and specific accumulation of probes at the tumor sites in vivo with improved dual modality imaging of mammary tumors.

Methods: 4T1 breast tumor bearing mice were used in this study. DNA Origami-QD655-AuNR (DO-QD-AuNR) probe was uniquely designed to avoid the fluorescence quenching of QD655 and was injected intratumorally. The AuNR alone, QD655 alone, and the mixture of DNA origami and QD655 and AuNR (DO+QD+AuNR), were used as control. Small animal optical molecular imaging system (IVIS Imaging System, Caliper, USA) was used for FMI acquisition, and MSOT (128 elements) were used for animal OAI acquisition.

Results: Both the in vitro and in vivo intratumoral FMI results showed that DO-QD-AuNR exhibited the fluorescence signal, which is comparable to QD655 alone, but there was no signal in the DO+QD+AuNR mixture and AuNR alone groups (Fig A). The OAI signal was observed for the DO-QD-AuNR, DO+QD+AuNR mixture and AuNR alone, but not in the QD655 group both in phantom and intratumoral injection experiment (Fig B). The data suggested that our carefully designed DO-QD-AuNR was successfully assembled to maintain the fluorescence and optoacoustic signal of QD655 and AuNR properties.

Conclusion: The DNA Origami assembled with QD655 and gold nanorod possesses potential to be applied as an efficient dual modality imaging contrast medium for both FMI and OAI imaging.

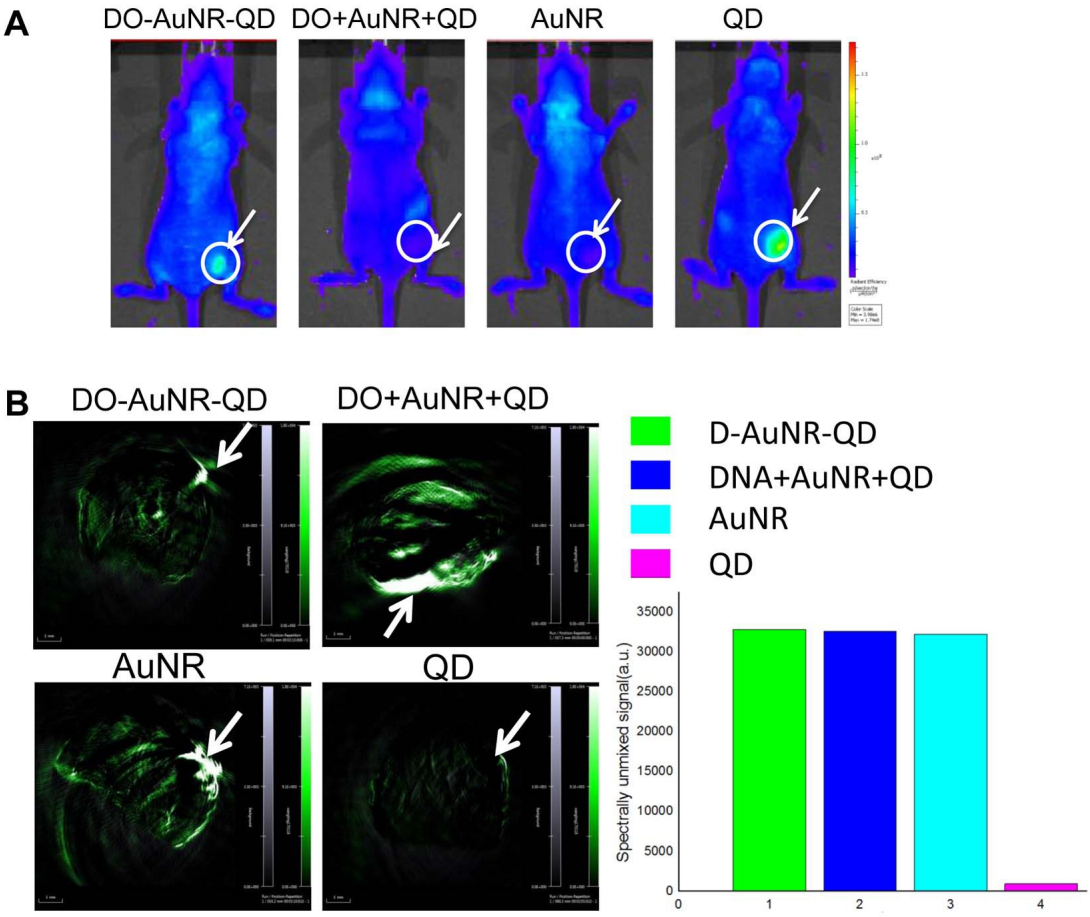
A
DO-AuNR-QD
DO+AuNR+QD
AuNR
QD
B
DO-AuNR-QD
DO+AuNR+QD
AuNR
QD
D-AuNR-QD
DNA+AuNR+QD
AuNR
QD
Spectrally unmixed signal(a.u.)
35000
30000
25000
20000
15000
10000
5000
0
0
1
2
3
4

IMAGE CAPTION:

SESSION TITLE: Scientific Session 10: Oncology Probes

CONTROL ID: 2734724

TITLE: A molecular imaging biosensor monitors the chemosensitizing effects of drugs that restore mutant p53 function and enhance combination chemotherapy for glioblastoma

PRESENTER: Ramasamy Paulmurugan

AUTHORS (FIRST NAME, LAST NAME): Ramasamy Paulmurugan[1], Rayhaneh Afjei[2], Sekar V. Thillai[1], Husam Bibikir Abdelsalam[2], Tarik F. Massoud[2]

INSTITUTIONS (ALL):

1. Radiology, Stanford University, Palo Alto, CA, United States.
2. Radiology and MIPS, Stanford University School of Medicine, Palo Alto, CA, United States.

ABSTRACT BODY:

Abstract Body: Misfolding mutations in p53 are found in >50% of cancers, including glioblastoma. Small molecule drugs that bind to mutant p53 and structurally induce a refolding to a wild-type p53 conformation may restore its biological function. We developed a molecular imaging biosensor that detects drug-modulated changes in p53 folding in cells and in vivo. We validate the specificity of this biosensor for drugs that efficiently bind to various mutant p53 proteins and recover their function. We also evaluate the potential role of these drugs in sensitizing glioblastoma cells that are endogenously mutant for p53 protein but that we subsequently engineered by stably transducing with four different biosensors to have the corresponding genetic backgrounds (wt-p53 or three other misfolding-mutant p53s).

We developed separate Ln229 cells (endogenously mt-p53^{P98L}) each to stably express one of four varieties of a split-Renilla luciferase reporter protein complementation biosensor (NRLuc-p53-CRLuc), to thus achieve four different cellular p53 statuses (wt-p53, mt-p53^{Y220C}, mt-p53^{G245S} and mt-p53^{G282W}). We first studied if these transduced fusion proteins could induce changes in the background p53 cellular status. We then evaluated these cells for luciferase complementation after exposure to drugs that induce structural changes in mt-p53 protein (PhiKan083, a drug of high affinity for p53^{Y220C}, and SCH-529074, a small molecule of high affinity for p53^{G245S}). We used RITA that stabilizes p53 protein without direct binding as a control to prove the specificity of our sensor. Further, we tested the apoptotic effects of these drugs when combined with standard chemotherapies in all transduced Ln229 cells, and wild type U87MG cells (that are endogenously wild-type for p53 status).
Ln229 cells changed their endogenous phenotype with respect to p53 status by adopting a p53 phenotype that reflects the transduced biosensor fusion protein. There was activation of p53 structural change and associated luciferase signal when we treated cells with PhiKan083 and SCH-529074. Indeed, cells treated with PhiKan083 showed significant levels of p53 refolding not only for mt-p53^{Y220C}, as expected, but also in cells transduced with the wt-p53 and all other mutant biosensors. The Ln229 cells treated with doxorubicin (Dox) or temozolomide (TMZ) in combination with PhiKan083 (12.5-50μM) or SCH (1.25-5.0μM) showed significant dose dependent enhancement of apoptotic effect (>40% increase) within 24 h after treatment when compared to respective drugs as monotherapy, an effect also observed in U87MG glioblastoma cells.

A molecular imaging biosensor consisting of p53 protein flanked by split luciferase fragments and expressed as a fusion protein maintains its particular p53 function (whether wild-type or mutant) within cells, and also induces a change in the genetic background of cells with respect to that p53 status accordingly. The use of PhiKan083 and SCH-529074 improves the therapeutic effects of Dox and TMZ in Ln229 and U87MG cells. Applications of this biosensor will be useful for discovery of new p53 anti-misfolding drugs and subsequent validation of drug hits in small animal models.

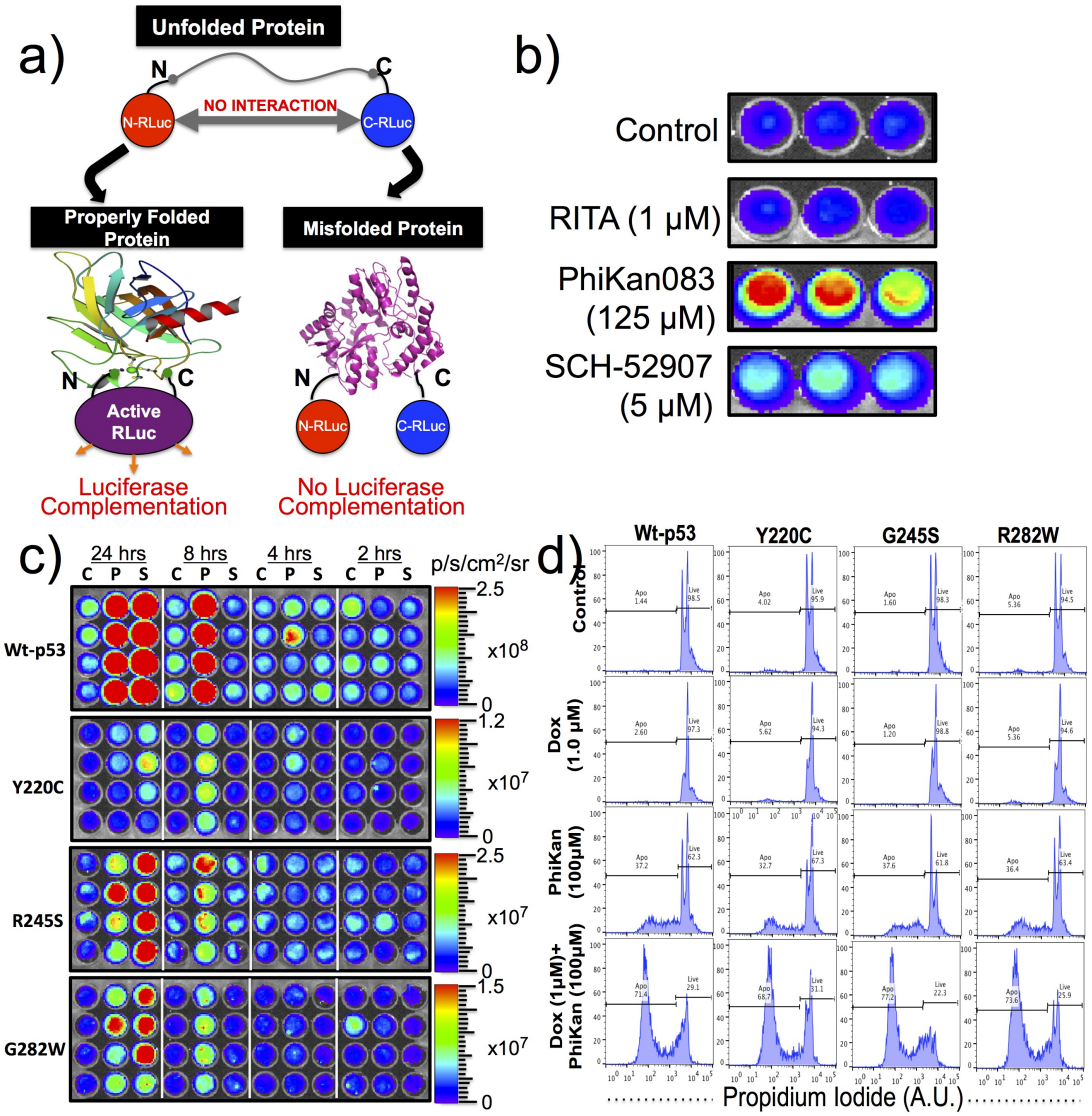

Figure 1: a) Schematic figure describes the functionality by which Split-*Renilla luciferase* complementation sensor differentiate folded and misfolded proteins in cells. **b)** Ln229 cells stably expressing Split-*Renilla luciferase* complementation biosensor with mutant *p53* ^{Y220C} protein measures drug (PhiKan083 and SCH-529074) modulated *p53* folding in cells. **c)** PhiKan083 (125 mM) and SCH-529074 (5 mM) mediated folding changes in Ln229 cells stably expressing Split-*Renilla luciferase* complementation sensor with *wt-p53* and *mt-p53* at different time points after treatment. **d)** Ln229 cells with altered genetic background for *p53* status derived from sensor fusion proteins for their differential response to Doxorubicin in combination with PhiKan083.

IMAGE CAPTION: Figure 1: a) Schematic figure describes the functionality by which Split-*Renilla luciferase* complementation sensor differentiate folded and misfolded proteins in cells. **b)** Ln229 cells stably expressing Split-*Renilla luciferase* complementation biosensor with mutant $p53^{Y220C}$ protein measures drug (PhiKan083 and SCH-529074) modulated *p53* folding in cells. **c)** PhiKan083 (125 mM) and SCH-529074 (5 mM) mediated folding changes in Ln229 cells stably expressing Split-*Renilla luciferase* complementation sensor with *wt-p53* and *mt-p53* at different time points after treatment. **d)** Ln229 cells with altered genetic background for *p53* status derived from sensor fusion proteins for their differential response to Doxorubicin in combination with PhiKan083.

SESSION TITLE: Scientific Session 15: Basic Biology - Imaging Biochemistry

CONTROL ID: 2727321

TITLE: Bisphosphonate functionalization of gadolinium nanoparticle contrast agent increases affinity to calcium phosphate-based bone substitutes and allows long term in vivo MR imaging

PRESENTER: Simone Mastrogiacomo

AUTHORS (FIRST NAME, LAST NAME): Simone Mastrogiacomo[2], Alicja E. Kownacka[4], Weiqiang Dou[5], Benjamin P. Burke[4], Arend Heerschap[5], Steve Archibald[3], X. Frank Walboomers[1]

INSTITUTIONS (ALL):

1. RadboudUMC, Nijmegen, Netherlands.
2. Biomaterials, RadboudUMC, Nijmegen, Netherlands.
3. University of Hull, Hull, United Kingdom.
4. Chemistry, University of Hull, Kingston upon Hull, YORKSHIRE, United Kingdom.
5. Radiology and Nuclear Medicine, RadboudUMC, Nijmegen, Netherlands.

ABSTRACT BODY:

Abstract Body: Introduction

Calcium phosphate cements (CPCs) are biocompatible materials widely used as bone filler. However, due to the high similarity to the osseous phase, CPCs lack in imaging contrast in conventional X-ray technologies as well as in radiation-free imaging modalities (i.e. magnetic resonance imaging, MRI). Poor imaging contrast limits the visualization of CPC once implanted into the body and makes the monitoring of its degradation problematic[1]. To improve imaging contrast, different contrast agents (CAs) have been proposed to enhance X-ray (e.g. barium sulfate) and MRI (e.g. superparamagnetic iron oxide) contrast. However, the in vivo degradation of the CPC causes leaching of the CA component from the implant resulting in signal loss over time[2]. In this study, the surface of a gadolinium-based CA was functionalized with bisphosphonate groups in order to increase the binding affinity to the CPC phase and to allow long term MR imaging in vivo (Fig. 1).

Material and Methods

Gadolinium nanoparticle contrast agents (GNCAs, <5 nm diameter) were first chemically functionalised with bisphosphonate groups (i.e. alendronic acid derivatives) and then combined with the CPC composite. Release studies were performed in vitro to evaluate the binding affinity of the functionalised GNCAs to the CPC phase. Imaging properties of the obtained CPC nanocomposite were first investigated in vitro. Afterwards, long term imaging properties and biological response of the CPC doped with functionalized GBCAs were evaluated by implantation in vivo in rat model (i.e. condyle defect) for 8 weeks. MRI measurements were performed on an 11.7 Tesla MR system (Brucker, Germany) using a quadrature ^{1}H volume coil with 40 mm inner diameter. Images were acquired using a zero echo time (ZTE) sequence with repetition time (TR)=2 ms, image resolution 0.31 mm^3, acquisition time (TA)=6.53 min.

Results

Release studies showed a high binding affinity of the functionalized GNCAs (up to 98 wt%) to the CPC matrix. As previously reported[1], the CPC could not be distinguished from the natural bone on ^{1}H-ZTE images because of the similar T_2^* relaxation times (i.e. <1 ms). However, after combination with GBCAs, the T_2^* relaxation time of CPC was significantly shortened resulting in a dark area on ZTE images. Moreover, 8 weeks after the in vivo implantation, the GNCAs loaded CPC could be still clearly detected by MRI (Fig 1). A bright signal in the middle of the implant surrounded by a dark region could be explained by the combination of T_1 and T_2^* effects. Finally, histological analysis showed no adverse inflammatory reaction from the CPC doped with GNCAs from the surrounding bone.

Conclusion

In the current study, an innovative strategy was developed to attach GNCAs directly to a calcium phosphate-based bone filler. The resultant gadolinium doped CPC can be successfully monitored in vivo by using MRI. The proved biological compatibility warrants its further investigation for use in clinical applications.

Acknowledgement

This project is supported by FP7-PEOPLE-2013-ITN under grant no 607868 (iTERM).

References

1. Tissue Eng Part C Methods 2013, 19, 281

2. Biomaterials 2014, 35, 2227

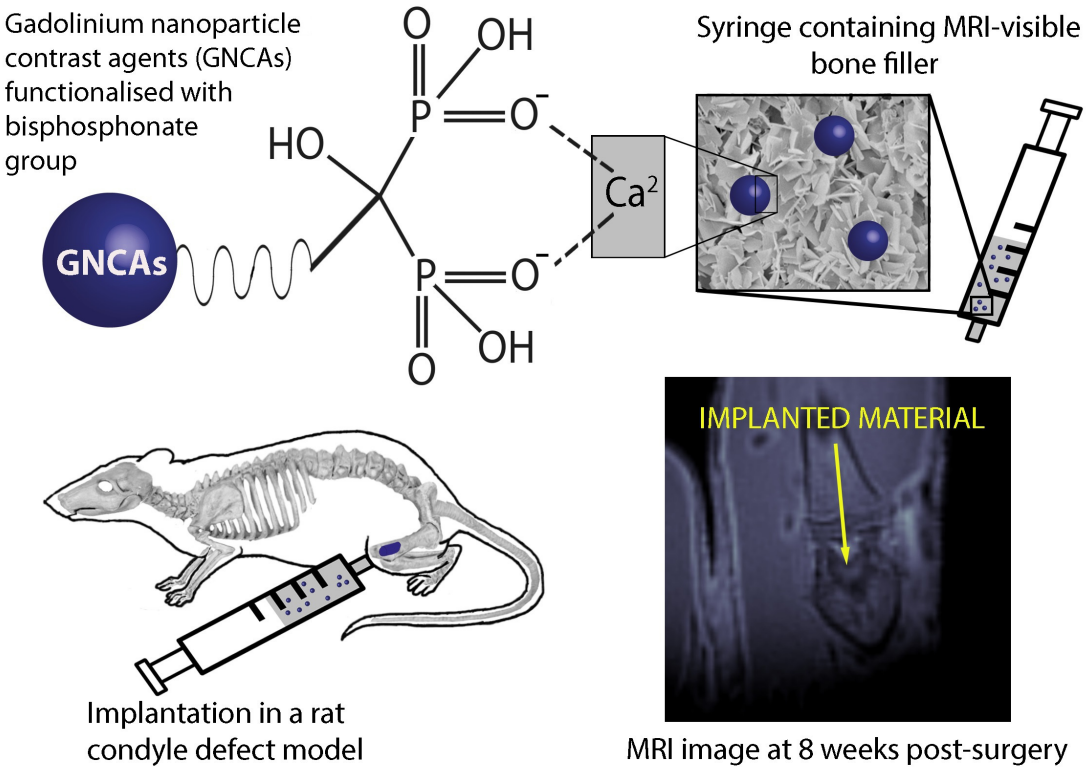

Fig. 1. Schematic representation of the material composition (on the top) and of its implantation in a femoral condyle defect model (on bottom left). On the bottom right a ^{1}H-ZTE MR image of the implanted materials at 8 weeks post-surgery. The yellow arrow points out the implanted material represented by a bright signal surrounded by a dark area as consequence of the T_1 / T_2^*-shortening effect due to the presence of the GNCAs.

IMAGE CAPTION: Fig. 1. Schematic representation of the material composition (on the top) and of its implantation in a femoral condyle defect model (on bottom left). On the bottom right a ^{1}H-ZTE MR image of the implanted materials at 8 weeks post-surgery. The yellow arrow points out the implanted material represented by a bright signal surrounded by a dark area as consequence of the T_1 / T_2^* -shortening effect due to the presence of the GNCAs.

SESSION TITLE: Scientific Session 15: Basic Biology - Imaging Biochemistry

CONTROL ID: 2731061

TITLE: Site-Specific Localization of Near Infrared-Light Activated Upconversion Nanoprobes for Precise Regulation of Membrane Functions

PRESENTER: Bengang Xing

AUTHORS (FIRST NAME, LAST NAME): Bengang Xing[1, 2], xiangzhao ai[1], Linna Lyu[1]

INSTITUTIONS (ALL):

1. Division of chemistry and Biological Chemistry , Nanyang Technological University, Singapore , Singapore.
2. Agency for , Institute of Materials Research & Engineering (IMRE), Singapore, Singapore.

ABSTRACT BODY:

Abstract Body: The spatiotemporal regulation of light-gated ion channels will be a powerful tool to study basic physiological processes and develop personalized theranostic modalities for biomedical applications. However, most existing light-gated channels are limited by their action spectra in the ultraviolet (UV) or visible region, which may raise concerns regarding photodamage and limited light penetration depth. Therefore, simple and innovative strategies that allows specific localization of photoswitchable platforms on the cell surface without modifying or genetically encoding channel protein structures, and more importantly, that enable the remote activation of ion-channel functions within near-infrared (NIR) spectral window in living systems, remain a challenging concern. Herein, a native metabolic glycan biosynthesis is utilized to achieve site-specific covalent attachment of NIR-light-responsive lanthanide-doped upconversion nanocrystals (UCNs) on the cell surface through copper-free click cyclization. Upon irradiation with NIR light at 808nm, the converted blue emission at 480 nm from UCNs could effectively activate a light-gated ion channel, channelrhodopsins-2 (ChR2) on cell surface, thus remotely manipulate the cation influx and precisely regulate the cellular functions (e.g., apoptosis) in living cells and animals, such as, zebrafish etc. Such unique strategy not only provides a site-specific and effective approach for the covalently localization of nanoparticles on the cell membrane, it also holds great potential to precisely regulate the membrane-associated activities under in vivo conditions, which could act as personalized nanomedicines for various pathological disorders in the future.

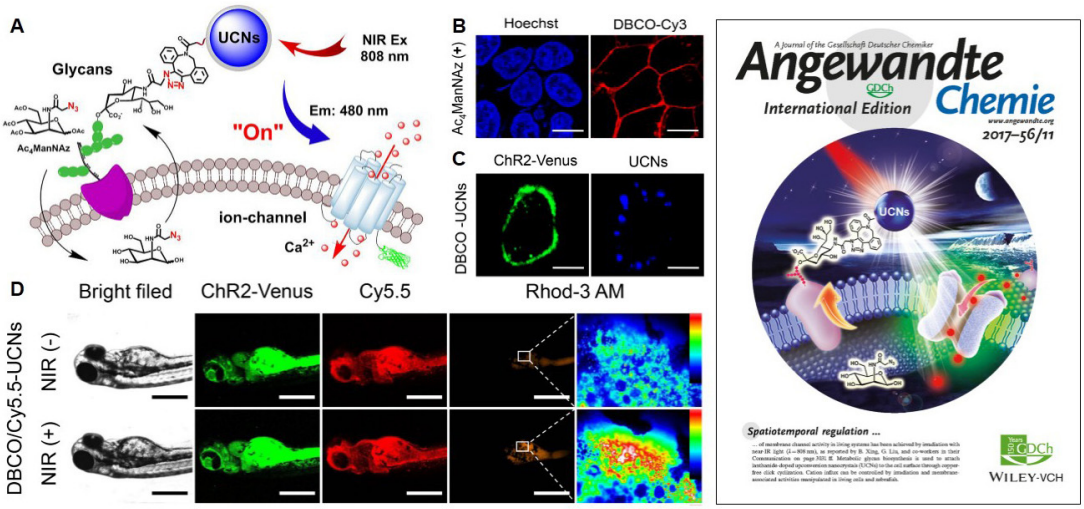
A
UCNs
NIR Ex
808 nm
Glycans
Em: 480 nm
"On"
Ac4ManNAz
ion-channel
Ca2+
B
Hoechst
DBCO-Cy3
Ac4ManNAz (+)
C
ChR2-Venus
UCNs
DBCO -UCNs
Rhod-3 AM
D
Bright filed
ChR2-Venus
Cy5.5
DBCO/Cy5.5-UCNs
NIR (-)
NIR (+)

A Journal of the Gesellschaft Deutscher Chemiker
Angewandte
International Edition
Chemie
www.angewandte.org
2017–56/11
UCNs
Spatiotemporal regulation ...
WILEY-VCH

IMAGE CAPTION:

SESSION TITLE: Scientific Session 15: Basic Biology - Imaging Biochemistry

CONTROL ID: 2732405

TITLE: Hydrazo-CEST: A carbonyl-activatable CEST-MRI contrast agent towards aldehyde imaging in vivo

PRESENTER: Adam Shuhendler

AUTHORS (FIRST NAME, LAST NAME): Trina Dang[1], Caitlin Lazurko[1], Mojmir Suchy[1], Wendy Oakden[3], Yen Truong[1], Wilfred Lam[3], Glenn Facey[1], Greg J. Stanisz[3, 4], Adam Shuhendler[1, 2]

INSTITUTIONS (ALL):

1. Chemistry and Biomolecular Sciences, University of Ottawa, Ottawa, ON, Canada.
2. University of Ottawa Heart Institute, Ottawa, ON, Canada.
3. Physical Sciences, Sunnybrook Research Institute, Toronto, ON, Canada.
4. Medical Biophysics, University of Toronto, Toronto, ON, Canada.

ABSTRACT BODY:

Abstract Body: Reactive carbonyls, including aldehydes, are regularly produced in cells through both anabolic and catabolic processes necessary for life. The production of aldehydes is tightly regulated[1], however chemical or physical stress on our cells can throw aldehyde levels into dysregulation, resulting in the initiation and progression of a variety of disease and injury states[2]. While some aldehydes have been investigated for assessing injury[3] or cancer therapy response[4], the use of reactive carbonyls as biomarkers are infrequent and limited to ex vivo detection. The non-invasive mapping of aldehydes in living systems provides unexplored potential as novel early imaging biomarkers for injury and a variety of diseases.

Building upon previous work establishing rapid, catalyst-free trapping of aldehydes using N-amino anthranilic acids[5], we have developed activatable molecular MRI contrast agents providing imaging signal through chemical exchange saturation transfer (CEST)[6]. These hydrazine-containing agents, collectively termed Hydrazo-CEST, are CEST-inactive until they trap reactive carbonyls to form hydrazones (Fig. 1a). Upon hydrazone formation, proton exchange from the ring-proximal nitrogen falls into the CEST regime and produces high CEST-MRI contrast ($\%MTR_{asym}$ >20%). Using a variety of control probes, we have identified that both the hydrazone proton and the ortho-carboxylic acid are necessary requirements for CEST-MRI. Hydrazo-CEST contrast is sensitive to the electronics of both hydrazine and carbonyl components: the more electron-withdrawing the combined substituents, the lower the CEST signal (Fig. 1b). The loss of observable CEST-MRI contrast was correlated with alterations in the proton exchange rates, deviating from that required for contrast production. The trapping of reactive carbonyls by our probes proceeds rapidly under physiological conditions (k_{obs}~0.1 min^{-1}) and to near completion (>90%) within 15 min (Fig. 1c). The presence of the ortho-carboxylic acid substantially increased the degree of reaction completion and the stability of the hydrazone product relative to control compounds lacking the ortho-carboxylic acid or containing an ortho-methyl ester instead. Through in silico molecular modeling and ^{1}H-NMR experiments, the dual effect of the ortho-carboxylic acid group (i.e. CEST-active and stabilizing reaction products) appears to derive from the formation of a pseudo-six-membered system through an intramolecular hydrogen bond. Finally, we have verified that our probes are biocompatible even at high doses (Fig. 1d), supporting the application of these agents towards in vivo imaging of aldehydes in living subjects.

The development of Hydrazo-CEST, comprised of a set of CEST-MRI probes conditionally activated when bound to bioactive carbonyls, and the rational investigation of the chemical determinants of CEST signal production, places the mapping of aldehydes in vivo by MRI within reach. These probes could provide novel diagnostic and prognostic strategies for diseases and injuries that are initiated and evolved through the biogenesis of aldehydes, including heart disease, neurodegeneration, and traumatic brain injury.

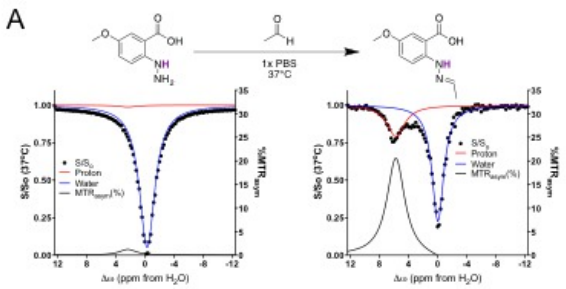

1A. **Hydrazo-CEST is activated upon hydrazone formation.** In the hydrazine form (*left*), negligible CEST signal is detected (black solid line). Upon hydrazone formation under physiological conditions, a significant CEST signal is produced (*right*).

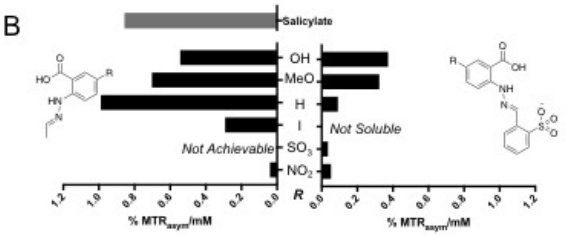

1B. **Hydrazo-CEST is sensitive to hydrazone electronics.** The concentration-normalized CEST signal is plotted for hydrazones formed from aliphatic (*left*) and aromatic (*right*) aldehydes across a variety of substituent groups at *R*. The more electron-withdrawing the substituent, the lower the CEST signal. The Hydrazo-CEST compounds (*black bars*) are compared to salicylate (*grey bar*), a gold standard CEST agent.

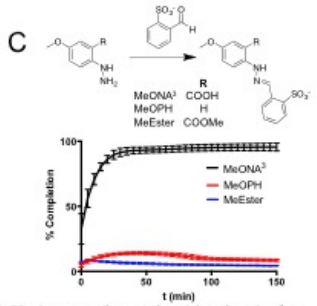

1C. **Hydrazone formation kinetics.** In the presence of the carboxylic acid (*black*), hydrazone formation is rapid and approaches 100% completion. Without the carboxylate (*red*) or with a methyl ester (*blue*) a significantly lower percentage of hydrazone is produced.

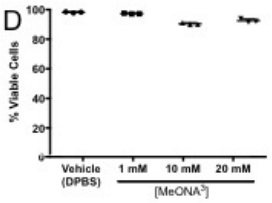

1D. **Hydrazo-CEST probe is non-toxic *in vitro*.** The methoxy-substituted probe was incubated with A549 cells for 60 min at indicated concentrations, and viable cell fraction was determined by flow cytometry Live-Dead Assay.

References. [1] Niki E, Free Radical Biology and Medicine (2009) 47:469-84.[2] Ellis EM, Pharmacology & Therapeutics (2007) 115:13-24. [3] Cebak JE et al., Journal of Neurotrauma (2016) 33:1-16; Halstrom A et al., Journal of Clinical Neuroscience (2017) 35:104-8. [4] Gomes Junior AL, et al., Oxidative Medicine and Cellular Longevity (2015) 212964; Kumaraguruparan R et al., Clinical Biochemistry (2005) 38:154-8. [5] Kool ET et al., JACS (2013) 135:17663-6; Kool ET et al., Organic Letters (2014)16:1454-7.[6] Bar-Shir A et al., ACS Chemical Biology (2015) 10:1160

IMAGE CAPTION: References. [1] Niki E, Free Radical Biology and Medicine (2009) 47:469-84.[2] Ellis EM, Pharmacology & Therapeutics (2007) 115:13-24. [3] Cebak JE et al., Journal of Neurotrauma (2016) 33:1-16; Halstrom A et al., Journal of Clinical Neuroscience (2017) 35:104-8. [4] Gomes Junior AL, et al., Oxidative Medicine and Cellular Longevity (2015) 212964; Kumaraguruparan R et al., Clinical Biochemistry (2005) 38:154-8. [5] Kool ET et al., JACS (2013) 135:17663-6; Kool ET et al., Organic Letters (2014)16:1454-7.[6] Bar-Shir A et al., ACS Chemical Biology (2015) 10:1160

SESSION TITLE: Scientific Session 19: Basic Biology - Cell Imaging & Bioengineering

CONTROL ID: 2686914

TITLE: Zirconium-89 tetraazamacrocycle complexes may provide a new strategy in ^{89}Zr radiopharmaceutical development

PRESENTER: Thaddeus Wadas

AUTHORS (FIRST NAME, LAST NAME): Darpan N. Pandya[1], Nikunj B. Bhatt[1], Cynthia S. Day[2], Hong Yuan[3], Thaddeus J. Wadas[1]

INSTITUTIONS (ALL):

1. Cancer Biology, Wake Forest University Health Sciences, Winston-Salem, NC, United States.
2. Chemistry, Wake Forest University, Winston-Salem, NC, United States.
3. Radiology, University of North Carolina, Chapel Hill, NC, United States.

ABSTRACT BODY:

Abstract Body: Introduction: The development of bifunctional chelators (BFCs) that can stably chelate zirconium-89 (^{89}Zr) while being conjugated to targeting molecules is an area of active research. Given the dearth of reports describing the use of tetraazamacrocycles in ^{89}Zr radiopharmaceutical development, we chose to investigate their potential as ^{89}Zr chelators.

Methods: The non-radioactive Zr tetraazamacrocycle complexes, Zr-DOTA, Zr-DOTAM and Zr-DOTP were prepared using standard procedures, and the molecular structure of Zr-DOTA was elucidated using single crystal x-ray diffraction analysis. The radioactive analogs were prepared using $^{89}ZrCl_4$ as a radioactive precursor. In vitro, the radiometal complexes were challenged with exogenous chelating ligands, biologically relevant metal ions and human serum. Biodistribution and small animal PET studies were conducted in normal mice to examine the in vivo behavior of the radiometal complexes.

Results: Single crystal analysis of Zr-DOTA revealed an octa-coordinate complex with square anti-prism geometry and a tetragonal (P4cc) space group. Radiochemistry studies revealed ^{89}Zr-DOTA to be extraordinarily inert to exogenous ligand, metal and serum challenge in vitro. Furthermore, biodistribution and small animal PET imaging revealed rapid systemic clearance and low tissue retention of this radiometal complex. In particular, mice injected with ^{89}Zr-DOTA retained less radioactivity in their liver, kidney and bone tissue than did mice receiving an injection of ^{89}Zr-DFO (^{89}Zr-DOTA vs. ^{89}Zr-DFO; %ID/g ± SD, p value: blood, 0.0003 ± 0.0008 vs. 0.0003 ± 0.0005, 1.00; liver, 0.021 ± 0.002 vs. 0.066 ± 0.009, < 0.0001; kidney, 0.078 ± 0.009 vs. 0.69 ± 0.098, < 0.0001; bone, 0.025 ± 0.009 vs. 0.079 ± 0.014, < 0.0001).

Conclusion: The structural characterization of Zr-DOTA using single crystal x-ray diffraction and the use of tetraazamacrocycles as ^{89}Zr chelators is described. In all studies, ^{89}Zr-DOTA demonstrated superior in vivo behaviour compared to ^{89}Zr-DFO, which is considered the “gold standard” in clinical ^{89}Zr radiopharmaceutical development. These results refute current thinking regarding the use of tetraazamacrocycles as ^{89}Zr chelators, and may provide a new strategy in ^{89}Zr radiopharmaceutical development.

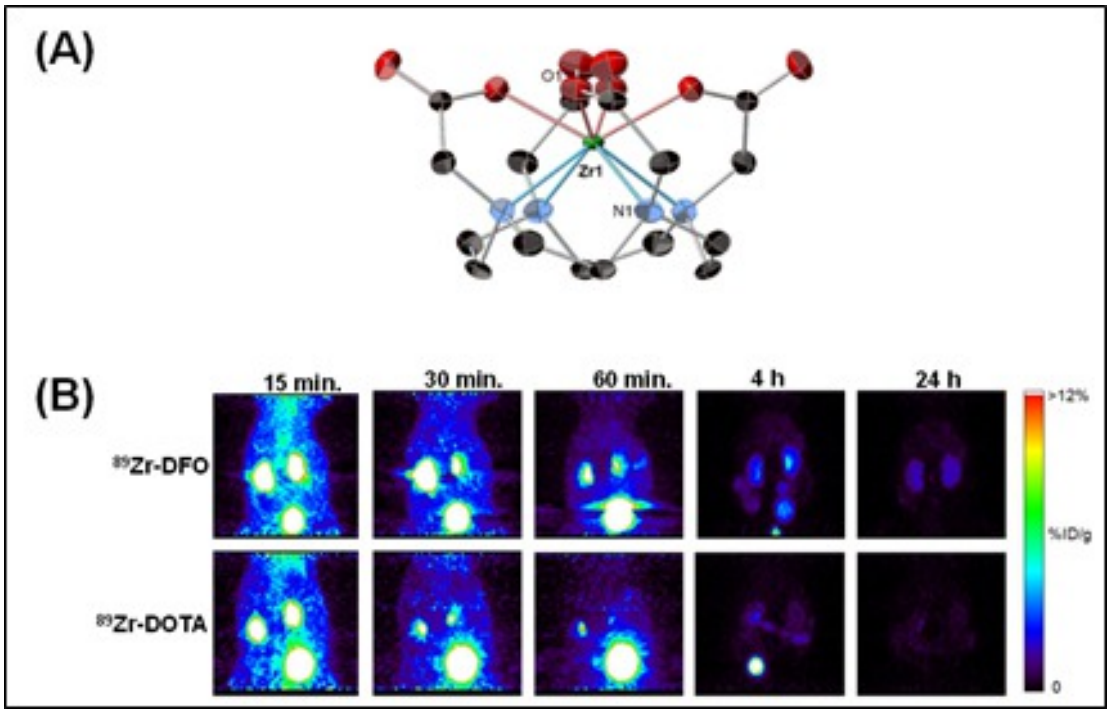

Figure 1. Tetraazamacrocycles are efficient ^{89}Zr chelators. (A) The single crystal structure of Zr-DOTA. (B) Maximum intensity projection images comparing the clearance of ^{89}Zr-DFO and ^{89}Zr-DOTA in normal mice. ^{89}Zr-DOTA demonstrates superior *in vivo* behavior, which refutes scientific consensus.

IMAGE CAPTION:

Figure 1. Tetraazamacrocycles are efficient ^{89}Zr chelators. (A) The single crystal structure of Zr-DOTA. (B) Maximum intensity projection images comparing the clearance of ^{89}Zr-DFO and ^{89}Zr-DOTA in normal mice. ^{89}Zr-DOTA demonstrates superior *in vivo* behavior, which refutes scientific consensus.

SESSION TITLE: Scientific Session 19: Basic Biology - Cell Imaging & Bioengineering

CONTROL ID: 2723909

TITLE: Manganese-zinc ferrites for cell labeling and imaging in vivo

PRESENTER: Vít Herynek

AUTHORS (FIRST NAME, LAST NAME): Vít Herynek[1], Andrea Gálisová[1], Ondrej Kaman[2], Magda Vosmanská[3], Jakub Koktan[2, 3], Lucie Kosinová[4], Milan Hajek[1]

INSTITUTIONS (ALL):

1. MR Unit, Department of Diagnostic and Interventional Radiology, Institute for Clinical and Experimental Medicine, Prague, Czech Republic.
2. Institute of Physics, Czech Academy of Sicences, Prague, Czech Republic.
3. Faculty of Chemical Engineering, University of Chemistry and Technology, Prague, Czech Republic.
4. Experimental Medicine Department, Institute for Clinical and Experimental Medicine, Prague, Czech Republic.

ABSTRACT BODY:

Abstract Body: Introduction

Iron oxide nanoparticles represent traditional cell labels for cell tracking using MRI. However, nanoparticles based on other metal oxides may show higher magnetization, which implicates high transverse relaxivity (r_2). Their properties can be further improved by optimization of the crystallite size, clustering and coating. We tested novel manganese ferrites doped with zinc (Mn-Zn ferrites).

Materials and Methods

Mn-Zn ferrite nanoparticles synthesized by hydrothermal treatment of precursors obtained by alkaline precipitation under inert atmosphere were coated by silica (1). Crystalline structure and mean size of crystallites were determined by X-ray diffraction (XRD). Particle size and silica coating thickness was evaluated from TEM images. Magnetization was measured by SQUID magnetometry. Relaxometry was performed at magnetic fields 0.5 - 4.7 T.

Silica-coated nanoparticles at three concentrations were tested in vitro on mesenchymal stem cells from the adipose tissue of luciferase-expressing Lewis rats. Cell viability (Trypan blue exclusion test, bioluminiscence following luciferin application) after 24 hour labeling was evaluated as well as relaxation rates of the labeled cells. The ferrite content in the cells was determined by ICP-MS.

The labeled cells were transplanted into the muscle of standard Lewis rats and imaged in vivo by MRI (Bruker BioSpec 4.7 T) and optical imaging (PerkinElmer IVIS Lumina imager) after intravenous luciferin administration, which also confirmed cell viability.

Results and Discussion

XRD patterns proved spinel structure of the nanoparticles. The nanoparticle chemical composition ($Mn_{0.61}Zn_{0.42}Fe_{1.97}O_4$) closely reflected the metal ratio employed for the synthesis. The crystallite diameter was $d_{XRD} \approx 10$ nm, core size 30 nm, and silica coating thickness 17 nm (Fig. A). Magnetization of bare cores reached $M_{796\ kA/m} = 107.1$ and 53.3 Am^2/kg at 5 and 300 K, respectively. Relaxometry revealed transverse relaxivity with a pronounced dependence on temperature (604 s^{-1}/mM at 5 °C, 260 s^{-1}/mM at 37 °C). Labeled cells showed relaxation rates higher than commercially available iron oxide nanoparticles (6.1 $s^{-1}/10^6$ cells/mL at 4.7 T) whereas metal content was lower (0.13 pg Mn/cell, 0.42 pg Fe/cell). Cell viability was not compromised by the nanoparticles in the medium and remained comparable to the unlabeled control sample.

Transplanted labeled cells were clearly visible on MR images (Fig. B) and viable (producing bioluminiscent signal after luciferin administration, Fig. C). Lower bioluminiscent signal from labeled cells was caused by uneven geometry during examination and by quenching of the optical signal by the nanoparticles.

Conclusion

Nanoparticles based on manganese-zinc ferrites with silica coating represent safe cell labels with high relaxivity, which enables decreasing of nanoparticle concentration during labeling and thus prevents adverse effects on cell viability.

Grant support: Czech Science Foundation - project No. 16-04340S, Ministry of Health of the Czech Republic (Institute for Clinical and Experimental Medicine – IKEM, Project IN 00023001).

References

1. Kaman O et al. J Magn Magn Mater. 2017; 427:251–257.

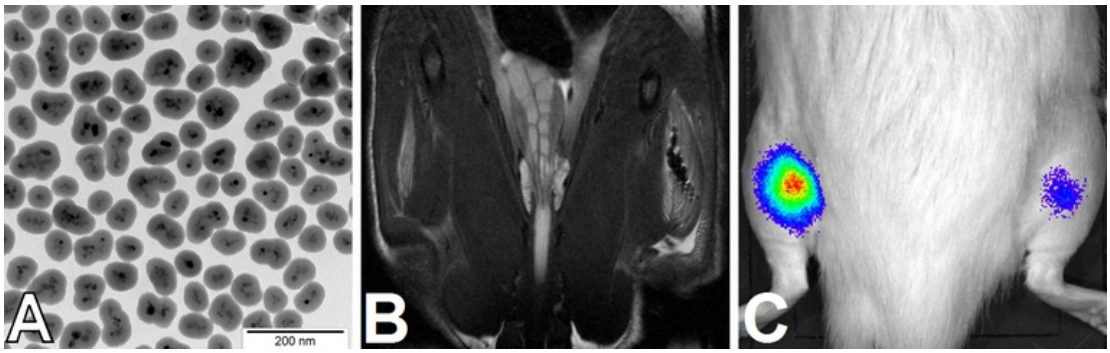

(A) Transmission electron microscopy image of the Mn-Zn ferrite nanoparticles coated by silica. (B) *In vivo* MRI image of cells transplanted into the muscle: unlabeled – left, labeled - right. (C) Biolumiscence of transplanted cells *in vivo:* unlabeled – left, labeled – right.

IMAGE CAPTION: (A) Transmission electron microscopy image of the Mn-Zn ferrite nanoparticles coated by silica. (B) *In vivo* MRI image of cells transplanted into the muscle: unlabeled – left, labeled - right. (C) Biolumiscence of transplanted cells *in vivo:* unlabeled – left, labeled – right.

SESSION TITLE: Scientific Session 19: Basic Biology - Cell Imaging & Bioengineering

CONTROL ID: 2730093

TITLE: Acoustic Reporter Genes for Non-Invasive Deep Tissue Imaging of Engineered Cells

PRESENTER: Arash Farhadi

AUTHORS (FIRST NAME, LAST NAME): Arash Farhadi[1], Raymond W. Bourdeau[3], Gabrielle Ho[3], Audrey Lee-Gosselin[3], Anupama Lakshmanan[1], Sripriya Ravindra Kumar[2], Suchita P. Nety[3], Mikhail G. Shapiro[3, 1]

INSTITUTIONS (ALL):

1. Bioengineering, California Institute of Technology, Pasadena, CA, United States.
2. Biology, California Institute of Technology, Pasadena, CA, United States.
3. Chemistry and Chemical Engineering, California Institute of Technology, Pasadena, CA, United States.

ABSTRACT BODY:

Abstract Body: Genetically encoded fluorescent proteins are used in virtually every study in basic and synthetic biology to observe specific cellular and molecular processes. However, the poor penetration of visible light into opaque tissues limits the utility of optical imaging in living animals. Conversely, non-invasive imaging modalities such as ultrasound are able to image deep tissues but lack genetically encoded molecular reporters. If such reporters could be developed, they would transform our ability to study the function of natural and engineered cells and genetic circuits in vivo. To address this need, we recently discovered that a unique class of gas-filled protein nanostructures, called gas vesicles (GVs), are able to serve as biomolecular reporters for ultrasound[1]. Naturally expressed in buoyant waterborne microbes, GVs comprise all-protein shells with sizes on the order of 250 nm that are filled with gas. To use these biomolecules as genetically encoded reporters, it is necessary to transfer the 8-14 gene operons encoding them from their native hosts into heterologous cells. Here we describe how we have used synthetic biology techniques to achieve this goal in bacteria and mammalian cells. First, we describe a 6-kilobase gene cluster that we engineered for functional GV expression in E. coli and Salmonella, allowing the use of this “acoustic reporter gene” for non-invasive ultrasound imaging of microbes in mammalian hosts[2]. We then describe our progress in developing GVs as acoustic reporter genes for mammalian cells. To enable this challenging transfer of a large operon from prokaryotes to eukaryotes, we have used a combination of viral elements and engineered promoters to design a minimized mammalian gene cluster with appropriate inter-gene stoichiometry for GV expression. We anticipate that the resulting acoustic reporter genes will enable previously impossible approaches to monitoring the location, viability and function of a large variety of engineered cells in vivo with applications in basic biology, cellular diagnostics and therapeutics.

1. Shapiro MG, Goodwill PW, Neogy A, Yin M, Foster FS, Schaffer DV, et al. Biogenic gas nanostructures as ultrasonic molecular reporters. Nat Nanotechnol 2014, 9(4): 311-316.
2. Bourdeau RW, Lee-Gosselin A, Lakshmanan A, Kumar SR, Farhadi A, Shapiro MG. Acoustic reporter genes for non-invasive imaging of microbes in mammalian hosts. In revision.

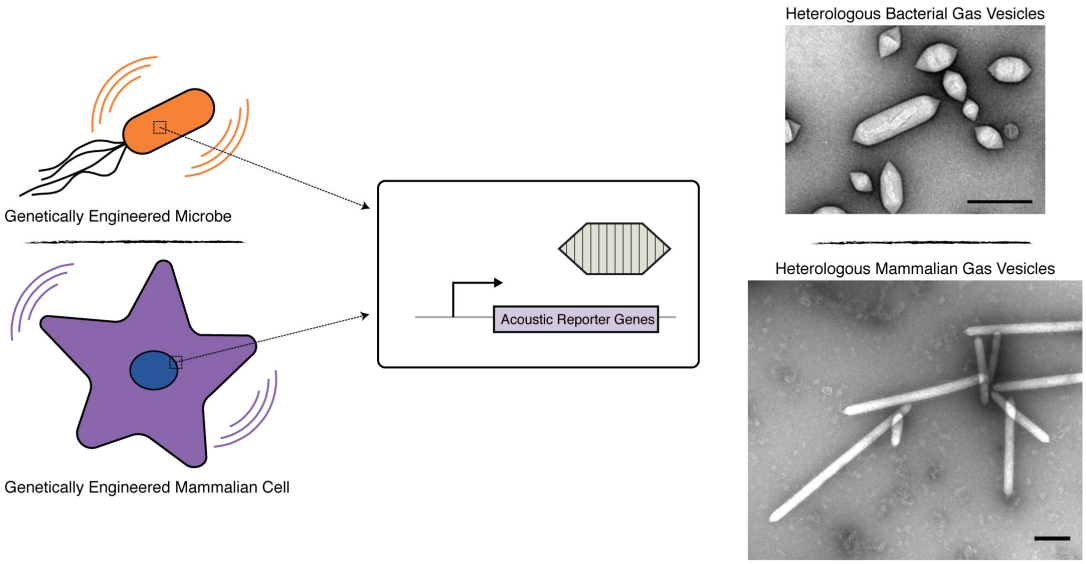

Figure 1 – **Heterologous expression of acoustic reporter genes in bacterial and mammalian hosts.** Schematic of genetically engineering microbes and mammalian cells containing genetically encoded acoustic reporter genes (left). Representative transmission electron micrographs of bacterial and mammalian ARG after protein expression, cell lysis and buoyancy enrichment to obtain purified proteins (right). Scale bars represent 250 nm.

IMAGE CAPTION: Figure 1 – **Heterologous expression of acoustic reporter genes in bacterial and mammalian hosts.** Schematic of genetically engineering microbes and mammalian cells containing genetically encoded acoustic reporter genes (left). Representative transmission electron micrographs of bacterial and mammalian ARG after protein expression, cell lysis and buoyancy enrichment to obtain purified proteins (right). Scale bars represent 250 nm.

SESSION TITLE: Scientific Session 19: Basic Biology - Cell Imaging & Bioengineering

CONTROL ID: 2734321

TITLE: Red blood cells as a carrier for targeted imaging and ultrasound-triggered contents release.

PRESENTER: Alexander Klibanov

AUTHORS (FIRST NAME, LAST NAME): Justin M. Farry[2], Johnny Chen[2], Adam J. Dixon[2], Ali H. Dhanaliwala[2], Zhongmin Du[1], John A. Hossack[2], Alexander L. Klibanov[3, 1]

INSTITUTIONS (ALL):

1. CVRC, University of Virginia, Charlottesville, VA, United States.
2. Biomedical Engineering, University of Virginia, Charlottesville, VA, United States.
3. Dept. of Medicine, Cardiovascular Div., University of Virginia, Charlottesville, VA, United States.

ABSTRACT BODY:

Abstract Body: Targeted delivery with red blood cells (RBCs) as carrier systems has been investigated for decades. These natural drug carriers are fully natural and stay in the bloodstream for many days; they possess significant internal volume for loading of drugs and/or imaging agents. In this study we investigate simple yet efficient tools to achieve molecular and magnetic targeting of RBCs, loading of dyes and drugs, photoacoustic imaging of dye-loaded RBCs, and rapid release of entrapped contents by focused ultrasound.

Dyes (calcein or ICG) were entrapped inside RBCs by a hypotonic loading procedure: washed murine RBCs were incubated in a medium with low osmolarity, with the dye present. Following addition of high salt buffer, RBCs were resealed, and external dye was removed by centrifugal wash. Contents leakage from the resealed RBCs was slow, ~10% per day. Targeting ligands were attached to RBCs by a simple co-incubation of ligand-PEG-DSPE micelles. A simple model, fluorescein-PEG-DSPE, demonstrated ~60% of the added anchor bound to the surface of RBCs, with estimated ~100,000 molecules per RBC (confirmed by fluorescence microscopy). A cyclic RGD peptide ligand, cRGDfK-PEG-DSPE, was bound to RBC membrane as well, resulting in an excellent in vitro targeting to recombinant $alpha_v beta_3$-coated dish, and minimal adhesion to the control albumin-only dish (~65-fold difference).

Magnetic targeting was performed by co-entrapping iron oxide nanoparticles (20 nm diameter) along with the ICG dye inside RBC by hypotonic hemolysis; unentrapped materials were removed by centrifugation. ICG- and magnet-loaded RBCs were tested in an in vitro channel phantom, with and without the action of neodymium magnet. Photoacoustic imaging of the magnetic RBCs in the phantom channel was performed with pulsed infrared laser irradiation (750-830 nm, up to 5 mJ/cm^2) and Verasonics ultrasound detection (CL15-7 or L22-14v probes) and confirmed the ability to attract and retain magnetic RBCs with a small neodymium magnet, as well as the ability to detect them by photoacoustic imaging of entrapped ICG. ICG-loaded RBCs could be detected in the presence of 40% hematocrit.

For focused ultrasound triggering, RBCs were decorated with perfluorocarbon nanodroplets, which convert to gas bubbles upon the action of focused ultrasound. Nanodroplets (~200 nm diameter) were prepared from perfluorobutane or perfluoropentane gas and stabilized with a lipid monolayer shell (DSPC and PEG stearate) and contained positively charged lipid (DSTAP); attachment of these particles to RBC membrane was by electrostatic interaction. Nanodroplet-decorated RBCs were radiolabeled with Cr-51 and ~90% stayed in the bloodstream for two hours following intravenous injection in mice, with minimal accumulation in RES or other organs. Calcein-loaded RBCs, complexed with perfluorocarbon nanodroplets rapidly released entrapped dye, following a single pulse of focused ultrasound (1 us, 10 MHz, 11 MPa), confirmed by video microscopy and fluorescence spectroscopy.

Overall, RBCs can become an attractive platform for image-guided and ultrasound-triggered targeted drug delivery.

(No Image Selected)